

EUROPEAN ORGANISATION FOR NUCLEAR RESEARCH (CERN)



Eur. Phys. J. C 78 (2018) 171
 DOI: [10.1140/epjc/s10052-018-5624-4](https://doi.org/10.1140/epjc/s10052-018-5624-4)



CERN-EP-2017-197
 13th March 2022

Measurement of quarkonium production in proton–lead and proton–proton collisions at 5.02 TeV with the ATLAS detector

The ATLAS Collaboration

The modification of the production of J/ψ , $\psi(2S)$, and $\Upsilon(nS)$ ($n = 1, 2, 3$) in $p+\text{Pb}$ collisions with respect to their production in pp collisions has been studied. The $p+\text{Pb}$ and pp datasets used in this paper correspond to integrated luminosities of 28 nb^{-1} and 25 pb^{-1} respectively, collected in 2013 and 2015 by the ATLAS detector at the LHC, both at a centre-of-mass energy per nucleon pair of 5.02 TeV. The quarkonium states are reconstructed in the dimuon decay channel. The yields of J/ψ and $\psi(2S)$ are separated into prompt and non-prompt sources. The measured quarkonium differential cross sections are presented as a function of rapidity and transverse momentum, as is the nuclear modification factor, $R_{p\text{Pb}}$ for J/ψ and $\Upsilon(nS)$. No significant modification of the J/ψ production is observed while $\Upsilon(nS)$ production is found to be suppressed at low transverse momentum in $p+\text{Pb}$ collisions relative to pp collisions. The production of excited charmonium and bottomonium states is found to be suppressed relative to that of the ground states in central $p+\text{Pb}$ collisions.

1 Introduction

The study of heavy quarkonium bound states ($c\bar{c}$ and $b\bar{b}$) in ultra-relativistic heavy-ion collisions [1, 2] has been a subject of intense theoretical and experimental efforts since it was initially proposed by Matsui and Satz [3] as a probe to study a deconfined quark–gluon plasma (QGP) created in nucleus–nucleus (A+A) collisions. In order to understand quarkonium yields in A+A collisions it is necessary to disentangle effects due to interaction between quarkonium and the QGP medium from those that can be ascribed to cold nuclear matter (CNM). In proton (deuteron)–nucleus collisions, $p(d)+A$, the formation of a large region of deconfined and hot QGP matter was not expected to occur. Therefore, the observed suppression of quarkonium yields in these systems with respect to pp collisions [4–7] has traditionally been attributed to CNM effects.

Among the CNM effects, three primary initial-state effects are: modifications of the nuclear parton distribution functions [8–11], parton saturation effects in the incident nucleus [12], and parton energy loss through interactions with the nuclear medium [13, 14]. On the other hand, the absorption of the heavy quark–antiquark pair through interactions with the co-moving nuclear medium [15–18] is considered to be a final-state effect. In proton–lead ($p+\text{Pb}$) collisions, the modification of quarkonium production with respect to that in pp collisions may be quantified by the nuclear modification factor, $R_{p\text{Pb}}$, which is defined as the ratio of the quarkonium production cross section in $p+\text{Pb}$ collisions to the cross section measured in pp collisions at the same centre-of-mass energy, scaled by the number of nucleons in the lead nucleus:

$$R_{p\text{Pb}} = \frac{1}{208} \frac{\sigma_{p+\text{Pb}}^{O(nS)}}{\sigma_{pp}^{O(nS)}},$$

where $O(nS)$ represents one of five measured quarkonium states, J/ψ , $\psi(2S)$, $\Upsilon(1S)$, $\Upsilon(2S)$ and $\Upsilon(3S)$. Several measurements of CNM effects in quarkonium production were performed with $p+\text{Pb}$ data collected in 2013 at the LHC at a centre-of-mass energy per nucleon pair $\sqrt{s_{\text{NN}}} = 5.02$ TeV. Measurements of the J/ψ nuclear modification factor and forward (p beam direction) to backward (Pb beam direction) cross-section ratio by the ALICE [19, 20] and LHCb [21] experiments show strong suppression at large rapidity and low transverse momentum. However, no strong modification of J/ψ production is observed at small rapidities and high transverse momentum by the ATLAS [22] or CMS [23] experiments indicating that the CNM effects have strong rapidity and/or transverse momentum dependence. The CNM effects in excited quarkonium states with respect to the ground state can be quantified by the double ratio, $\rho_{p\text{Pb}}^{O(nS)/O(1S)}$, defined as:

$$\rho_{p\text{Pb}}^{O(nS)/O(1S)} = \frac{R_{p\text{Pb}}(O(nS))}{R_{p\text{Pb}}(O(1S))} = \frac{\sigma_{p+\text{Pb}}^{O(nS)}}{\sigma_{p+\text{Pb}}^{O(1S)}} / \frac{\sigma_{pp}^{O(nS)}}{\sigma_{pp}^{O(1S)}},$$

where $n = 2$ for charmonium and $n = 2$ or 3 for bottomonium. In the double ratio, most sources of detector systematic uncertainty cancel out, and measurements of this quantity by different experiments can easily be compared. The initial-state effects are expected to be largely cancelled out in double ratio due to the same modifications affecting partons before the formation of the quarkonium state, so measuring the relative suppression of different quarkonium states should help in understanding the properties of the final-state effects separately from the initial ones. The PHENIX experiment at RHIC has presented measurements of $\psi(2S)$ suppression at mid-rapidity for $d+\text{Au}$ interactions at $\sqrt{s_{\text{NN}}} = 200$ GeV, showing

that the charmonium double ratio is smaller than unity, and decreases from peripheral to central collisions [24]. At the LHC, inclusive J/ψ [19] and $\psi(2S)$ [25] production has been measured by the ALICE experiment in $p+\text{Pb}$ collisions at $\sqrt{s_{\text{NN}}} = 5.02$ TeV at forward rapidity. Those measurements show a significantly larger suppression of the $\psi(2S)$ compared to that measured for J/ψ .

The $\Upsilon(nS)$ ($n = 2, 3$) to $\Upsilon(1S)$ double ratios are both found to be less than unity by the CMS experiment in $p+\text{Pb}$ collisions at $\sqrt{s_{\text{NN}}} = 5.02$ TeV [26]. A double ratio which is smaller than unity suggests the presence of final-state interactions that affect the excited states more strongly than the ground state, since initial-state effects are expected to cancel. The CMS $p+\text{Pb}$ results indicate that the CNM effect partially contributes to the strong relative suppression found in previous CMS measurements [27–29] of $\text{Pb}+\text{Pb}$ collisions at $\sqrt{s_{\text{NN}}} = 2.76$ TeV.

In this paper, four classes of experimental measurements are presented. The first class of measurements is differential production cross sections of J/ψ , $\psi(2S)$, and $\Upsilon(nS)$ ($n = 1, 2, 3$) in pp collisions at $\sqrt{s} = 5.02$ TeV and $p+\text{Pb}$ collisions at $\sqrt{s_{\text{NN}}} = 5.02$ TeV. The second is the centre-of-mass rapidity dependence and transverse momentum dependence of J/ψ and $\Upsilon(1S)$ nuclear modification factors, $R_{p\text{Pb}}$. The third is the evolution of the quarkonium yields with $p+\text{Pb}$ collision centrality [30] studied using ratios of the yields of quarkonia to that of Z bosons and the correlation between quarkonium yields and event activity, where both are normalised by their average values over all events. The fourth is the charmonium and bottomonium double ratios, $\rho_{p\text{Pb}}^{O(nS)/O(1S)}$, presented as a function of centre-of-mass rapidity and centrality.

2 ATLAS detector

The ATLAS experiment [31] at the LHC is a multi-purpose detector with a forward-backward symmetric cylindrical geometry and a nearly 4π coverage in solid angle.¹ It consists of an inner tracking detector (ID) surrounded by a thin superconducting solenoid providing a 2 T axial magnetic field, electromagnetic and hadron calorimeters, and a muon spectrometer (MS). The ID covers the pseudorapidity range $|\eta| < 2.5$. It consists of silicon pixel, silicon micro-strip, and gaseous transition radiation tracking detectors. A new innermost insertable B-layer [32] installed during the first LHC long shutdown (2013 to 2015) has been operating as a part of the silicon pixel detector since 2015. The calorimeter system covers the pseudorapidity range $|\eta| < 4.9$. Within the region $|\eta| < 3.2$, electromagnetic calorimetry is provided by barrel and endcap high-granularity lead/liquid-argon (LAr) electromagnetic calorimeters, with an additional thin LAr presampler covering $|\eta| < 1.8$ to correct for energy loss in material upstream of the calorimeters. Hadronic calorimetry is provided by a steel/scintillator tile calorimeter, segmented into three barrel structures within $|\eta| < 1.7$, and two copper/LAr hadronic endcap calorimeters. The solid angle coverage is completed with forward copper/LAr and tungsten/LAr calorimeter (FCal) modules optimised for electromagnetic and hadronic measurements respectively. The MS comprises separate trigger and high-precision tracking chambers measuring the deflection of muons in a magnetic field generated by superconducting air-core toroids. Monitored drift tubes and cathode strip chambers are designed to

¹ ATLAS uses a right-handed coordinate system with its origin at the nominal interaction point (IP) in the centre of the detector and the z -axis along the beam pipe. The x -axis points from the IP to the centre of the LHC ring, and the y -axis points upward. Cylindrical coordinates (r, ϕ) are used in the transverse plane, ϕ being the azimuthal angle around the beam pipe. The pseudorapidity is defined in terms of the polar angle θ as $\eta = -\ln \tan(\theta/2)$ and the transverse momentum p_T is defined as $p_T = p \sin \theta$. Angular distance is measured in units of $\Delta R \equiv \sqrt{(\Delta\eta)^2 + (\Delta\phi)^2}$.

provide precise position measurements in the bending plane in the range $|\eta| < 2.7$. Resistive plate chambers (RPCs) and thin gap chambers (TGCs) with a coarse position resolution but a fast response time are used primarily to trigger on muons in the ranges $|\eta| < 1.05$ and $1.05 < |\eta| < 2.4$ respectively.

The ATLAS trigger system [33, 34] is separated into two levels: the hardware-based level-1 (L1) trigger and the software-based high level trigger (HLT), which reduce the proton–proton/lead collision rate to several-hundred Hz of events of interest for data recording to mass storage. The L1 muon trigger requires coincidences between hits on different RPC or TGC planes, which are used as a seed for the HLT algorithms. The HLT uses dedicated algorithms to incorporate information from both the MS and the ID, achieving position and momentum resolution close to that provided by the offline muon reconstruction, as shown in Ref. [33]. During the first LHC long shutdown additional RPCs were installed to cover the acceptance holes at the bottom of the MS and additional TGC coincidence logic was implemented for the region $1.3 < |\eta| < 1.9$ to reduce backgrounds. More details about the improvement in the trigger system during the long shutdown can be found in Ref. [34].

3 Datasets and Monte Carlo samples

This analysis includes data from $p+\text{Pb}$ collisions recorded at the LHC in 2013 and pp collisions recorded in 2015, both at a centre-of-mass energy of 5.02 TeV per nucleon pair. These data samples correspond to a total integrated luminosity of 28 nb^{-1} and 25 pb^{-1} for $p+\text{Pb}$ and pp collisions respectively.

The $p+\text{Pb}$ collisions result from the interactions of a proton beam with an energy of 4 TeV and a lead beam with an energy of 1.58 TeV per nucleon. The usual rapidity, y , in the laboratory frame is defined as $y = 0.5 \ln[(E + p_z)/(E - p_z)]$, where E and p_z refer to energy and longitudinal momentum respectively. In the $p+\text{Pb}$ collision configuration, the proton–nucleon centre-of-mass rapidity, y^* , had a shift of $\Delta y = 0.465$ with respect to y in the laboratory frame. After 60% of the data were recorded the directions of the proton and lead beams were reversed. In this paper, all data from both periods are presented in y^* , using an additional convention that the proton beam always travels in the direction of positive y^* .

Monte Carlo (MC) simulations [35] of $p+\text{Pb}$ and pp collision events are used to study muon trigger and reconstruction efficiencies, and quarkonium signal yields extraction. Events were generated using PYTHIA 8 [36] with the CTEQ61L [37] parton distribution functions. In each event, one of the five quarkonium states, J/ψ , $\psi(2S)$, and $\Upsilon(nS)$ ($n = 1, 2, 3$), was produced unpolarised, as motivated by previous measurements at the LHC energy [38–40], and forced to decay via the dimuon channel. The response of the ATLAS detector was simulated using GEANT 4 [41]. The simulated events were reconstructed with the same algorithms used for data.

4 Event selection

Candidate events in $p+\text{Pb}$ collisions were collected with a dimuon trigger which requires one muon to pass the identification requirement at L1. In addition, the L1 muon candidate must be confirmed in the HLT as a muon with $p_T > 2 \text{ GeV}$, and at least one more muon candidate with $p_T > 2 \text{ GeV}$ must be found in a search over the full MS system. In pp collisions the candidate events were collected with a different dimuon trigger which requires at least two L1 muon candidates with $p_T > 4 \text{ GeV}$. Subsequently

in the HLT, the two L1 candidates must be confirmed as muons from a common vertex with opposite-sign charges.

In the offline analysis, events are required to have at least one reconstructed primary vertex with at least four tracks and at least two muons originating from a common vertex, each with $p_T > 4$ GeV and matching an HLT muon candidate associated with the event trigger. The selected muons are required to be *Combined* [42] and *Tight* [43] in $p+\text{Pb}$ and pp collisions respectively, where *Combined* implies that a muon results from a track in the ID which can be combined with one in the MS, and *Tight* requires a strict compatibility between the two segments. To ensure high-quality triggering and accurate track measurement, each muon track is further restricted to $|\eta| < 2.4$. Pairs of muon candidates satisfying these quality requirements, and with opposite charges, are selected as quarkonia candidate pairs. All candidate pairs that satisfy the criteria discussed above, including those events with additional interactions in the same bunch crossing (known as "pile-up" events), are used for the cross-section measurements.

In order to characterise the $p+\text{Pb}$ collision geometry, each event is assigned to a centrality class based on the total transverse energy measured in the FCal on the Pb-going side (backwards). Collisions with more (fewer) participating nucleons are referred to as central (peripheral). Following Ref. [30], the centrality classes used for this analysis, in order from most central to most peripheral, are 0–5%, 5–10%, 10–20%, 20–30%, 30–40%, 40–60%, and 60–90%.

5 Analysis

5.1 Cross-section determination

The double-differential cross section multiplied by the dimuon decay branching fraction is calculated for each measurement interval as:

$$\frac{d^2\sigma_{O(nS)}}{dp_T dy^*} \times B(O(nS) \rightarrow \mu^+ \mu^-) = \frac{N_{O(nS)}}{\Delta p_T \times \Delta y \times L}, \quad (1)$$

where L is the integrated luminosity, Δp_T and Δy are the interval sizes in terms of dimuon transverse momentum and centre-of-mass rapidity respectively, and $N_{O(nS)}$ is the observed quarkonium yield in the kinematic interval under study, extracted from fits and corrected for acceptance, trigger and reconstruction efficiencies. The total correction weight assigned to each selected dimuon candidate is given by:

$$w_{\text{total}}^{-1} = \mathcal{A}(O(nS)) \cdot \varepsilon_{\text{reco}} \cdot \varepsilon_{\text{trig}}, \quad (2)$$

where $\mathcal{A}(O(nS))$ is the acceptance of the dimuon system for one of the five quarkonium states, $\varepsilon_{\text{reco}}$ is the dimuon reconstruction efficiency and $\varepsilon_{\text{trig}}$ is the trigger efficiency.

5.2 Acceptance

The acceptance of quarkonium decays into muon pairs is defined as the probability of both muons from the decay falling in the fiducial region ($p_T(\mu^\pm) > 4$ GeV, $|\eta(\mu^\pm)| < 2.4$). The acceptance depends on transverse momentum, rapidity, invariant mass and the spin-alignment of the quarkonium state. The invariant mass of each state is taken to be the generator-level mass. Previous measurements in pp collisions [38–40]

indicate that decays of quarkonia produced at LHC energies are consistent with the assumption that they are unpolarised. Based on this assumption, and with a further assumption that the nuclear medium does not modify the average polarisation of produced quarkonia, all quarkonium states in both the $p+\text{Pb}$ and pp collisions are considered to be produced unpolarised in this paper. The acceptance, $\mathcal{A}(O(nS))$, for each of J/ψ , $\psi(2\text{S})$, and $\Upsilon(n\text{S})$ ($n = 1, 2, 3$) as a function of quarkonium transverse momentum and $|y|$ is calculated using generator-level MC, applying cuts on the p_{T} and η of the muons to emulate the fiducial volume as described in Refs. [44, 45]. The reconstructed dimuon transverse momentum, $p_{\text{T}}^{\mu\mu}$, is used for obtaining the acceptance correction for a given event. However, the reconstructed dimuon transverse momentum and the quarkonium transverse momentum could be different due to final-state radiation from muons. Corrections for final-state radiation are obtained by comparing acceptances calculated from generator-level muons with those after full detector simulation. The final-state radiation corrections as a function of $p_{\text{T}}^{\mu\mu}$ are applied to the acceptance corrections. The correction factors are different for charmonium and bottomonium states but are the same for ground and excited states. Finally, the same correction factors are used in pp and $p+\text{Pb}$ data.

5.3 Muon reconstruction and trigger efficiency

The single muon reconstruction efficiency in $p+\text{Pb}$ data is determined directly from data using $J/\psi \rightarrow \mu^+\mu^-$ tag-and-probe method as used in Ref. [22, 42], in which the tag muon is required to match with the trigger used to select the sample such that the probe muon is unbiased from the sample selection trigger, and the purity of the probe is guaranteed by background subtraction based on $J/\psi \rightarrow \mu^+\mu^-$ decay. The dimuon trigger efficiency in $p+\text{Pb}$ data is factorised into single-muon trigger efficiencies for reconstructed muons at the L1 and HLT, with the correlation between the L1 and HLT trigger algorithms taken into account. The single-muon trigger efficiencies are obtained from data, based on $J/\psi \rightarrow \mu^+\mu^-$ tag-and-probe method as described in Ref. [22], in intervals of $p_{\text{T}}(\mu)$ and $q \times \eta(\mu)$, where q is the charge of the muon.

For the pp data, the same $J/\psi \rightarrow \mu^+\mu^-$ tag-and-probe technique as for $p+\text{Pb}$ data is used to determine single muon reconstruction and trigger efficiencies. The dimuon trigger efficiency in the pp data consists of two components. The first part represents the trigger efficiency for a single muon in intervals of $p_{\text{T}}(\mu)$ and $q \times \eta(\mu)$. The second part is a dimuon correction term to account for reductions in the trigger efficiency due to close-by muon pairs identified as single muon candidates at L1. The dimuon correction term, which is determined separately for charmonium and bottomonium candidates, also accounts for inefficiency due to the vertex-quality requirement and opposite-sign charge requirement on the two online candidates. The efficiency and the dimuon correction term obtained from the MC simulation are used to correct data in order to suppress the statistical fluctuations of measured corrections. The measured average single-muon trigger efficiency is about 80% (95%) in the range $|\eta(\mu)| < 1.05$ ($1.05 < |\eta(\mu)| < 2.4$). In addition to the main corrections derived from simulation, data-to-simulation scale factors, which are simple linear factors to account for the differences between data and MC simulation, are also applied. The resulting scale factor is found to be about 92% in the range $|\eta(\mu)| < 1.05$ and about 98% in the range $1.05 < |\eta(\mu)| < 2.4$ without apparent p_{T} dependence in both η regions.

5.4 Yield extraction

Charmonium

Table 1: Probability density functions for individual components in the central fit model used to extract the prompt and non-prompt contributions for charmonium signals and backgrounds. The composite PDF terms are defined as follows: *CB* - Crystal Ball; *G* - Gaussian; *E* - Exponential; *F* - constant distribution; δ - delta function. The parameter ω_i is the fraction of CB component in signal.

i	Type	Source	$f_i(m_{\mu\mu})$	$h_i(\tau_{\mu\mu})$
1	J/ψ	Prompt	$\omega_1 CB_1(m_{\mu\mu}) + (1 - \omega_1) G_1(m_{\mu\mu})$	$\delta(\tau_{\mu\mu})$
2	J/ψ	Non-prompt	$\omega_1 CB_1(m_{\mu\mu}) + (1 - \omega_1) G_1(m_{\mu\mu})$	$E_1(\tau_{\mu\mu})$
3	$\psi(2S)$	Prompt	$\omega_2 CB_2(m_{\mu\mu}) + (1 - \omega_2) G_2(m_{\mu\mu})$	$\delta(\tau_{\mu\mu})$
4	$\psi(2S)$	Non-prompt	$\omega_2 CB_2(m_{\mu\mu}) + (1 - \omega_2) G_2(m_{\mu\mu})$	$E_2(\tau_{\mu\mu})$
5	Background	Prompt	F	$\delta(\tau_{\mu\mu})$
6	Background	Non-prompt	$E_3(m_{\mu\mu})$	$E_4(\tau_{\mu\mu})$
7	Background	Non-prompt	$E_5(m_{\mu\mu})$	$E_6(\tau_{\mu\mu})$

The charmonium yield determination decomposes the yields into two sources of muon pairs referred to as "prompt" and "non-prompt". The prompt J/ψ and $\psi(2S)$ signal originates from the strong production of short-lived particles, including feed-down from other short-lived charmonium states, while non-prompt refers to J/ψ and $\psi(2S)$ mesons which are the decay products of b -hadrons. To distinguish between these prompt and non-prompt processes, the pseudo-proper lifetime, $\tau_{\mu\mu} = (L_{xy}m_{\mu\mu})/p_T^{\mu\mu}$, is used. The transverse displacement, L_{xy} , is the distance of the dimuon secondary vertex from the primary vertex along the dimuon momentum direction in the transverse plane. Two-dimensional unbinned maximum-likelihood fits, as used in a previous ATLAS measurement [46], are performed on weighted distributions of the dimuon invariant mass ($m_{\mu\mu}$) and pseudo-proper lifetime ($\tau_{\mu\mu}$) to extract prompt and non-prompt signal yields, in intervals of $p_T^{\mu\mu}$, rapidity and centrality. The event weight is given by Eq. (2). To obtain the acceptance corrections, J/ψ acceptance is applied to events with $m_{\mu\mu} < 3.2$ GeV, $\psi(2S)$ acceptance is applied to events with $m_{\mu\mu} > 3.5$ GeV and a linear interpolation of the two acceptances is used for events with $3.2 < m_{\mu\mu} < 3.5$ GeV. Each interval of $p_T^{\mu\mu}$, rapidity and centrality is fitted independently in the RooFit framework [47]. The two-dimensional probability density function (PDF) in $m_{\mu\mu}$ and $\tau_{\mu\mu}$ for the fit model is defined as:

$$\text{PDF}(m_{\mu\mu}, \tau_{\mu\mu}) = \sum_{i=1}^7 \kappa_i f_i(m_{\mu\mu}) \cdot h_i(\tau_{\mu\mu}) \otimes g(\tau_{\mu\mu}),$$

where \otimes implies a convolution, κ_i is the normalisation factor of each component and $g(\tau_{\mu\mu})$ is a double Gaussian $\tau_{\mu\mu}$ resolution function. The two Gaussian components share a fixed mean at $\tau_{\mu\mu} = 0$. One of the two widths in the resolution function is free, while the other width is fixed at the first one multiplied by a constant factor, determined from MC simulation. The relative fraction of the two Gaussian components is a free parameter. The details of the seven components in the nominal fit model are summarised in Table 1 and described below.

The signal charmonium line shape in $m_{\mu\mu}$ is described by the sum of a Crystal Ball shape (CB) [48] and a single Gaussian function with a common mean. The width parameter in the CB function is free, while the Gaussian width is fixed with respect to the CB width by a constant factor motivated by the ratio of muon transverse momentum resolutions in different parts of the detector. The rest of the parameters in the CB function are fixed to values obtained from MC simulation. The mean and width of the $\psi(2S)$ are fixed to those of the J/ψ multiplied by a factor equal to the ratio of the measured masses of the $\psi(2S)$

and the J/ψ [49]. The relative fraction of the CB and Gaussian components is considered to be a free parameter, but one that is common to both the J/ψ and $\psi(2S)$. The prompt charmonium line shapes in $\tau_{\mu\mu}$ are described by a δ function convolved with the resolution function $g(\tau_{\mu\mu})$, whereas the non-prompt charmonium signals have pseudo-proper lifetime line shapes given by an exponential function convolved with $g(\tau_{\mu\mu})$.

The background contribution contains one prompt component and two non-prompt components. The prompt background is given by a δ function convolved with $g(\tau_{\mu\mu})$ in $\tau_{\mu\mu}$ and a constant distribution in $m_{\mu\mu}$. One of the non-prompt background contributions is described by a single-sided exponential function convolved with $g(\tau_{\mu\mu})$ (for positive $\tau_{\mu\mu}$ only), and the other non-prompt background contribution is described by a double-sided exponential function convolved with $g(\tau_{\mu\mu})$ accounting for misreconstructed or combinatoric dimuon pairs. The two non-prompt backgrounds are parameterised as two independent exponential functions in $m_{\mu\mu}$.

There are in total seventeen free parameters in the charmonium fit model. The normalisation factor κ_i of each component is extracted from each fit. From these parameters, and the weighted sum of events, all measured values are calculated. Figure 1 shows examples of charmonium fit projections onto invariant mass and pseudo-proper lifetime axes. The fit projections are shown for the total prompt signal, total non-prompt signal and total background contributions.

Bottomonium

The yields of bottomonium states are obtained by performing unbinned maximum likelihood fits of the weighted invariant mass distribution, in intervals of $p_T^{\mu\mu}$, rapidity and centrality. Due to overlaps between the invariant mass peaks of different bottomonium states, the linear acceptance interpolation used for the charmonium states is not appropriate to the bottomonium states. Instead, each interval is fitted three times to extract the corrected yields of the three different bottomonium states, each time with the acceptance weight of one of the three states assigned to all candidates. Each of the fits in each interval of $p_T^{\mu\mu}$, rapidity and centrality is independent of all the others.

The bottomonium signal invariant mass model is essentially the same as the charmonium model. The mean and width of the $\Upsilon(1S)$ is free, while the means and widths of $\Upsilon(2S)$ and $\Upsilon(3S)$ are fixed with respect to parameters of $\Upsilon(1S)$ with a constant scaling factor equal to the $\Upsilon(nS)$ to $\Upsilon(1S)$ mass ratio taken from Ref. [49]. The bottomonium background parameterisation varies with $p_T^{\mu\mu}$. At low $p_T^{\mu\mu}$ ($p_T^{\mu\mu} < 6$ GeV), and for all rapidity intervals, an error function multiplied by an exponential function is used to model the $m_{\mu\mu}$ turn-on effects due to decreasing acceptance with decreasing invariant mass, which originates from the p_T selection applied to each muon. At low $p_T^{\mu\mu}$, the background model's parameters are constrained by using a background control sample. The control sample is selected from dimuon events in which at least one of the muons has a transverse impact parameter with respect to the primary vertex larger than 0.2 mm. This criterion causes the control sample to be dominated by muon pairs from the decay of b -hadrons. For candidates with higher $p_T^{\mu\mu}$, a second-order polynomial is used to describe the background contribution. At low $p_T^{\mu\mu}$, the background model is first fitted to the control sample, then the parameters of the error function are fixed at their fitted values, and finally the full fit model with the constrained background is applied to the data sample. Some selected bottomonium fits are shown in Figure 2.

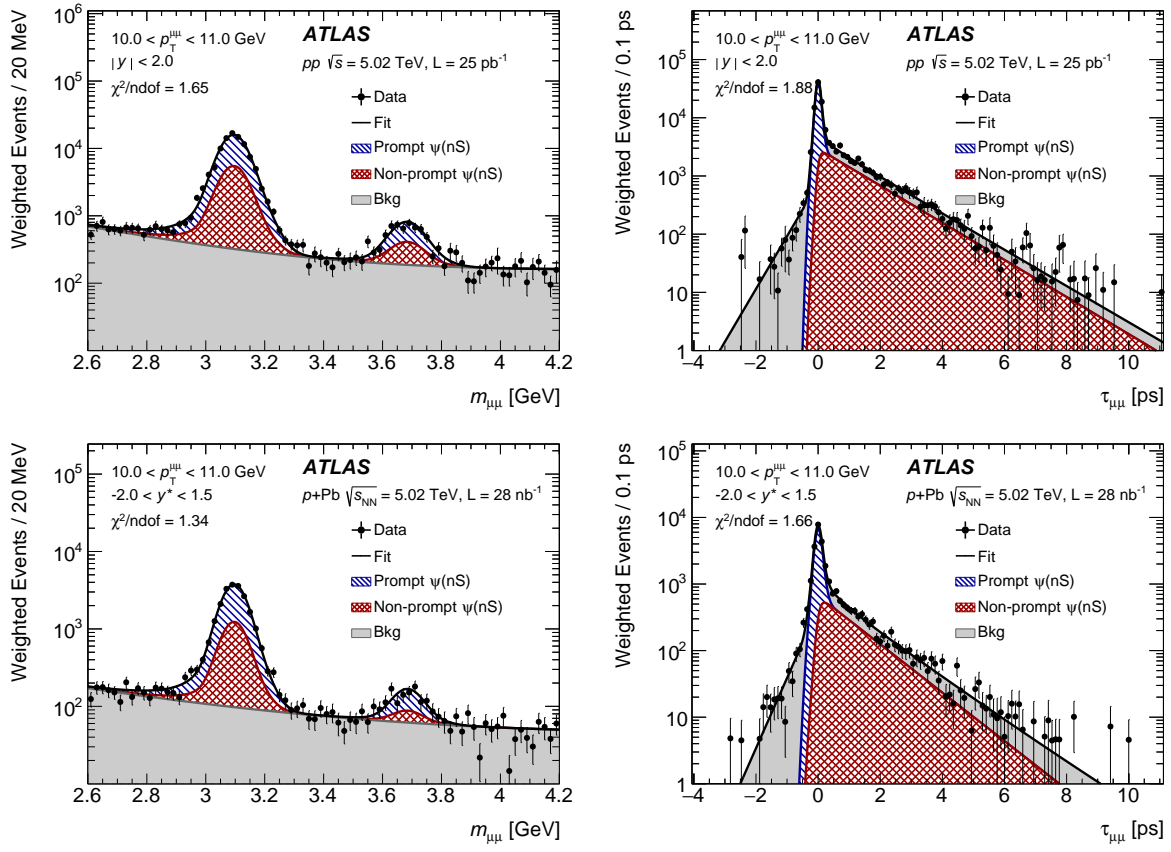


Figure 1: Projections of the charmonium fit results onto dimuon invariant mass $m_{\mu\mu}$ (left) and pseudo-proper lifetime $\tau_{\mu\mu}$ (right) for pp collisions at $\sqrt{s} = 5.02$ TeV (top) for the kinematic ranges $10 < p_T^{\mu\mu} < 11$ GeV and $|y| < 2.0$, and $p+\text{Pb}$ collisions at $\sqrt{s_{\text{NN}}} = 5.02$ TeV (bottom) for the kinematic ranges $10 < p_T^{\mu\mu} < 11$ GeV and $-2.0 < y^* < 1.5$. The goodneses of the invariant mass fits with $\text{ndof} = 63$ and the pseudo-proper lifetime fits with $\text{ndof} = 153$ are also presented.

6 Systematic uncertainties

The sources of systematic uncertainty in the quarkonium yields include acceptance, muon reconstruction and trigger efficiency corrections, the fit model parameterisation and bin migration corrections and the luminosity. For the ratio measurements the systematic uncertainties are assessed in the same manner as for the yields, except that in the ratios the correlated systematic uncertainties, such as the luminosity uncertainty, cancel out.

Luminosity

The uncertainty in integrated luminosity is 2.7% (5.4%) for 2013 $p+\text{Pb}$ (2015 pp) data-taking. The luminosity calibration is based on data from dedicated beam-separation scans, also known as van der Meer scans, as described in Ref. [50].

Acceptance

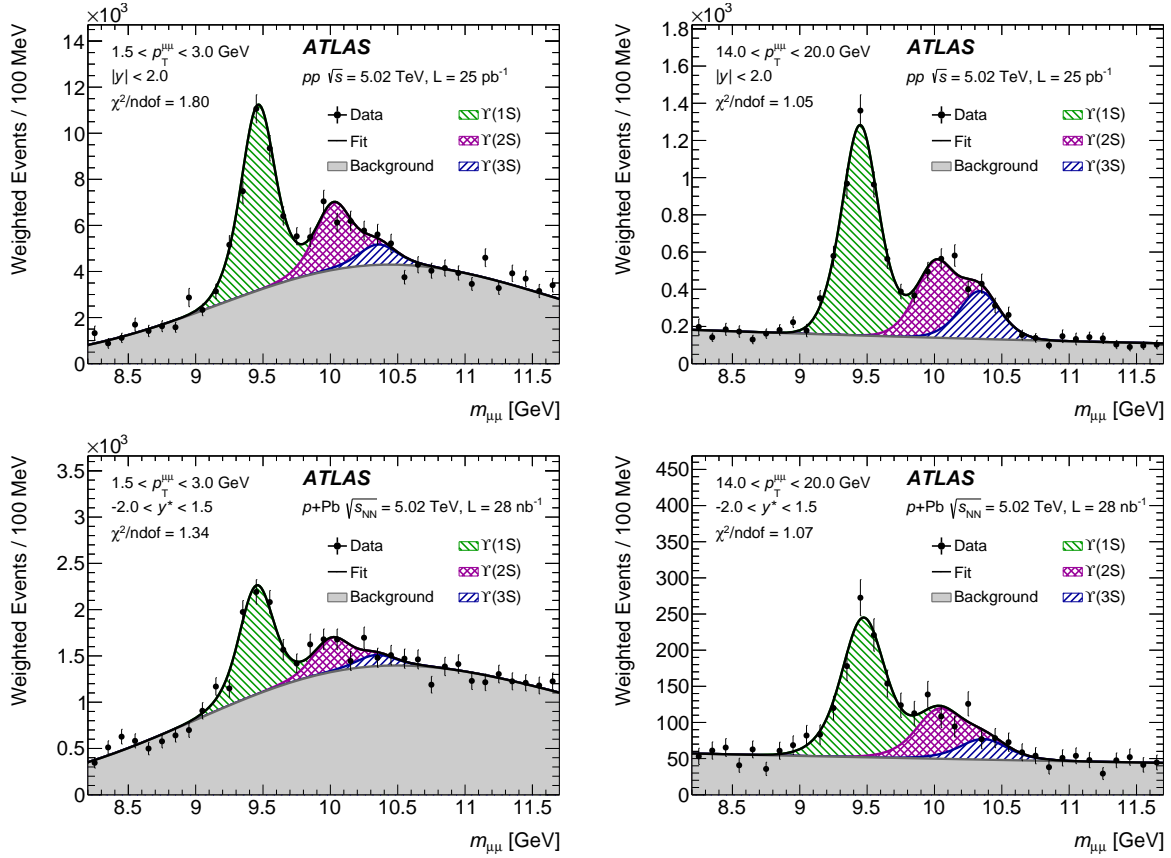


Figure 2: Bottomonium fit results in dimuon invariant mass $m_{\mu\mu}$ for pp collisions at $\sqrt{s} = 5.02$ TeV (top) and $p+Pb$ collisions at $\sqrt{s_{NN}} = 5.02$ TeV (bottom) for one typical low $p_T^{\mu\mu}$ interval of $1.5 < p_T^{\mu\mu} < 3$ GeV (left) and one high $p_T^{\mu\mu}$ interval of $14.0 < p_T^{\mu\mu} < 20$ GeV (right). For all the shown fits, $\Upsilon(1S)$ acceptance weights are assigned. The goodness of the bottomonium fit with $ndof = 24$ is also presented.

A systematic uncertainty for the final-state radiation corrections is assigned to cover the differences between correction factors obtained for ground and excited states of quarkonium and for different rapidity slices. The systematic uncertainties fully cancel out in ratio measurements in the same datasets and between different datasets.

Muon reconstruction and trigger efficiencies in $p+Pb$ collisions

The dominant source of uncertainty in the muon reconstruction and trigger efficiency in $p+Pb$ collisions is statistical. Therefore, the uncertainty in each bin is treated as uncorrelated and the corresponding uncertainties are propagated to the measured observables by using pseudo-experiments as in previous ATLAS measurements [46]. For each pseudo-experiment a new efficiency map is created by varying independently the content of each bin according to a Gaussian distribution. The mean and width parameters of the Gaussian distribution are respectively the value and uncertainty of the bin in the original map. In each pseudo-experiment, the total weight is recalculated for each dimuon kinematic interval of the analysis. A distribution of total weight is obtained from repeating pseudo-experiments for 200 times, which is sufficient to suppress the statistical fluctuation of the sample used in each experiment. For each efficiency type, the RMS of the total weight distributions is assigned as the systematic uncertainty.

An additional uncertainty of 1% is applied to cover the small muon reconstruction inefficiency in the inner detector in p +Pb collisions. The dimuon trigger efficiency factorisation is tested in simulation, and a bias of at most 4% is found in yield observables. The bias stems from the imperfect approximation of the correlation between trigger algorithms at different levels in the dimuon trigger factorisation. An additional correlated uncertainty of 4% is added to cover this bias. This uncertainty is applied to quarkonium yields in p +Pb collisions, but is assumed to cancel in ratios measured in the same datasets.

Muon reconstruction and trigger efficiencies in pp collisions

For the pp measurements, the efficiency maps are determined from MC simulation and corrected with measured data-to-simulation scale factors as detailed in Ref. [43]. The statistical uncertainty associated with efficiency scale factor is evaluated using random replicas of the efficiency maps as for p +Pb and the different sources of uncertainty described below are treated as correlated. The systematic uncertainty in reconstruction efficiency is obtained by varying the signal and background models in the fits used to extract the efficiency in data, and taking the difference between the reconstruction efficiency calculated using generator-level information and the value obtained with the tag-and-probe method in MC simulation. An additional 1% correlated uncertainty is added to cover a systematic variation due to a small misalignment in the ID. For the trigger efficiency, the following variations of the analysis are studied and the effects are combined in quadrature:

- variations of signal and background fit model used to extract the data efficiency;
- variations of the matching criteria between a muon and a trigger element;
- using dimuon correction terms determined at positive (or negative) rapidity for whole rapidity range.

A test of the approximation of muon–muon correlation at L1 in the pp dimuon trigger factorisation in MC simulation results in a bias of at most 4%, which is the same size as the factorisation bias of the p +Pb trigger but with totally different origins. An additional 4% correlated uncertainty is added to quarkonium yields to cover the bias. This uncertainty cancels out in ratio observables that are measured in the same datasets.

Bin migrations

Corrections due to bin migration factors were evaluated in Refs. [45, 46] and are determined to be less than 0.5% of the measured values. For this reason, bin migration correction factors and their uncertainties are neglected in this analysis.

Charmonium fit

The uncertainty from the signal and background line shapes is estimated from variations of the fit model. To remove the statistical component, each variation is repeated with pseudo-experiments, generated using the bootstrap method [51]. First, for each toy sample, every event from the original data is filled into the toy sample n times, where n is a random integer obtained from a Poisson distribution with a mean of one. Then the central model and a set of ‘variation’ models are fitted to the toy sample, and all measured quantities are recalculated. The difference between the central model and a given variation model is extracted and recorded. After repeating the pseudo-experiment 100 times, the systematic uncertainty due to the line shape is defined as the mean difference of a given variation model from the nominal model. Up to ten variation models are considered for the charmonium fit model, categorised into four groups:

- *Signal tail due to final-state radiation.* Evaluated by replacing the CB plus Gaussian model with a double Gaussian function, and varying the tail parameters of the CB model, which are originally fixed.
- *Pseudo-proper lifetime resolution.* Evaluated by replacing the double Gaussian function with a single Gaussian function to model pseudo-proper lifetime resolution.
- *Signal pseudo-proper lifetime shape.* Evaluated by using a double exponential function to describe the pseudo-proper lifetime distribution of the signal.
- *Background mass shapes.* Evaluated by using a second-order Chebyshev polynomial to describe the prompt, non-prompt and double-sided background terms.

The total systematic uncertainty from the line shape fit is determined by combining the maximum variation found in each of the four groups in quadrature. In order to estimate the possible bias introduced by the line shape assumptions in the nominal fit model parameterisation, the nominal model is tested using the $J/\psi \rightarrow \mu^+ \mu^-$ MC sample in which random numbers of prompt and non-prompt J/ψ are mixed. About 1% difference between the random input and fit model output is found for the yield and non-prompt fraction in the MC test. An additional systematic uncertainty of 1% is assigned to charmonium yields and non-prompt fractions to cover the nominal fit model parameterisation bias. This uncertainty cancels out in the $\psi(2S)$ to J/ψ yield ratio.

Bottomonium fit

The systematic uncertainty from varying the fit model is estimated based on the same method as used for the charmonium fit uncertainty, and there are six variation models for bottomonium categorised into three groups:

- *Signal resolution.* Evaluated by replacing the CB plus Gaussian model with a single CB function and a triple Gaussian function, and varying the constant width scaling term between the CB function and the Gaussian function.
- *Signal tail due to final-state radiation.* Evaluated by replacing the CB plus Gaussian model with a double Gaussian function, and treating the tail parameters in the CB function as free parameters.
- *Background shapes.* Evaluated by replacing the low p_T background distribution with a fourth-order Chebyshev polynomial, and replacing the high p_T distribution by an exponential function or a second-order Chebyshev polynomial.

The total systematic uncertainty from the line shape fit is given by combining the maximum variation found in each of the three groups in quadrature. An additional systematic uncertainty of 1.5% is assigned to $\Upsilon(1S)$ yields and 2% for $\Upsilon(nS)$ yields and $\Upsilon(nS)$ to $\Upsilon(1S)$ ratios ($n = 2, 3$), in order to cover the bias of the nominal model found in MC tests similar to those for the charmonium fit model.

Table 2 summarises the systematic uncertainties in the ground-state and excited-state yields and their ratio. The dominant sources of systematic uncertainty for the yields are the fit model and muon trigger efficiency. The ranges of uncertainties shown in the table indicate the minimum and maximum values found in all $p_T^{\mu\mu}$, rapidity and centrality intervals. The large range of bottomonium fit systematic uncertainty is due to the different modelling of the background at low $p_T^{\mu\mu}$ ($p_T^{\mu\mu} < 6$ GeV) and high $p_T^{\mu\mu}$. The systematic uncertainty from fit model variations is much larger at low $p_T^{\mu\mu}$ than at high $p_T^{\mu\mu}$. For the ratios

Table 2: Summary of systematic uncertainties in the charmonium and bottomonium ground-state and excited-state yields and their ratio. The ranges of uncertainties indicate the minimum and maximum values found in all kinematic slices. Symbol “–” in the ratio observable column indicates the uncertainty fully cancels out.

Collision type	Sources	Ground-state yield [%]	Excited-state yield [%]	Ratio [%]
<i>p</i> +Pb collisions	Luminosity	2.7	2.7	–
	Acceptance	1–4	1–4	–
	Muon reco.	1–2	1–2	< 1
	Muon trigger	4–5	4–5	< 1
	Charmonium fit	2–5	4–10	7–15
	Bottomonium fit	2–15	2–15	5–12
<i>pp</i> collisions	Luminosity	5.4	5.4	–
	Acceptance	1–4	1–4	–
	Muon reco.	1–5	1–5	< 1
	Muon trigger	5–7	5–7	< 1
	Charmonium fit	2–7	4–10	7–11
	Bottomonium fit	1–15	2–15	5–12

measured in the same datasets, most sources of systematic uncertainty including the trigger efficiency largely cancel out.

The luminosity systematic uncertainties in *pp* and *p*+Pb collisions are considered to be totally uncorrelated. The acceptance systematic uncertainties in *pp* and *p*+Pb collisions are fully correlated. The reconstruction efficiency systematic uncertainties are treated as uncorrelated due to different muon selection criteria in *pp* and *p*+Pb collisions. The uncertainties in the trigger efficiencies are also treated as uncorrelated since different efficiency determination strategies are used in *pp* and *p*+Pb collisions and the factorisation biases originate from different types of trigger correlations. The fit model variation systematic uncertainties are found to be partially correlated and their effects on $R_{p\text{Pb}}$ and $\rho_{p\text{Pb}}^{O(nS)/O(1S)}$ are determined by studying these ratios obtained from simultaneous fits to *pp* and *p*+Pb collision data for each variation.

7 Results

7.1 Production cross sections

Following the yield correction and signal extraction, the cross sections of five quarkonium states are measured differentially in transverse momentum² and rapidity, as described in Eq. (1).

The results for non-prompt J/ψ and $\psi(2\text{S})$ cross sections in *pp* collisions at $\sqrt{s} = 5.02$ TeV compared to fixed-order next-to-leading-logarithm (FONLL) predictions [52] are shown in intervals of p_{T} for different rapidity slices in Figure 3. The FONLL uncertainties include renormalisation and factorisation scale variations, charm quark mass and parton distribution functions uncertainties as detailed in Ref. [52]. The measured non-prompt charmonium production cross sections agree with the FONLL predictions within uncertainties over the measured p_{T} range.

² The transverse momentum of the quarkonium state is denoted as p_{T} in the rest of the paper.

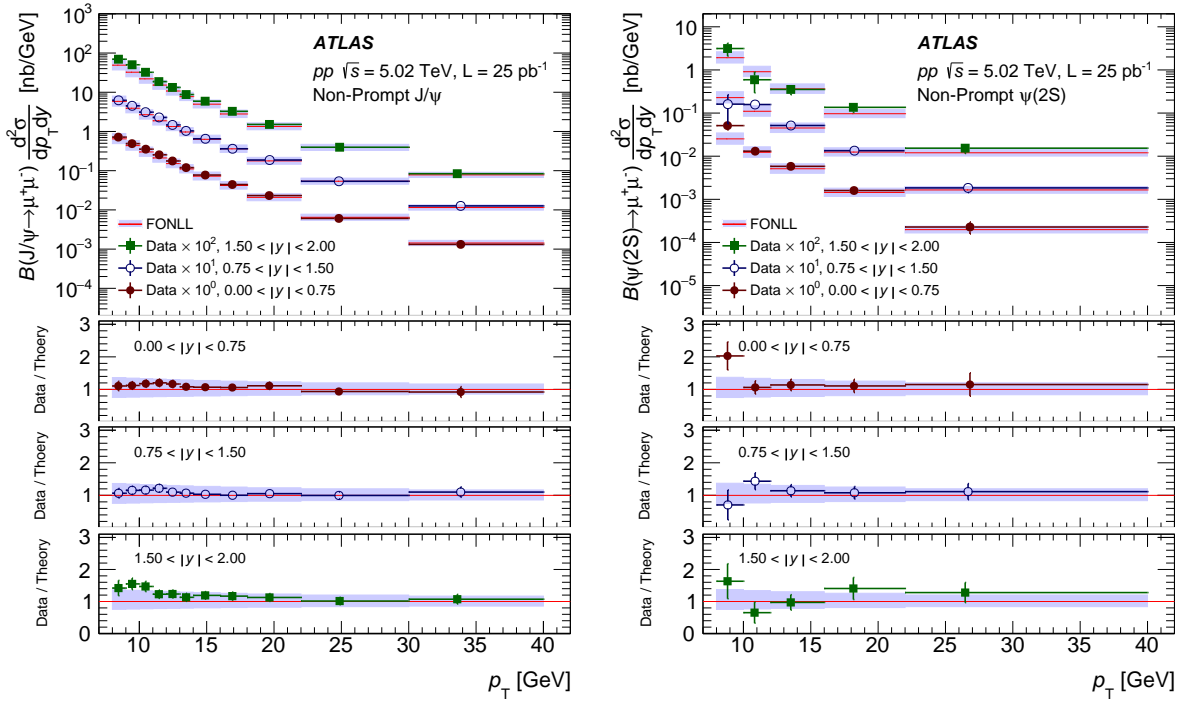


Figure 3: The differential non-prompt production cross section times dimuon branching fraction of J/ψ (left) and $\psi(2S)$ (right) as a function of transverse momentum p_T for three intervals of rapidity y in pp collisions at 5.02 TeV. For each increasing rapidity slice, an additional scaling factor of 10 is applied to the plotted points for visual clarity. The horizontal position of each data point indicates the mean of the weighted p_T distribution. The horizontal bars represent the range of p_T for the bin, and the vertical error bars correspond to the combined statistical and systematic uncertainties. The FONLL theory predictions (see text) are also shown, and the error bands in the prediction correspond to the combined factorisation scale, quark mass and parton distribution functions uncertainties.

The measured prompt J/ψ and $\psi(2S)$ cross sections in pp collisions at $\sqrt{s} = 5.02$ TeV are shown in Figure 4 in p_T and rapidity intervals, compared with non-relativistic QCD (NRQCD) predictions. The theory predictions are based on the long-distance matrix elements (LDMEs) from Refs. [53, 54], with uncertainties originating from the choice of scale, charm quark mass and LDMEs (see Refs. [53, 54] for more details). Figures 5 and 6 show the production cross section of $\Upsilon(nS)$ in pp collisions compared to similar NRQCD model calculations [55]. As stated in Ref. [55], the LDMEs for bottomonium production are only extracted from fitting experiment data at $p_T > 15$ GeV. At lower p_T , there might be non-perturbative effects which break the NRQCD factorization and perturbation expansion. As a consequence of its construction, the bottomonium NRQCD model gives a relatively good description of the measured $\Upsilon(nS)$ production cross section at $p_T > 15$ GeV, while overestimates the production cross section at lower p_T .

The results for prompt and non-prompt production cross sections of J/ψ and $\psi(2S)$ in $p+\text{Pb}$ collisions at $\sqrt{s_{\text{NN}}} = 5.02$ TeV are shown in intervals of p_T in Figure 7. The results for prompt and non-prompt production cross sections of J/ψ and $\psi(2S)$ in $p+\text{Pb}$ collisions in intervals of y^* are shown in Figure 8. Compared to the previous ATLAS measurement [22], improved muon trigger corrections which are smaller by 6% in central value and 4% in uncertainty and a more comprehensive fit model involving a wider mass range are used in the J/ψ cross-section measurements. The measured J/ψ cross sections are consist-

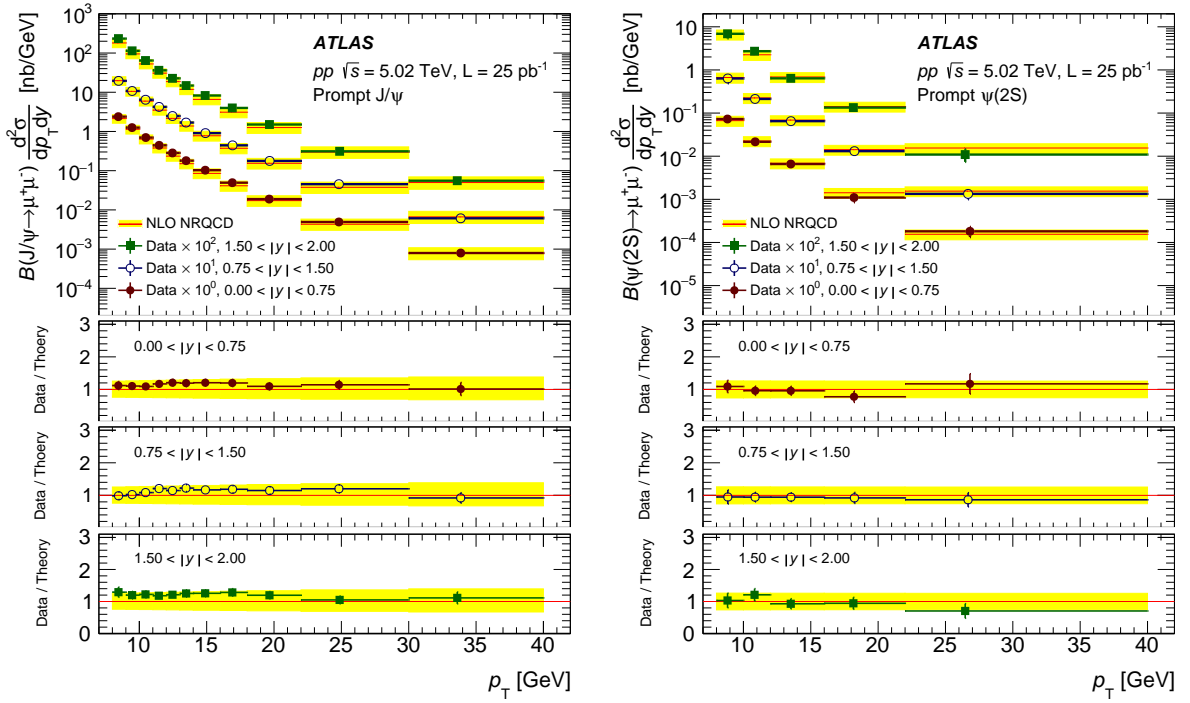


Figure 4: The differential prompt production cross section times dimuon branching fraction of J/ψ (left) and $\psi(2S)$ (right) as a function of transverse momentum p_T for three intervals of rapidity y in pp collisions at 5.02 TeV. For each increasing rapidity slice, an additional scaling factor of 10 is applied to the plotted points for visual clarity. The horizontal position of each data point indicates the mean of the weighted p_T distribution. The horizontal bars represent the range of p_T for the bin, and the vertical error bars correspond to the combined statistical and systematic uncertainties. The NRQCD theory predictions (see text) are also shown, and the error bands in the prediction correspond to the combined scale, quark mass and LDMEs uncertainties.

ent with previous results within uncertainties. The measured differential production cross section of $\Upsilon(nS)$ in $p+\text{Pb}$ collisions is shown in Figure 9. Due to difficulties in separating $\Upsilon(2S)$ and $\Upsilon(3S)$ at forward and backward y^* intervals in $p+\text{Pb}$ collisions, they are combined to obtain stable rapidity dependence of the production cross section.

7.2 Nuclear modification factor

The p_T dependence of $R_{p\text{Pb}}$ for the prompt and non-prompt J/ψ is shown in Figure 10. Taking into account the correlated and uncorrelated uncertainties, both the prompt and non-prompt $J/\psi R_{p\text{Pb}}$ are consistent with unity across the p_T range from 8 to 40 GeV. The rapidity dependence of prompt and non-prompt $J/\psi R_{p\text{Pb}}$ is shown in Figure 11. No significant rapidity dependence is observed. The p_T and rapidity dependence of $\Upsilon(1S) R_{p\text{Pb}}$ is shown in Figure 12. The $\Upsilon(1S)$ production in $p+\text{Pb}$ collisions is found to be suppressed compared to pp collisions at low p_T ($p_T < 15$ GeV), and increases with p_T . Low p_T $\Upsilon(1S)$ can probe smaller Bjorken-x region compared to J/ψ measured in $8 < p_T < 40$ GeV [56], so the observed suppression of $\Upsilon(1S)$ production at low p_T may come from the reduction of hard-scattering cross sections due to stronger nPDF shadowing at smaller Bjorken-x. No significant rapidity dependence is observed, which qualitatively agrees with a prediction of weak rapidity dependence for central rapidities.

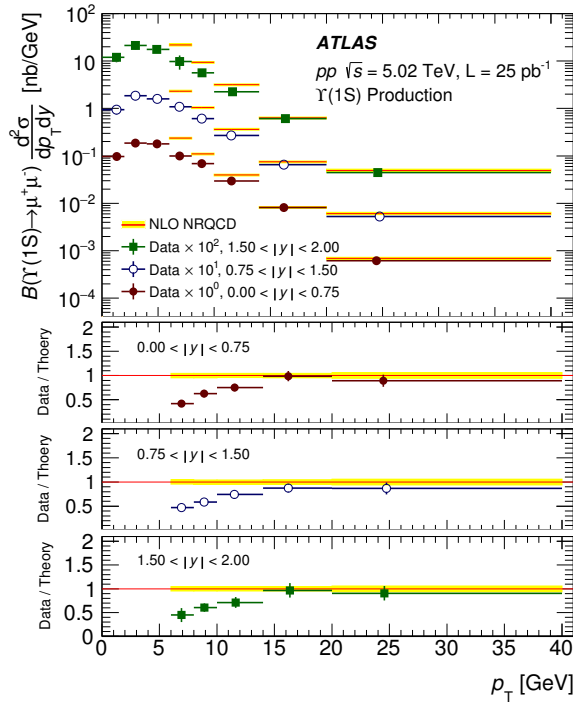


Figure 5: The differential production cross section times dimuon branching fraction of $\Upsilon(1S)$ as a function of transverse momentum p_T for three intervals of rapidity y in pp collisions at 5.02 TeV. For each increasing rapidity slice, an additional scaling factor of 10 is applied to the plotted points for visual clarity. The horizontal position of each data point indicates the mean of the weighted p_T distribution. The horizontal bars represent the range of p_T for the bin, and the vertical error bars correspond to the combined statistical and systematic uncertainties. The NRQCD theory predictions (see text) are also shown, and the error bands in the prediction correspond to the combined scale, quark mass and LDMEs uncertainties.

The Z boson does not interact with the nuclear medium via the strong interaction, so it is considered a good reference process in $p+Pb$ collisions for studying the centrality dependence of quarkonium production in a model-independent way. The quarkonium yield is compared to the Z boson yield from Ref. [57] in intervals of centrality. The ratio of quarkonium to the Z boson yield is defined as:

$$R_{p\text{Pb}}^Z(O(nS)) = \frac{N_{O(nS)}^{\text{cent}}/N_Z^{\text{cent}}}{N_{O(nS)}^{0-90\%}/N_Z^{0-90\%}}$$

where $N_{O(nS)}^{\text{cent}}$ (N_Z^{cent}) is the corrected quarkonium (Z boson) yield for one centrality class. The resulting $R_{p\text{Pb}}^Z(O(nS))$ is shown in Figure 13 for the different quarkonium states in intervals of centrality. In each centrality interval, $R_{p\text{Pb}}^Z(O(nS))$ is normalised to the ratio integrated in the centrality range 0–90% such that the normalised yield ratio is independent of production cross sections of the different quarkonium states. The prompt and non-prompt J/ψ are found to behave in a way very similar to the Z boson. The Z boson production is found to scale with the number of binary collisions in $p+Pb$ collisions after applying the centrality bias correction factor [57, 58]. The centrality bias correction factor proposed in Ref. [58] does not depend on the physics process, so the measured $R_{p\text{Pb}}^Z(J/\psi)$ suggests that centrality-bias-corrected J/ψ production also scales with the number of binary collisions. The measured $R_{p\text{Pb}}^Z(\Upsilon(1S))$ is consistent

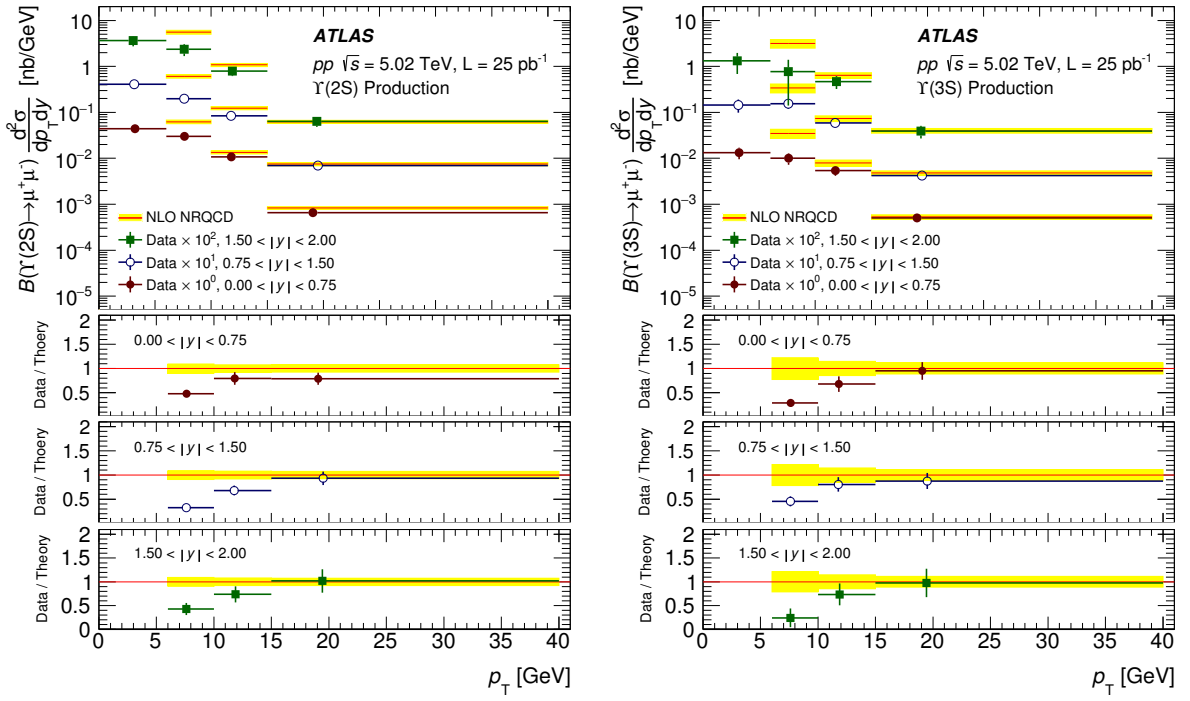


Figure 6: The differential production cross section times dimuon branching fraction of $\Upsilon(2S)$ (left) and $\Upsilon(3S)$ (right) as a function of transverse momentum p_T for three intervals of rapidity y in pp collisions at 5.02 TeV. For each increasing rapidity slice, an additional scaling factor of 10 is applied to the plotted points for visual clarity. The horizontal position of each data point indicates the mean of the weighted p_T distribution. The horizontal bars represent the range of p_T for the bin, and the vertical error bars correspond to the combined statistical and systematic uncertainties. The NRQCD theory predictions (see text) are also shown, and the error bands in the prediction correspond to the combined scale, quark mass and LDMEs uncertainties.

with being a constant except for the measurement in the most peripheral (60–90%) $p+\text{Pb}$ collisions, which is about two to three standard deviations away from the value observed in more central collisions. The current precision of $R_{p\text{Pb}}^Z(\psi(2S))$ does not allow conclusions to be drawn about the centrality dependence of prompt $\psi(2S)$ production with respect to Z bosons.

Quarkonium self-normalised yields, $O(nS)/\langle O(nS) \rangle$, are defined as the per-event yields of quarkonium in each centrality class normalised by the yield in the 0–90% centrality interval. The correlation of quarkonium production with the underlying event is traced by comparing the self-normalised quarkonium yields with the respective self-normalised event activity. The event activity is characterised by the total transverse energy deposition in the backward FCal ($3.1 < |\eta| < 4.9$), $\Sigma E_T^{\text{Backwards}}$, on the Pb-going side, and it is determined in a minimum-bias data sample as used in Ref. [30]. The self-normalised quantities $O(nS)/\langle O(nS) \rangle$ and $\Sigma E_T^{\text{Backwards}}/\langle \Sigma E_T^{\text{Backwards}} \rangle$ are defined as:

$$\frac{O(nS)}{\langle O(nS) \rangle} \equiv \frac{N_{O(nS)}^{\text{cent}}/N_{\text{evt}}^{\text{cent}}}{N_{O(nS)}^{0-90\%}/N_{\text{evt}}^{0-90\%}},$$

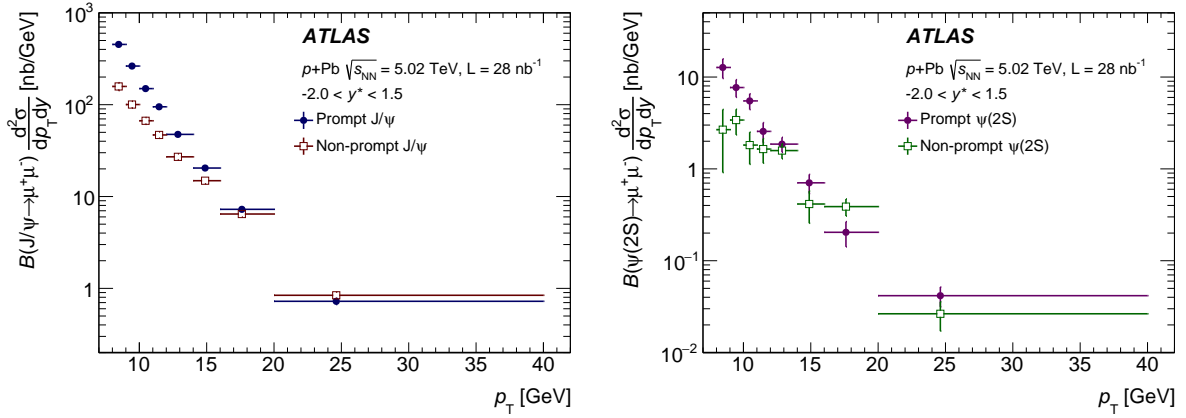


Figure 7: The differential cross section times dimuon branching fraction of prompt and non-prompt J/ψ (left) and $\psi(2S)$ (right) as a function of transverse momentum p_T in $p+Pb$ collisions at $\sqrt{s_{NN}} = 5.02$ TeV. The horizontal position of each data point indicates the mean of the weighted p_T distribution. The horizontal bars represent the range of p_T for the bin, and the vertical error bars correspond to the combined statistical and systematic uncertainties.

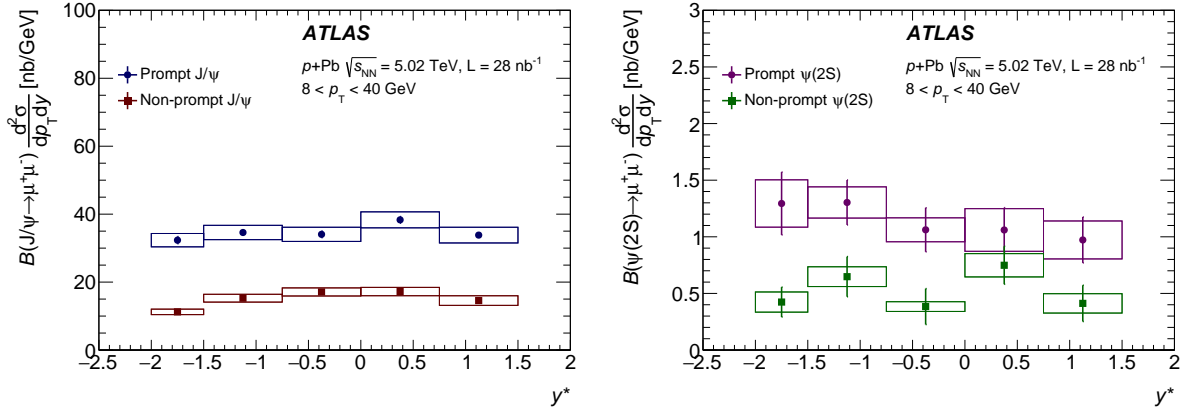


Figure 8: The differential cross section times dimuon branching fraction of prompt and non-prompt J/ψ (left) and $\psi(2S)$ (right) as a function of centre-of-mass rapidity y^* in $p+Pb$ collisions at $\sqrt{s_{NN}} = 5.02$ TeV. The horizontal position of each data point indicates the mean of the weighted y^* distribution. The vertical error bars correspond to statistical uncertainties. The vertical sizes of coloured boxes around the data points represent the systematic uncertainties, and the horizontal sizes of coloured boxes represent the range of y^* for the bin.

$$\frac{\sum E_T^{\text{Backwards}}}{\langle \sum E_T^{\text{Backwards}} \rangle} = \frac{\langle \sum E_T^{\text{Backwards}} \rangle_{\text{cent}}}{\langle \sum E_T^{\text{Backwards}} \rangle_{0-90\%}},$$

where $N_{\text{evt}}^{\text{cent}}$ is the number of events in the minimum-bias sample for one centrality class. The measured self-normalised yields for prompt J/ψ , non-prompt J/ψ and $\Upsilon(1S)$ in $p+Pb$ collisions are shown in Figure 14 in comparison with the same observable for $\Upsilon(1S)$ in a previous CMS measurement [26]. The event activity is determined in the range $4.0 < |\eta| < 5.2$ in CMS. The $\Upsilon(1S)$ self-normalised yields from ATLAS and CMS show a consistent trend. In the events with the highest event activity, a two-standard-deviation departure from the linear trend is observed. Since the same centrality dependence is found for

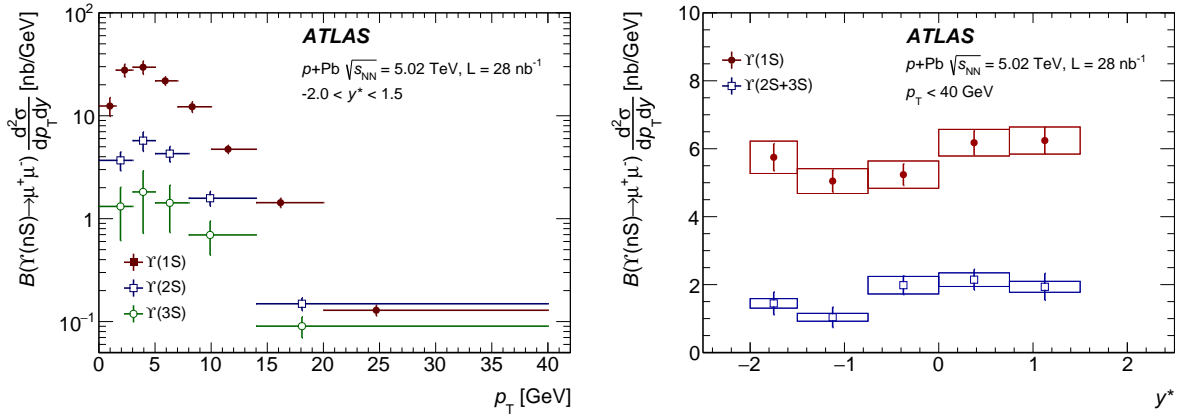


Figure 9: Left: the differential cross section times dimuon branching fraction of $\Upsilon(nS)$ as a function of transverse momentum p_T in $p+Pb$ collisions at $\sqrt{s_{NN}} = 5.02$ TeV. The horizontal position of each data point indicates the mean of the weighted p_T distribution. The horizontal bars represent the range of p_T for the bin, and the vertical error bars correspond to the combined statistical and systematic uncertainties. Right: the differential cross section times dimuon branching fraction of $\Upsilon(nS)$ as a function of centre-of-mass rapidity y^* in $p+Pb$ collisions. The horizontal position of each data point indicates the mean of the weighted y^* distribution. The vertical error bars correspond to statistical uncertainties. The vertical sizes of coloured boxes around the data points represent the systematic uncertainties, and the horizontal sizes of coloured boxes represent the range of y^* for the bin.

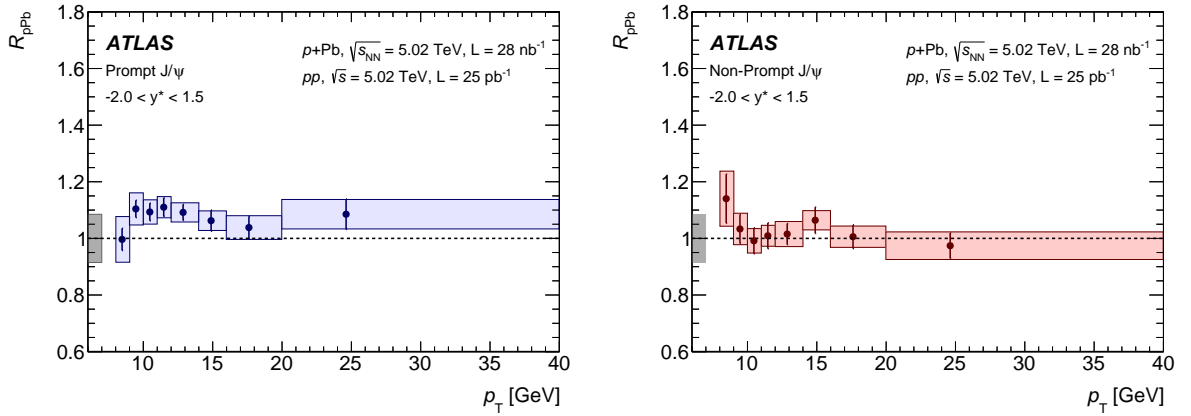


Figure 10: The nuclear modification factor, R_{pPb} , as a function of transverse momentum p_T for prompt J/ψ (left) and non-prompt J/ψ (right). The horizontal position of each data point indicates the mean of the weighted p_T distribution. The vertical error bars correspond to the statistical uncertainties. The vertical sizes of coloured boxes around the data points represent the uncorrelated systematic uncertainties, and the horizontal sizes of coloured boxes represent the p_T bin sizes. The vertical sizes of the leftmost grey boxes around $R_{pPb} = 1$ represent the correlated systematic uncertainty.

ground-state quarkonium states and Z bosons as seen in Figure 13, the deviation at highest event activity may suggest that the $\Sigma E_T^{\text{Backwards}}$ characterised event activity is not a robust scale parameter, but a more complicated geometry model is needed for instance as discussed in Ref. [57].

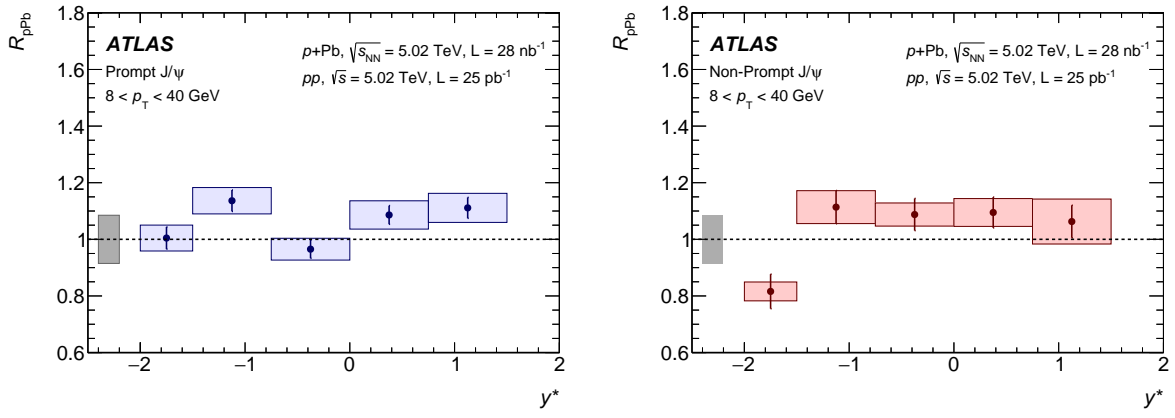


Figure 11: The nuclear modification factor, $R_{p\text{Pb}}$, as a function of centre-of-mass rapidity y^* for prompt J/ψ (left) and non-prompt J/ψ (right). The horizontal position of each data point indicates the mean of the weighted y^* distribution. The vertical error bars correspond to the statistical uncertainties. The vertical sizes of coloured boxes around the data points represent the uncorrelated systematic uncertainties, and the horizontal sizes of coloured boxes represent the y^* bin sizes. The vertical sizes of the leftmost grey boxes around $R_{p\text{Pb}} = 1$ represent the correlated systematic uncertainty.

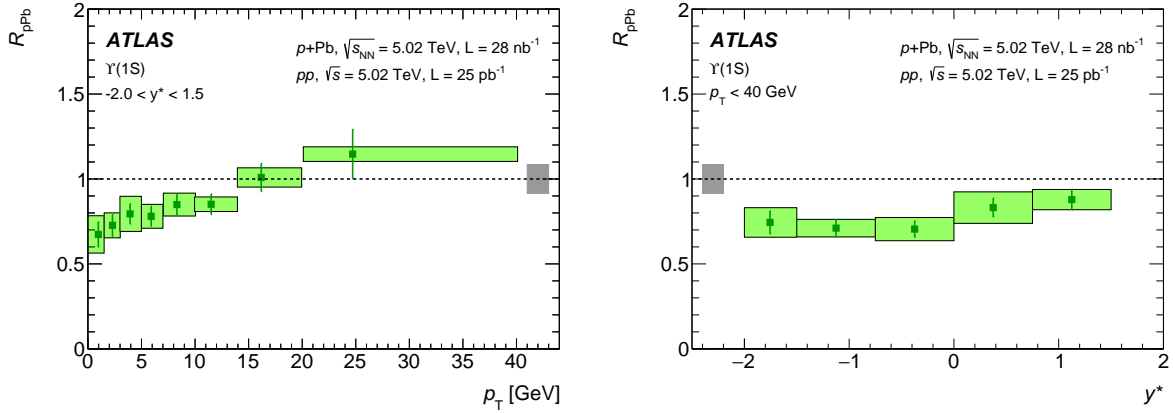


Figure 12: The nuclear modification factor, $R_{p\text{Pb}}$, as a function of transverse momentum p_T (left) and centre-of-mass rapidity y^* (right) for $\Upsilon(1\text{S})$. The horizontal position of each data point indicates the mean of the weighted p_T or y^* distribution. The vertical error bars correspond to the statistical uncertainties. The vertical sizes of coloured boxes around the data points represent the uncorrelated systematic uncertainties, and the horizontal sizes of coloured boxes represent the bin sizes. The vertical size of the rightmost (left) and leftmost (right) grey boxes around $R_{p\text{Pb}} = 1$ represent the correlated systematic uncertainty.

7.3 Double ratio

The prompt $\psi(2\text{S})$ to J/ψ production double ratio, $\rho_{p\text{Pb}}^{\psi(2\text{S})/J/\psi}$, is shown in Figure 15 in intervals of y^* . A decreasing trend with one-standard-deviation significance of the double ratio is observed from backward to forward centre-of-mass rapidity. The p_T and y^* integrated bottomonium double ratios, $\rho_{p\text{Pb}}^{\Upsilon(n\text{S})/\Upsilon(1\text{S})}$ ($n = 2, 3$) are shown in Figure 16. Both the integrated $\rho_{p\text{Pb}}^{\Upsilon(2\text{S})/\Upsilon(1\text{S})}$ and $\rho_{p\text{Pb}}^{\Upsilon(3\text{S})/\Upsilon(1\text{S})}$ are found to be less

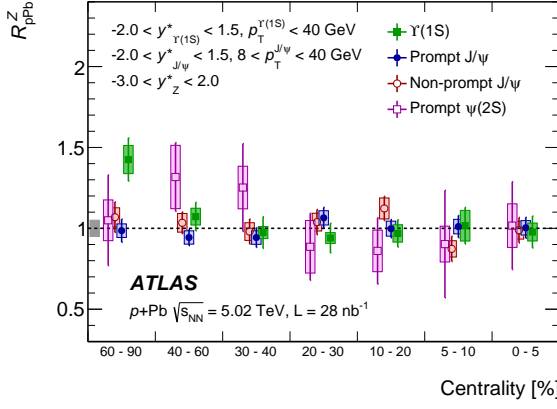


Figure 13: Prompt and non-prompt J/ψ , prompt $\psi(2S)$ and $\Upsilon(1S)$ to Z boson yield ratio, $R_{p\text{Pb}}^Z$, as a function of event centrality in $p+\text{Pb}$ collisions. The ratio is normalised to the ratio integrated in the centrality range 0–90%. The error bars represent statistical uncertainties. The vertical sizes of coloured boxes around the data points represent the uncorrelated systematic uncertainties, and the vertical size of the leftmost grey box around $R_{p\text{Pb}}^Z = 1$ represents the correlated systematic uncertainty.

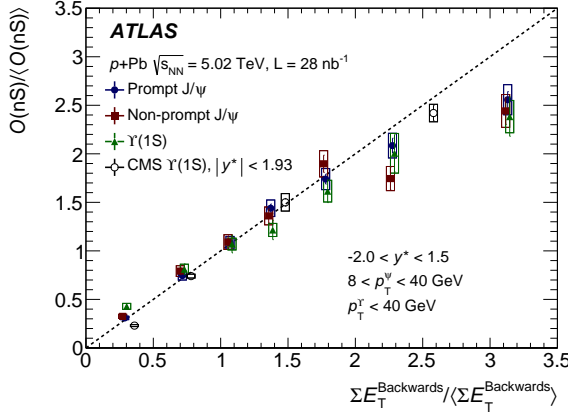


Figure 14: Self-normalised yield for prompt J/ψ , non-prompt J/ψ and $\Upsilon(1S)$, compared to $\Upsilon(1S)$ self-normalised yield ratio measured by CMS [26]. The horizontal position of each data point represents the normalised mean value of the $\Sigma E_T^{\text{Backwards}}$ distribution in minimum-bias data sample. The error bar represents statistical uncertainties, and the vertical size of box underneath the data point represents the systematic uncertainties. The dotted line is a linear function with a slope equal to unity.

than unity by two standard deviations, and they are consistent with each other within the uncertainties. The double ratio as a function of centrality is shown in Figure 17. Both $\rho_{p\text{Pb}}^{\psi(2S)/J/\psi}$ and $\rho_{p\text{Pb}}^{\Upsilon(2S)/\Upsilon(1S)}$ are found to decrease slightly with increasing centrality at the significance level of one-standard-deviation, while conclusions about $\rho_{p\text{Pb}}^{\Upsilon(3S)/\Upsilon(1S)}$ are precluded by the size of the statistical uncertainties.

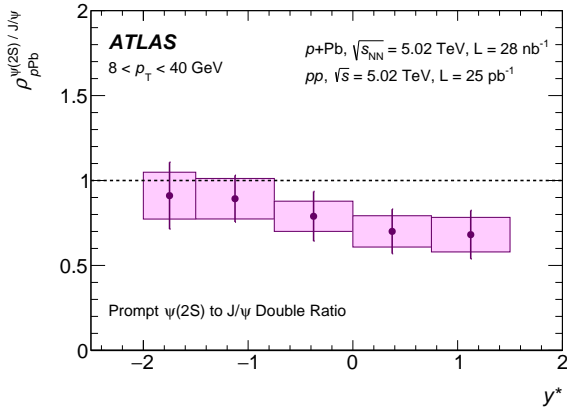


Figure 15: The prompt charmonium production double ratio, $\rho_{p\text{Pb}}^{\psi(2S)/J/\psi}$, as a function of the centre-of-mass rapidity, y^* . The vertical error bars correspond to the statistical uncertainties. The horizontal position of each data point indicates the mean of the weighted y^* distribution. The vertical sizes of coloured boxes around the data points represent the uncorrelated systematic uncertainties, and horizontal sizes of the coloured boxes represent the bin sizes.

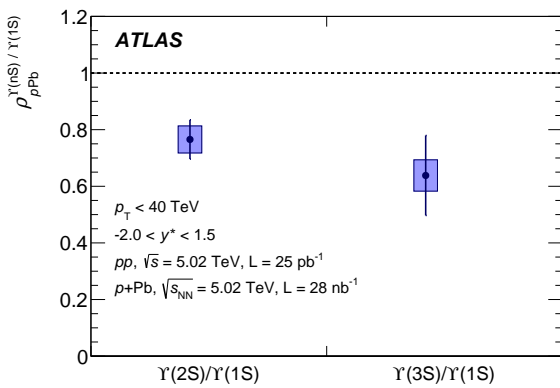


Figure 16: The bottomonium double ratio, $\rho_{p\text{Pb}}^{\Upsilon(nS)/\Upsilon(1S)}$, integrated in the whole measured p_T and y^* range. The vertical error bars correspond to the statistical uncertainties. The vertical sizes of boxes around the data points represent the systematic uncertainties.

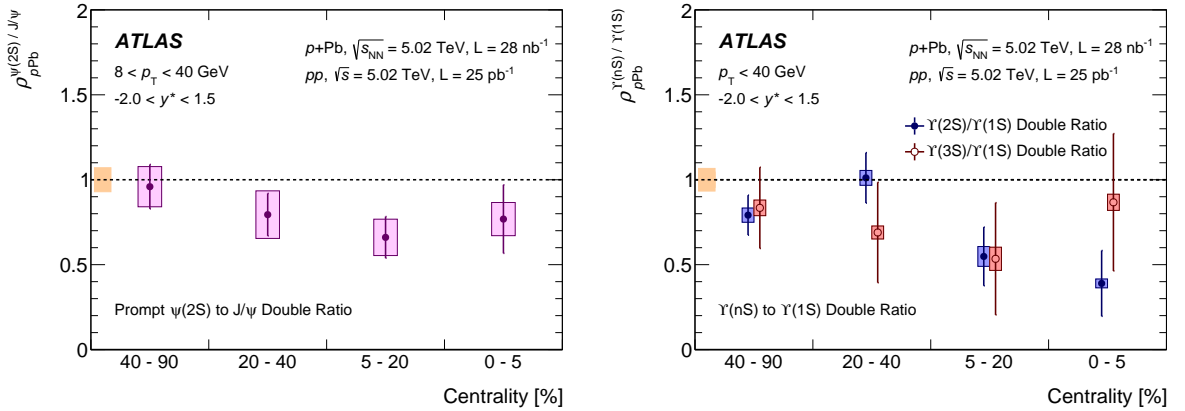


Figure 17: The prompt charmonium double ratio, $\rho_{pPb}^{\psi(2S)/J/\psi}$, (left) and the bottomonium double ratio, $\rho_{pPb}^{\Upsilon(nS)/\Upsilon(1S)}$, (right) as a function of event centrality in $p+Pb$ collisions. The vertical error bars correspond to the statistical uncertainties, and the vertical sizes of coloured boxes around the data points represent the uncorrelated systematic uncertainties in $p+Pb$ collisions. The vertical size of the leftmost yellow box around $\rho_{pPb}^{\Upsilon(nS)/\Upsilon(1S)} = 1$ represents the total uncertainty of the pp reference which is the same for all centralities.

8 Summary

The double-differential production cross sections of five quarkonium states, J/ψ , $\psi(2S)$, $\Upsilon(nS)$ ($n = 1, 2, 3$) are measured using $p+\text{Pb}$ (pp) collision data corresponding to an integrated luminosity of 28 nb^{-1} (25 pb^{-1}) at a centre-of-mass energy per nucleon pair of 5.02 TeV collected by the ATLAS experiment at the LHC. The measured prompt charmonium production cross section in the range of $8 < p_T < 40 \text{ GeV}$ is found to be compatible with non-relativistic QCD predictions, while only the bottomonium results at $p_T > 15 \text{ GeV}$ can be described by the non-relativistic QCD predictions. The measured non-prompt production cross sections of J/ψ and $\psi(2S)$ in pp collisions are found to be consistent with fixed-order next-to-leading-logarithm calculations.

The nuclear modification factors of prompt and non-prompt J/ψ in $p+\text{Pb}$ collisions, $R_{p\text{Pb}}$, measured for $8 < p_T < 40 \text{ GeV}$ are found to be consistent with unity, and no apparent dependence on p_T or rapidity is observed in the measured range, which indicates weak modification of J/ψ production due to cold nuclear matter effects at central rapidity and high p_T . The $R_{p\text{Pb}}$ for $\Upsilon(1S)$ is measured for $p_T < 40 \text{ GeV}$ and is found to be smaller than unity at $p_T < 15 \text{ GeV}$, increasing with p_T and becoming compatible with unity at high p_T . The observed suppression of $\Upsilon(1S)$ production in $p+\text{Pb}$ collisions at low p_T suggests that the nuclear parton distribution functions are modified relative to those of the nucleon. No apparent rapidity dependence of $\Upsilon(1S) R_{p\text{Pb}}$ is observed. The production ratios of prompt and non-prompt J/ψ to Z boson are found to be constant in bins of centrality. As the Z boson production in $p+\text{Pb}$ collisions was found to scale with the number of binary collisions after applying centrality bias correction factors, the same conclusion can be drawn for J/ψ production in $p+\text{Pb}$ collisions. The self-normalised yields of ground-state quarkonium states in $p+\text{Pb}$ collisions are found to correlate linearly with self-normalised event activity expected for events with the highest event activity where the self-normalised yields show two-standard-deviation departure from the linear correlation trend.

The prompt charmonium double ratio is found to decrease slightly from the backward to the forward centre-of-mass rapidity. The prompt $\psi(2S)$ production is suppressed with respect to prompt J/ψ production in $p+\text{Pb}$ collisions with a significance of one standard deviation. The production of excited bottomonium states, $\Upsilon(2S)$ and $\Upsilon(3S)$, is found to be suppressed with respect to $\Upsilon(1S)$ in the integrated kinematic ranges of $p_T < 40 \text{ GeV}$ and $-2 < y^* < 1.5$ in $p+\text{Pb}$ collisions with significance at the level of two standard deviations. Both the prompt $\psi(2S)$ to J/ψ and $\Upsilon(2S)$ to $\Upsilon(1S)$ double ratios show decreasing behaviour in more central collisions. The decreasing trends from peripheral to central are at the significance level of one standard deviation. A stronger cold nuclear matter effect is observed in excited quarkonium states compared to that in ground states.

This work expands the kinematic range of measured charmonium and bottomonium cross sections in pp and $p+\text{Pb}$ collisions. It thus serves as an additional dataset for constraining different models of cold nuclear matter effects and quantifying heavy quarkonium production. In particular, the behaviour of the ground-state yields as a function of centrality is found to match that of Z bosons, while excited states are relatively suppressed in more central collisions.

Acknowledgements

We thank CERN for the very successful operation of the LHC, as well as the support staff from our institutions without whom ATLAS could not be operated efficiently.

We acknowledge the support of ANPCyT, Argentina; YerPhI, Armenia; ARC, Australia; BMWFW and FWF, Austria; ANAS, Azerbaijan; SSTC, Belarus; CNPq and FAPESP, Brazil; NSERC, NRC and CFI, Canada; CERN; CONICYT, Chile; CAS, MOST and NSFC, China; COLCIENCIAS, Colombia; MSMT CR, MPO CR and VSC CR, Czech Republic; DNRF and DNSRC, Denmark; IN2P3-CNRS, CEA-DRF/IRFU, France; SRNSF, Georgia; BMBF, HGF, and MPG, Germany; GSRT, Greece; RGC, Hong Kong SAR, China; ISF, I-CORE and Benoziyo Center, Israel; INFN, Italy; MEXT and JSPS, Japan; CNRST, Morocco; NWO, Netherlands; RCN, Norway; MNiSW and NCN, Poland; FCT, Portugal; MNE/IFA, Romania; MES of Russia and NRC KI, Russian Federation; JINR; MESTD, Serbia; MSSR, Slovakia; ARRS and MIZŠ, Slovenia; DST/NRF, South Africa; MINECO, Spain; SRC and Wallenberg Foundation, Sweden; SERI, SNSF and Cantons of Bern and Geneva, Switzerland; MOST, Taiwan; TAEK, Turkey; STFC, United Kingdom; DOE and NSF, United States of America. In addition, individual groups and members have received support from BCKDF, the Canada Council, CANARIE, CRC, Compute Canada, FQRNT, and the Ontario Innovation Trust, Canada; EPLANET, ERC, ERDF, FP7, Horizon 2020 and Marie Skłodowska-Curie Actions, European Union; Investissements d’Avenir Labex and Idex, ANR, Région Auvergne and Fondation Partager le Savoir, France; DFG and AvH Foundation, Germany; Herakleitos, Thales and Aristea programmes co-financed by EU-ESF and the Greek NSRF; BSF, GIF and Minerva, Israel; BRF, Norway; CERCA Programme Generalitat de Catalunya, Generalitat Valenciana, Spain; the Royal Society and Leverhulme Trust, United Kingdom.

The crucial computing support from all WLCG partners is acknowledged gratefully, in particular from CERN, the ATLAS Tier-1 facilities at TRIUMF (Canada), NDGF (Denmark, Norway, Sweden), CC-IN2P3 (France), KIT/GridKA (Germany), INFN-CNAF (Italy), NL-T1 (Netherlands), PIC (Spain), ASGC (Taiwan), RAL (UK) and BNL (USA), the Tier-2 facilities worldwide and large non-WLCG resource providers. Major contributors of computing resources are listed in Ref. [59].

References

- [1] J. Lansberg et al., *Perspectives on heavy-quarkonium production at the LHC*, arXiv: [0807.3666 \[hep-ph\]](#).
- [2] N. Brambilla et al., *Heavy quarkonium: progress, puzzles, and opportunities*, *Eur. Phys. J. C* **71** (2011) 1534, arXiv: [1010.5827 \[hep-ph\]](#).
- [3] T. Matsui and H. Satz, *J/ψ suppression by quark-gluon plasma formation*, *Phys. Lett. B* **178** (1986) 416.
- [4] NA50 Collaboration, B. Alessandro et al., *Charmonium production and nuclear absorption in p - A interactions at 450 GeV*, *Eur. Phys. J. C* **33** (2004) 31.
- [5] PHENIX Collaboration, S. S. Adler et al., *J/ψ production and nuclear effects for d +Au and p + p collisions at $\sqrt{s_{NN}} = 200$ GeV*, *Phys. Rev. Lett.* **96** (2006) 012304, arXiv: [nucl-ex/0507032](#).
- [6] PHENIX Collaboration, A. Adare et al., *Cold Nuclear Matter Effects on J/Ψ as Constrained by Deuteron-Gold Measurements at $\sqrt{s_{NN}} = 200$ GeV*, *Phys. Rev. C* **77** (2008) 024912, arXiv: [0903.4845 \[nucl-ex\]](#), Erratum: *Phys. Rev. C* **79** (2009) 059901.

- [7] PHENIX Collaboration, A. Adare et al., *Cold Nuclear Matter Effects on J/ψ Yields as a Function of Rapidity and Nuclear Geometry in $d+A$ Collisions at $\sqrt{s_{NN}} = 200$ GeV*, *Phys. Rev. Lett.* **107** (2011) 142301, arXiv: [1010.1246 \[nucl-ex\]](#).
- [8] J. W. Cronin et al., *Production of hadrons at large transverse momentum at 200, 300, and 400 GeV*, *Phys. Rev. D* **11** (1975) 3105.
- [9] B. Kopeliovich, A. Tarasov and J. Hüfner, *Coherence phenomena in charmonium production off nuclei at the energies of RHIC and LHC*, *Nucl. Phys. A* **696** (2001) 669, arXiv: [hep-ph/0104256](#).
- [10] R. Vogt, *Shadowing and absorption effects on J/ψ production in dA collisions*, *Phys. Rev. C* **71** (2005) 054902, arXiv: [hep-ph/0411378](#).
- [11] R. E. Nelson, R. Vogt and A. D. Frawley, *Narrowing the uncertainty on the total charm cross section and its effect on the J/ψ cross section*, *Phys. Rev. C* **87** (2013) 014908, arXiv: [1210.4610 \[hep-ph\]](#).
- [12] H. Fujii and K. Watanabe, *Heavy quark pair production in high-energy pA collisions: Quarkonium*, *Nucl. Phys. A* **915** (2013) 1, arXiv: [1304.2221 \[hep-ph\]](#).
- [13] S. Gavin and J. Milana, *Energy loss at large x_F in nuclear collisions*, *Phys. Rev. Lett.* **68** (1992) 1834.
- [14] F. Arleo and S. Peigné, *Heavy-quarkonium suppression in $p-A$ collisions from parton energy loss in cold QCD matter*, *JHEP* **03** (2013) 122, arXiv: [1212.0434 \[hep-ph\]](#).
- [15] A. Capella, J. A. Casado, C. Pajares, A. V. Ramallo and J. Tran Thanh Van, *Nuclear effects in J/ψ suppression*, *Phys. Lett. B* **206** (1988) 354.
- [16] D. Kharzeev and H. Satz, *Charmonium composition and nuclear suppression*, *Phys. Lett. B* **366** (1996) 316, arXiv: [hep-ph/9508276](#).
- [17] R. Vogt, *J/ψ production and suppression*, *Phys. Rept.* **310** (1999) 197.
- [18] E. G. Ferreiro, *Charmonium dissociation and recombination at LHC: Revisiting comovers*, *Phys. Lett. B* **731** (2014) 57, arXiv: [1210.3209 \[hep-ph\]](#).
- [19] ALICE Collaboration, B. Abelev et al., *J/ψ production and nuclear effects in $p-Pb$ collisions at $\sqrt{s_{NN}} = 5.02$ TeV*, *JHEP* **02** (2014) 073, arXiv: [1308.6726 \[nucl-ex\]](#).
- [20] ALICE Collaboration, J. Adam et al., *Rapidity and transverse-momentum dependence of the inclusive J/ψ nuclear modification factor in $p-Pb$ collisions at $\sqrt{s_{NN}} = 5.02$ TeV*, *JHEP* **06** (2015) 055, arXiv: [1503.07179 \[nucl-ex\]](#).
- [21] LHCb Collaboration, R. Aaij et al., *Study of J/ψ production and cold nuclear matter effects in pPb collisions at $\sqrt{s_{NN}} = 5$ TeV*, *JHEP* **02** (2014) 072, arXiv: [1308.6729 \[nucl-ex\]](#).
- [22] ATLAS Collaboration, *Measurement of differential J/ψ production cross-sections and forward-backward ratios in $p + Pb$ collisions with the ATLAS detector*, *Phys. Rev. C* **92** (2015) 034904, arXiv: [1505.08141 \[hep-ex\]](#).

- [23] CMS Collaboration, *Measurement of prompt and nonprompt J/ψ production in pp and pPb collisions at $\sqrt{s_{NN}} = 5.02$ TeV*, *Eur. Phys. J. C* **77** (2017) 269, arXiv: [1702.01462 \[nucl-ex\]](#).
- [24] PHENIX Collaboration, A. Adare et al.,
Nuclear Modification of ψ' , χ_c , and J/ψ Production in $d+Au$ Collisions at $\sqrt{s_{NN}} = 200$ GeV, *Phys. Rev. Lett.* **111** (2013) 202301, arXiv: [1305.5516 \[nucl-ex\]](#).
- [25] ALICE Collaboration, B. Abelev et al.,
Suppression of $\psi(2S)$ production in $p-Pb$ collisions at $\sqrt{s_{NN}} = 5.02$ TeV, *JHEP* **12** (2014) 073, arXiv: [1405.3796 \[nucl-ex\]](#).
- [26] CMS Collaboration, *Event activity dependence of $\Upsilon(nS)$ production in $\sqrt{s_{NN}} = 5.02$ TeV pPb and $\sqrt{s} = 2.76$ TeV pp collisions*, *JHEP* **04** (2014) 103, arXiv: [1312.6300 \[nucl-ex\]](#).
- [27] CMS Collaboration,
Indications of suppression of excited Υ states in $PbPb$ collisions at $\sqrt{s_{NN}} = 2.76$ TeV, *Phys. Rev. Lett.* **107** (2011) 052302, arXiv: [1105.4894 \[nucl-ex\]](#).
- [28] CMS Collaboration, *Observation of sequential Υ suppression in $PbPb$ collisions*, *Phys. Rev. Lett.* **109** (2012) 222301, arXiv: [1208.2826 \[nucl-ex\]](#).
- [29] CMS Collaboration, *Suppression of $\Upsilon(1S)$, $\Upsilon(2S)$ and $\Upsilon(3S)$ quarkonium states in $PbPb$ collisions at $\sqrt{s_{NN}} = 2.76$ TeV*, *Phys. Lett. B* **770** (2017) 357, arXiv: [1611.01510 \[nucl-ex\]](#).
- [30] ATLAS Collaboration,
Measurement of the centrality dependence of the charged-particle pseudorapidity distribution in proton–lead collisions at $\sqrt{s_{NN}} = 5.02$ TeV with the ATLAS detector, *Eur. Phys. J. C* **76** (2016) 199, arXiv: [1508.00848 \[hep-ex\]](#).
- [31] ATLAS Collaboration, *The ATLAS Experiment at the CERN Large Hadron Collider*, *JINST* **3** (2008) S08003.
- [32] ATLAS Collaboration, *ATLAS Insertable B-Layer Technical Design Report*, ATLAS-TDR-19, 2010, URL: <https://cds.cern.ch/record/1291633>,
ATLAS Insertable B-Layer Technical Design Report Addendum, ATLAS-TDR-19-ADD-1, 2012, URL: <https://cds.cern.ch/record/1451888>.
- [33] ATLAS Collaboration, *Performance of the ATLAS muon trigger in pp collisions at $\sqrt{s} = 8$ TeV*, *Eur. Phys. J. C* **75** (2015) 120, arXiv: [1408.3179 \[hep-ex\]](#).
- [34] ATLAS Collaboration, *Performance of the ATLAS Trigger System in 2015*, *Eur. Phys. J. C* **77** (2017) 317, arXiv: [1611.09661 \[hep-ex\]](#).
- [35] ATLAS Collaboration, *The ATLAS Simulation Infrastructure*, *Eur. Phys. J. C* **70** (2010) 823, arXiv: [1005.4568 \[physics.ins-det\]](#).
- [36] T. Sjöstrand, S. Mrenna and P. Skands, *A Brief Introduction to PYTHIA 8.1*, *Comput. Phys. Comm.* **178** (2008) 852, arXiv: [0710.3820 \[hep-ph\]](#).
- [37] J. Pumplin et al.,
New generation of parton distributions with uncertainties from global QCD analysis, *JHEP* **07** (2002) 012, arXiv: [hep-ph/0201195](#).
- [38] CMS Collaboration,
Measurement of the $\Upsilon(1S)$, $\Upsilon(2S)$ and $\Upsilon(3S)$ Polarizations in pp Collisions at $\sqrt{s} = 7$ TeV, *Phys. Rev. Lett.* **110** (2013) 081802, arXiv: [1209.2922 \[hep-ex\]](#).

- [39] CMS Collaboration, *Measurement of the prompt J/ψ and $\psi(2S)$ polarizations in pp collisions at $\sqrt{s} = 7$ TeV*, *Phys. Lett. B* **727** (2013) 381, arXiv: [1307.6070 \[hep-ex\]](#).
- [40] LHCb Collaboration, R. Aaij et al., *Measurement of J/ψ polarization in pp collisions at $\sqrt{s} = 7$ TeV*, *Eur. Phys. J. C* **73** (2013) 2631, arXiv: [1307.6379 \[hep-ex\]](#).
- [41] S. Agostinelli et al., *GEANT4: A simulation toolkit*, *Nucl. Instrum. Meth. A* **506** (2003) 250.
- [42] ATLAS Collaboration, *Measurement of the muon reconstruction performance of the ATLAS detector using 2011 and 2012 LHC proton–proton collision data*, *Eur. Phys. J. C* **74** (2014) 3130, arXiv: [1407.3935 \[hep-ex\]](#).
- [43] ATLAS Collaboration, *Muon reconstruction performance of the ATLAS detector in proton–proton collision data at $\sqrt{s} = 13$ TeV*, *Eur. Phys. J. C* **76** (2016) 292, arXiv: [1603.05598 \[hep-ex\]](#).
- [44] ATLAS Collaboration, *Measurement of the differential cross-sections of inclusive, prompt and non-prompt J/ψ production in proton–proton collisions at $\sqrt{s} = 7$ TeV*, *Nucl. Phys. B* **850** (2011) 387, arXiv: [1104.3038 \[hep-ex\]](#).
- [45] ATLAS Collaboration, *Measurement of Upsilon production in 7 TeV pp collisions at ATLAS*, *Phys. Rev. D* **87** (2013) 052004, arXiv: [1211.7255 \[hep-ex\]](#).
- [46] ATLAS Collaboration, *Measurement of the differential cross-sections of prompt and non-prompt production of J/ψ and $\psi(2S)$ in pp collisions at $\sqrt{s} = 7$ and 8 TeV with the ATLAS detector*, *Eur. Phys. J. C* **76** (2016) 283, arXiv: [1512.03657 \[hep-ex\]](#).
- [47] W. Verkerke and D. Kirkby, *The RooFit toolkit for data modeling*, arXiv: [physics/0306116 \[physics.data-an\]](#).
- [48] M. Oreglia, *A Study of the Reactions $\psi' \rightarrow \gamma\gamma\psi$* , 1980, URL: <https://www.slac.stanford.edu/cgi-wrap/getdoc/slac-r-236.pdf>.
- [49] Particle Data Group, C. Patrignani et al., *Review of Particle Physics*, *Chin. Phys. C* **40** (2016) 100001.
- [50] ATLAS Collaboration, *Luminosity determination in pp collisions at $\sqrt{s} = 8$ TeV using the ATLAS detector at the LHC*, *Eur. Phys. J. C* **76** (2016) 653, arXiv: [1608.03953 \[hep-ex\]](#).
- [51] D. D. Boos, *Introduction to the bootstrap world*, *Statist. Sci.* **18** (2003) 168.
- [52] M. Cacciari et al., *Theoretical predictions for charm and bottom production at the LHC*, *JHEP* **10** (2012) 137, arXiv: [1205.6344 \[hep-ph\]](#).
- [53] Y. Ma, K. Wang and K. Chao, *$J/\psi(\psi')$ production at the Tevatron and LHC at $O(\alpha_s^4 v^4)$ in nonrelativistic QCD*, *Phys. Rev. Lett.* **106** (2011) 042002, arXiv: [1009.3655 \[hep-ph\]](#).
- [54] H. Shao et al., *Yields and polarizations of prompt J/ψ and $\psi(2S)$ production in hadronic collisions*, *JHEP* **05** (2015) 103, arXiv: [1411.3300 \[hep-ph\]](#).
- [55] H. Han et al., *$\Upsilon(nS)$ and $\chi_b(nP)$ production at hadron colliders in nonrelativistic QCD*, *Phys. Rev. D* **94** (2016) 014028, arXiv: [1410.8537 \[hep-ph\]](#).
- [56] J. L. Albacete et al., *Predictions for $p+Pb$ Collisions at $\sqrt{s_{NN}} = 5.02$ TeV*, *Int. J. Mod. Phys. E* **22** (2013) 1330007, arXiv: [1301.3395 \[hep-ph\]](#).

- [57] ATLAS Collaboration,
Z boson production in p + Pb collisions at $\sqrt{s_{\text{NN}}} = 5.02 \text{ TeV}$ measured with the ATLAS detector,
Phys. Rev. C **92** (2015) 044915, arXiv: [1507.06232 \[hep-ex\]](https://arxiv.org/abs/1507.06232).
- [58] D. V. Perepelitsa and P. A. Steinberg, *Calculation of centrality bias factors in p+A collisions based on a positive correlation of hard process yields with underlying event activity*,
arXiv: [1412.0976 \[nucl-ex\]](https://arxiv.org/abs/1412.0976).
- [59] ATLAS Collaboration, *ATLAS Computing Acknowledgements 2016–2017*,
ATL-GEN-PUB-2016-002, URL: <https://cds.cern.ch/record/2202407>.

The ATLAS Collaboration

M. Aaboud^{137d}, G. Aad⁸⁸, B. Abbott¹¹⁵, J. Abdallah⁸, O. Abdinov^{12,*}, B. Abeloos¹¹⁹, S.H. Abidi¹⁶¹, O.S. AbouZeid¹³⁹, N.L. Abraham¹⁵¹, H. Abramowicz¹⁵⁵, H. Abreu¹⁵⁴, R. Abreu¹¹⁸, Y. Abulaiti^{148a,148b}, B.S. Acharya^{167a,167b,a}, S. Adachi¹⁵⁷, L. Adamczyk^{41a}, J. Adelman¹¹⁰, M. Adersberger¹⁰², T. Adye¹³³, A.A. Affolder¹³⁹, T. Agatonovic-Jovin¹⁴, C. Agheorghiesei^{28c}, J.A. Aguilar-Saavedra^{128a,128f}, S.P. Ahlen²⁴, F. Ahmadov^{68,b}, G. Aielli^{135a,135b}, S. Akatsuka⁷¹, H. Akerstedt^{148a,148b}, T.P.A. Åkesson⁸⁴, A.V. Akimov⁹⁸, G.L. Alberghi^{22a,22b}, J. Albert¹⁷², M.J. Alconada Verzini⁷⁴, M. Aleksa³², I.N. Aleksandrov⁶⁸, C. Alexa^{28b}, G. Alexander¹⁵⁵, T. Alexopoulos¹⁰, M. Alhroob¹¹⁵, B. Ali¹³⁰, M. Aliev^{76a,76b}, G. Alimonti^{94a}, J. Alison³³, S.P. Alkire³⁸, B.M.M. Allbrooke¹⁵¹, B.W. Allen¹¹⁸, P.P. Allport¹⁹, A. Aloisio^{106a,106b}, A. Alonso³⁹, F. Alonso⁷⁴, C. Alpigiani¹⁴⁰, A.A. Alshehri⁵⁶, M.I. Alstaty⁸⁸, B. Alvarez Gonzalez³², D. Álvarez Piqueras¹⁷⁰, M.G. Alviggi^{106a,106b}, B.T. Amadio¹⁶, Y. Amaral Coutinho^{26a}, C. Amelung²⁵, D. Amidei⁹², S.P. Amor Dos Santos^{128a,128c}, A. Amorim^{128a,128b}, S. Amoroso³², G. Amundsen²⁵, C. Anastopoulos¹⁴¹, L.S. Ancu⁵², N. Andari¹⁹, T. Andeen¹¹, C.F. Anders^{60b}, J.K. Anders⁷⁷, K.J. Anderson³³, A. Andreazza^{94a,94b}, V. Andrei^{60a}, S. Angelidakis⁹, I. Angelozzi¹⁰⁹, A. Angerami³⁸, A.V. Anisenkov^{111,c}, N. Anjos¹³, A. Annovi^{126a,126b}, C. Antel^{60a}, M. Antonelli⁵⁰, A. Antonov^{100,*}, D.J. Antrim¹⁶⁶, F. Anulli^{134a}, M. Aoki⁶⁹, L. Aperio Bella³², G. Arabidze⁹³, Y. Arai⁶⁹, J.P. Araque^{128a}, V. Araujo Ferraz^{26a}, A.T.H. Arce⁴⁸, R.E. Ardell⁸⁰, F.A. Arduh⁷⁴, J-F. Arguin⁹⁷, S. Argyropoulos⁶⁶, M. Arik^{20a}, A.J. Armbruster³², L.J. Armitage⁷⁹, O. Arnaez¹⁶¹, H. Arnold⁵¹, M. Arratia³⁰, O. Arslan²³, A. Artamonov⁹⁹, G. Artoni¹²², S. Artz⁸⁶, S. Asai¹⁵⁷, N. Asbah⁴⁵, A. Ashkenazi¹⁵⁵, L. Asquith¹⁵¹, K. Assamagan²⁷, R. Astalos^{146a}, M. Atkinson¹⁶⁹, N.B. Atlay¹⁴³, K. Augsten¹³⁰, G. Avolio³², B. Axen¹⁶, M.K. Ayoub¹¹⁹, G. Azuelos^{97,d}, A.E. Baas^{60a}, M.J. Baca¹⁹, H. Bachacou¹³⁸, K. Bachas^{76a,76b}, M. Backes¹²², M. Backhaus³², P. Bagnaia^{134a,134b}, H. Bahrasemani¹⁴⁴, J.T. Baines¹³³, M. Bajic³⁹, O.K. Baker¹⁷⁹, E.M. Baldin^{111,c}, P. Balek¹⁷⁵, F. Balli¹³⁸, W.K. Balunas¹²⁴, E. Banas⁴², Sw. Banerjee^{176,e}, A.A.E. Bannoura¹⁷⁸, L. Barak³², E.L. Barberio⁹¹, D. Barberis^{53a,53b}, M. Barbero⁸⁸, T. Barillari¹⁰³, M-S Barisits³², J.T. Barkeloo¹¹⁸, T. Barklow¹⁴⁵, N. Barlow³⁰, S.L. Barnes^{36c}, B.M. Barnett¹³³, R.M. Barnett¹⁶, Z. Barnovska-Blenessy^{36a}, A. Baroncelli^{136a}, G. Barone²⁵, A.J. Barr¹²², L. Barranco Navarro¹⁷⁰, F. Barreiro⁸⁵, J. Barreiro Guimarães da Costa^{35a}, R. Bartoldus¹⁴⁵, A.E. Barton⁷⁵, P. Bartos^{146a}, A. Basalaev¹²⁵, A. Bassalat^{119,f}, R.L. Bates⁵⁶, S.J. Batista¹⁶¹, J.R. Batley³⁰, M. Battaglia¹³⁹, M. Bauce^{134a,134b}, F. Bauer¹³⁸, H.S. Bawa^{145,g}, J.B. Beacham¹¹³, M.D. Beattie⁷⁵, T. Beau⁸³, P.H. Beauchemin¹⁶⁵, P. Bechtle²³, H.P. Beck^{18,h}, K. Becker¹²², M. Becker⁸⁶, M. Beckingham¹⁷³, C. Becot¹¹², A.J. Beddall^{20e}, A. Beddall^{20b}, V.A. Bednyakov⁶⁸, M. Bedognetti¹⁰⁹, C.P. Bee¹⁵⁰, T.A. Beermann³², M. Begalli^{26a}, M. Begel²⁷, J.K. Behr⁴⁵, A.S. Bell⁸¹, G. Bella¹⁵⁵, L. Bellagamba^{22a}, A. Bellerive³¹, M. Bellomo¹⁵⁴, K. Belotskiy¹⁰⁰, O. Beltramello³², N.L. Belyaev¹⁰⁰, O. Benary^{155,*}, D. Benchekroun^{137a}, M. Bender¹⁰², K. Bendtz^{148a,148b}, N. Benekos¹⁰, Y. Benhammou¹⁵⁵, E. Benhar Noccioli¹⁷⁹, J. Benitez⁶⁶, D.P. Benjamin⁴⁸, M. Benoit⁵², J.R. Bensinger²⁵, S. Bentvelsen¹⁰⁹, L. Beresford¹²², M. Beretta⁵⁰, D. Berge¹⁰⁹, E. Bergeaas Kuutmann¹⁶⁸, N. Berger⁵, J. Beringer¹⁶, S. Berlendis⁵⁸, N.R. Bernard⁸⁹, G. Bernardi⁸³, C. Bernius¹⁴⁵, F.U. Bernlochner²³, T. Berry⁸⁰, P. Berta¹³¹, C. Bertella^{35a}, G. Bertoli^{148a,148b}, F. Bertolucci^{126a,126b}, I.A. Bertram⁷⁵, C. Bertsche⁴⁵, D. Bertsche¹¹⁵, G.J. Besjes³⁹, O. Bessidskaia Bylund^{148a,148b}, M. Bessner⁴⁵, N. Besson¹³⁸, C. Betancourt⁵¹, A. Bethani⁸⁷, S. Bethke¹⁰³, A.J. Bevan⁷⁹, R.M. Bianchi¹²⁷, O. Biebel¹⁰², D. Biedermann¹⁷, R. Bielski⁸⁷, N.V. Biesuz^{126a,126b}, M. Biglietti^{136a}, J. Bilbao De Mendizabal⁵², T.R.V. Billoud⁹⁷, H. Bilokon⁵⁰, M. Bindi⁵⁷, A. Bingul^{20b}, C. Bini^{134a,134b}, S. Biondi^{22a,22b}, T. Bisanz⁵⁷, C. Bittrich⁴⁷, D.M. Bjergaard⁴⁸, C.W. Black¹⁵², J.E. Black¹⁴⁵, K.M. Black²⁴, D. Blackburn¹⁴⁰, R.E. Blair⁶, T. Blazek^{146a}, I. Bloch⁴⁵, C. Blocker²⁵, A. Blue⁵⁶, W. Blum^{86,*}, U. Blumenschein⁷⁹,

S. Blunier^{34a}, G.J. Bobbink¹⁰⁹, V.S. Bobrovnikov^{111,c}, S.S. Bocchetta⁸⁴, A. Bocci⁴⁸, C. Bock¹⁰²,
 M. Boehler⁵¹, D. Boerner¹⁷⁸, D. Bogavac¹⁰², A.G. Bogdanchikov¹¹¹, C. Bohm^{148a}, V. Boisvert⁸⁰,
 P. Bokan^{168,i}, T. Bold^{41a}, A.S. Boldyrev¹⁰¹, A.E. Bolz^{60b}, M. Bomben⁸³, M. Bona⁷⁹, M. Boonekamp¹³⁸,
 A. Borisov¹³², G. Borissov⁷⁵, J. Bortfeldt³², D. Bortoletto¹²², V. Bortolotto^{62a}, D. Boscherini^{22a},
 M. Bosman¹³, J.D. Bossio Sola²⁹, J. Boudreau¹²⁷, J. Bouffard², E.V. Bouhova-Thacker⁷⁵,
 D. Boumediene³⁷, C. Bourdarios¹¹⁹, S.K. Boutle⁵⁶, A. Boveia¹¹³, J. Boyd³², I.R. Boyko⁶⁸, J. Bracinik¹⁹,
 A. Brandt⁸, G. Brandt⁵⁷, O. Brandt^{60a}, U. Bratzler¹⁵⁸, B. Brau⁸⁹, J.E. Brau¹¹⁸, W.D. Breaden Madden⁵⁶,
 K. Brendlinger⁴⁵, A.J. Brennan⁹¹, L. Brenner¹⁰⁹, R. Brenner¹⁶⁸, S. Bressler¹⁷⁵, D.L. Briglin¹⁹,
 T.M. Bristow⁴⁹, D. Britton⁵⁶, D. Britzger⁴⁵, F.M. Brochu³⁰, I. Brock²³, R. Brock⁹³, G. Brooijmans³⁸,
 T. Brooks⁸⁰, W.K. Brooks^{34b}, J. Brosamer¹⁶, E. Brost¹¹⁰, J.H. Broughton¹⁹,
 P.A. Bruckman de Renstrom⁴², D. Bruncko^{146b}, A. Bruni^{22a}, G. Bruni^{22a}, L.S. Bruni¹⁰⁹, BH Brunt³⁰,
 M. Bruschi^{22a}, N. Bruscino²³, P. Bryant³³, L. Bryngemark⁴⁵, T. Buanes¹⁵, Q. Buat¹⁴⁴, P. Buchholz¹⁴³,
 A.G. Buckley⁵⁶, I.A. Budagov⁶⁸, F. Buehrer⁵¹, M.K. Bugge¹²¹, O. Bulekov¹⁰⁰, D. Bullock⁸,
 H. Burckhart³², S. Burdin⁷⁷, C.D. Burgard⁵¹, A.M. Burger⁵, B. Burghgrave¹¹⁰, K. Burka⁴², S. Burke¹³³,
 I. Burmeister⁴⁶, J.T.P. Burr¹²², E. Busato³⁷, D. Büscher⁵¹, V. Büscher⁸⁶, P. Bussey⁵⁶, J.M. Butler²⁴,
 C.M. Buttar⁵⁶, J.M. Butterworth⁸¹, P. Butti³², W. Buttlinger²⁷, A. Buzatu^{35c}, A.R. Buzykaev^{111,c},
 S. Cabrera Urbán¹⁷⁰, D. Caforio¹³⁰, V.M. Cairo^{40a,40b}, O. Cakir^{4a}, N. Calace⁵², P. Calafiura¹⁶,
 A. Calandri⁸⁸, G. Calderini⁸³, P. Calfayan⁶⁴, G. Callea^{40a,40b}, L.P. Caloba^{26a}, S. Calvente Lopez⁸⁵,
 D. Calvet³⁷, S. Calvet³⁷, T.P. Calvet⁸⁸, R. Camacho Toro³³, S. Camarda³², P. Camarri^{135a,135b},
 D. Cameron¹²¹, R. Caminal Armadans¹⁶⁹, C. Camincher⁵⁸, S. Campana³², M. Campanelli⁸¹,
 A. Camplani^{94a,94b}, A. Campoverde¹⁴³, V. Canale^{106a,106b}, M. Cano Bret^{36c}, J. Cantero¹¹⁶, T. Cao¹⁵⁵,
 M.D.M. Capeans Garrido³², I. Caprini^{28b}, M. Caprini^{28b}, M. Capua^{40a,40b}, R.M. Carbone³⁸,
 R. Cardarelli^{135a}, F. Cardillo⁵¹, I. Carli¹³¹, T. Carli³², G. Carlino^{106a}, B.T. Carlson¹²⁷, L. Carminati^{94a,94b},
 R.M.D. Carney^{148a,148b}, S. Caron¹⁰⁸, E. Carquin^{34b}, S. Carrá^{94a,94b}, G.D. Carrillo-Montoya³²,
 J. Carvalho^{128a,128c}, D. Casadei¹⁹, M.P. Casado^{13,j}, M. Casolino¹³, D.W. Casper¹⁶⁶, R. Castelijn¹⁰⁹,
 V. Castillo Gimenez¹⁷⁰, N.F. Castro^{128a,k}, A. Catinaccio³², J.R. Catmore¹²¹, A. Cattai³², J. Caudron²³,
 V. Cavaliere¹⁶⁹, E. Cavallaro¹³, D. Cavalli^{94a}, M. Cavalli-Sforza¹³, V. Cavasinni^{126a,126b}, E. Celebi^{20a},
 F. Ceradini^{136a,136b}, L. Cerdá Alberich¹⁷⁰, A.S. Cerqueira^{26b}, A. Cerri¹⁵¹, L. Cerrito^{135a,135b}, F. Cerutti¹⁶,
 A. Cervelli¹⁸, S.A. Cetin^{20d}, A. Chafaq^{137a}, D. Chakraborty¹¹⁰, S.K. Chan⁵⁹, W.S. Chan¹⁰⁹,
 Y.L. Chan^{62a}, P. Chang¹⁶⁹, J.D. Chapman³⁰, D.G. Charlton¹⁹, C.C. Chau¹⁶¹, C.A. Chavez Barajas¹⁵¹,
 S. Che¹¹³, S. Cheatham^{167a,167c}, A. Chegwidden⁹³, S. Chekanov⁶, S.V. Chekulaev^{163a}, G.A. Chelkov^{68,l},
 M.A. Chelstowska³², C. Chen⁶⁷, H. Chen²⁷, S. Chen^{35b}, S. Chen¹⁵⁷, X. Chen^{35c,m}, Y. Chen⁷⁰,
 H.C. Cheng⁹², H.J. Cheng^{35a,35d}, Y. Cheng³³, A. Cheplakov⁶⁸, E. Cheremushkina¹³²,
 R. Cherkaoui El Moursli^{137e}, V. Chernyatin^{27,*}, E. Cheu⁷, L. Chevalier¹³⁸, V. Chiarella⁵⁰,
 G. Chiarella^{126a,126b}, G. Chiodini^{76a}, A.S. Chisholm³², A. Chitan^{28b}, Y.H. Chiu¹⁷², M.V. Chizhov⁶⁸,
 K. Choi⁶⁴, A.R. Chomont³⁷, S. Chouridou¹⁵⁶, V. Christodoulou⁸¹, D. Chromeck-Burckhart³²,
 M.C. Chu^{62a}, J. Chudoba¹²⁹, A.J. Chuinard⁹⁰, J.J. Chwastowski⁴², L. Chytka¹¹⁷, A.K. Ciftci^{4a},
 D. Cinca⁴⁶, V. Cindro⁷⁸, I.A. Cioara²³, C. Ciocca^{22a,22b}, A. Ciocio¹⁶, F. Cirotto^{106a,106b}, Z.H. Citron¹⁷⁵,
 M. Citterio^{94a}, M. Ciubancan^{28b}, A. Clark⁵², B.L. Clark⁵⁹, M.R. Clark³⁸, P.J. Clark⁴⁹, R.N. Clarke¹⁶,
 C. Clement^{148a,148b}, Y. Coadou⁸⁸, M. Cobal^{167a,167c}, A. Coccaro⁵², J. Cochran⁶⁷, L. Colasurdo¹⁰⁸,
 B. Cole³⁸, A.P. Colijn¹⁰⁹, J. Collot⁵⁸, T. Colombo¹⁶⁶, P. Conde Muiño^{128a,128b}, E. Coniavitis⁵¹,
 S.H. Connell^{147b}, I.A. Connelly⁸⁷, S. Constantinescu^{28b}, G. Conti³², F. Conventi^{106a,n}, M. Cooke¹⁶,
 A.M. Cooper-Sarkar¹²², F. Cormier¹⁷¹, K.J.R. Cormier¹⁶¹, M. Corradi^{134a,134b}, F. Corriveau^{90,o},
 A. Cortes-Gonzalez³², G. Cortiana¹⁰³, G. Costa^{94a}, M.J. Costa¹⁷⁰, D. Costanzo¹⁴¹, G. Cottin³⁰,
 G. Cowan⁸⁰, B.E. Cox⁸⁷, K. Cranmer¹¹², S.J. Crawley⁵⁶, R.A. Creager¹²⁴, G. Cree³¹,
 S. Crépé-Renaudin⁵⁸, F. Crescioli⁸³, W.A. Cribbs^{148a,148b}, M. Cristinziani²³, V. Croft¹⁰⁸,
 G. Crosetti^{40a,40b}, A. Cueto⁸⁵, T. Cuhadar Donszelmann¹⁴¹, A.R. Cukierman¹⁴⁵, J. Cummings¹⁷⁹,

M. Curatolo⁵⁰, J. Cúth⁸⁶, H. Czirr¹⁴³, P. Czodrowski³², G. D’amen^{22a,22b}, S. D’Auria⁵⁶, M. D’Onofrio⁷⁷,
 M.J. Da Cunha Sargedas De Sousa^{128a,128b}, C. Da Via⁸⁷, W. Dabrowski^{41a}, T. Dado^{146a}, T. Dai⁹²,
 O. Dale¹⁵, F. Dallaire⁹⁷, C. Dallapiccola⁸⁹, M. Dam³⁹, J.R. Dandoy¹²⁴, N.P. Dang⁵¹, A.C. Daniells¹⁹,
 N.S. Dann⁸⁷, M. Danninger¹⁷¹, M. Dano Hoffmann¹³⁸, V. Dao¹⁵⁰, G. Darbo^{53a}, S. Darmora⁸,
 J. Dassoulas³, A. Dattagupta¹¹⁸, T. Daubney⁴⁵, W. Davey²³, C. David⁴⁵, T. Davidek¹³¹, M. Davies¹⁵⁵,
 P. Davison⁸¹, E. Dawe⁹¹, I. Dawson¹⁴¹, K. De⁸, R. de Asmundis^{106a}, A. De Benedetti¹¹⁵,
 S. De Castro^{22a,22b}, S. De Cecco⁸³, N. De Groot¹⁰⁸, P. de Jong¹⁰⁹, H. De la Torre⁹³, F. De Lorenzi⁶⁷,
 A. De Maria⁵⁷, D. De Pedis^{134a}, A. De Salvo^{134a}, U. De Sanctis^{135a,135b}, A. De Santo¹⁵¹,
 K. De Vasconcelos Corga⁸⁸, J.B. De Vie De Regie¹¹⁹, W.J. Dearnaley⁷⁵, R. Debbe²⁷,
 C. Debenedetti¹³⁹, D.V. Dedovich⁶⁸, N. Dehghanian³, I. Deigaard¹⁰⁹, M. Del Gaudio^{40a,40b},
 J. Del Peso⁸⁵, T. Del Prete^{126a,126b}, D. Delgove¹¹⁹, F. Deliot¹³⁸, C.M. Delitzsch⁵², A. Dell’Acqua³²,
 L. Dell’Asta²⁴, M. Dell’Orso^{126a,126b}, M. Della Pietra^{106a,106b}, D. della Volpe⁵², M. Delmastro⁵,
 C. Delporte¹¹⁹, P.A. Delsart⁵⁸, D.A. DeMarco¹⁶¹, S. Demers¹⁷⁹, M. Demichev⁶⁸, A. Demilly⁸³,
 S.P. Denisov¹³², D. Denysiuk¹³⁸, D. Derendarz⁴², J.E. Derkaoui^{137d}, F. Derue⁸³, P. Dervan⁷⁷,
 K. Desch²³, C. Deterre⁴⁵, K. Dette⁴⁶, M.R. Devesa²⁹, P.O. Deviveiros³², A. Dewhurst¹³³, S. Dhaliwal²⁵,
 F.A. Di Bello⁵², A. Di Ciaccio^{135a,135b}, L. Di Ciaccio⁵, W.K. Di Clemente¹²⁴, C. Di Donato^{106a,106b},
 A. Di Girolamo³², B. Di Girolamo³², B. Di Micco^{136a,136b}, R. Di Nardo³², K.F. Di Petrillo⁵⁹,
 A. Di Simone⁵¹, R. Di Sipio¹⁶¹, D. Di Valentino³¹, C. Diaconu⁸⁸, M. Diamond¹⁶¹, F.A. Dias⁴⁹,
 M.A. Diaz^{34a}, E.B. Diehl⁹², J. Dietrich¹⁷, S. Díez Cornell⁴⁵, A. Dimitrievska¹⁴, J. Dingfelder²³,
 P. Dita^{28b}, S. Dita^{28b}, F. Dittus³², F. Djama⁸⁸, T. Djobava^{54b}, J.I. Djuvsland^{60a}, M.A.B. do Vale^{26c},
 D. Dobos³², M. Dobre^{28b}, C. Doglioni⁸⁴, J. Dolejsi¹³¹, Z. Dolezal¹³¹, M. Donadelli^{26d},
 S. Donati^{126a,126b}, P. Dondero^{123a,123b}, J. Donini³⁷, J. Dopke¹³³, A. Doria^{106a}, M.T. Dova⁷⁴,
 A.T. Doyle⁵⁶, E. Drechsler⁵⁷, M. Dris¹⁰, Y. Du^{36b}, J. Duarte-Campderros¹⁵⁵, E. Duchovni¹⁷⁵,
 G. Duckeck¹⁰², A. Ducourthial⁸³, O.A. Ducu^{97,p}, D. Duda¹⁰⁹, A. Dudarev³², A.Chr. Dudder⁸⁶,
 E.M. Duffield¹⁶, L. Duflot¹¹⁹, M. Dührssen³², M. Dumancic¹⁷⁵, A.E. Dumitriu^{28b}, A.K. Duncan⁵⁶,
 M. Dunford^{60a}, H. Duran Yildiz^{4a}, M. Düren⁵⁵, A. Durglishvili^{54b}, D. Duschinger⁴⁷, B. Dutta⁴⁵,
 M. Dyndal⁴⁵, C. Eckardt⁴⁵, K.M. Ecker¹⁰³, R.C. Edgar⁹², T. Eifert³², G. Eigen¹⁵, K. Einsweiler¹⁶,
 T. Ekelof¹⁶⁸, M. El Kacimi^{137c}, R. El Kosseifi⁸⁸, V. Ellajosyula⁸⁸, M. Ellert¹⁶⁸, S. Elles⁵,
 F. Ellinghaus¹⁷⁸, A.A. Elliot¹⁷², N. Ellis³², J. Elmsheuser²⁷, M. Elsing³², D. Emeliyanov¹³³, Y. Enari¹⁵⁷,
 O.C. Endner⁸⁶, J.S. Ennis¹⁷³, J. Erdmann⁴⁶, A. Ereditato¹⁸, G. Ernis¹⁷⁸, M. Ernst²⁷, S. Errede¹⁶⁹,
 E. Ertel⁸⁶, M. Escalier¹¹⁹, C. Escobar¹²⁷, B. Esposito⁵⁰, O. Estrada Pastor¹⁷⁰, A.I. Etienne¹³⁸,
 E. Etzion¹⁵⁵, H. Evans⁶⁴, A. Ezhilov¹²⁵, M. Ezzi^{137e}, F. Fabbri^{22a,22b}, L. Fabbri^{22a,22b}, G. Facini³³,
 R.M. Fakhrutdinov¹³², S. Falciano^{134a}, R.J. Falla⁸¹, J. Faltova³², Y. Fang^{35a}, M. Fanti^{94a,94b}, A. Farbin⁸,
 A. Farilla^{136a}, C. Farina¹²⁷, E.M. Farina^{123a,123b}, T. Farooque⁹³, S. Farrell¹⁶, S.M. Farrington¹⁷³,
 P. Farthouat³², F. Fassi^{137e}, P. Fassnacht³², D. Fassouliotis⁹, M. Faucci Giannelli⁸⁰, A. Favareto^{53a,53b},
 W.J. Fawcett¹²², L. Fayard¹¹⁹, O.L. Fedin^{125,q}, W. Fedorko¹⁷¹, S. Feigl¹²¹, L. Feligioni⁸⁸, C. Feng^{36b},
 E.J. Feng³², H. Feng⁹², M.J. Fenton⁵⁶, A.B. Fenyuk¹³², L. Feremenga⁸, P. Fernandez Martinez¹⁷⁰,
 S. Fernandez Perez¹³, J. Ferrando⁴⁵, A. Ferrari¹⁶⁸, P. Ferrari¹⁰⁹, R. Ferrari^{123a}, D.E. Ferreira de Lima^{60b},
 A. Ferrer¹⁷⁰, D. Ferrere⁵², C. Ferretti⁹², F. Fiedler⁸⁶, A. Filipčič⁷⁸, M. Filipuzzi⁴⁵, F. Filthaut¹⁰⁸,
 M. Fincke-Keeler¹⁷², K.D. Finelli¹⁵², M.C.N. Fiolhais^{128a,128c,r}, L. Fiorini¹⁷⁰, A. Fischer², C. Fischer¹³,
 J. Fischer¹⁷⁸, W.C. Fisher⁹³, N. Flaschel⁴⁵, I. Fleck¹⁴³, P. Fleischmann⁹², R.R.M. Fletcher¹²⁴,
 T. Flick¹⁷⁸, B.M. Flierl¹⁰², L.R. Flores Castillo^{62a}, M.J. Flowerdew¹⁰³, G.T. Forcolin⁸⁷, A. Formica¹³⁸,
 F.A. Förster¹³, A. Forti⁸⁷, A.G. Foster¹⁹, D. Fournier¹¹⁹, H. Fox⁷⁵, S. Fracchia¹⁴¹, P. Francavilla⁸³,
 M. Franchini^{22a,22b}, S. Franchino^{60a}, D. Francis³², L. Franconi¹²¹, M. Franklin⁵⁹, M. Frate¹⁶⁶,
 M. Fraternali^{123a,123b}, D. Freeborn⁸¹, S.M. Fressard-Batraneanu³², B. Freund⁹⁷, D. Froidevaux³²,
 J.A. Frost¹²², C. Fukunaga¹⁵⁸, T. Fusayasu¹⁰⁴, J. Fuster¹⁷⁰, C. Gabaldon⁵⁸, O. Gabizon¹⁵⁴,
 A. Gabrielli^{22a,22b}, A. Gabrielli¹⁶, G.P. Gach^{41a}, S. Gadatsch³², S. Gadomski⁸⁰, G. Gagliardi^{53a,53b},

L.G. Gagnon⁹⁷, C. Galea¹⁰⁸, B. Galhardo^{128a,128c}, E.J. Gallas¹²², B.J. Gallop¹³³, P. Gallus¹³⁰,
 G. Galster³⁹, K.K. Gan¹¹³, S. Ganguly³⁷, J. Gao^{36a}, Y. Gao⁷⁷, Y.S. Gao^{145,g}, F.M. Garay Walls⁴⁹,
 C. García¹⁷⁰, J.E. García Navarro¹⁷⁰, M. Garcia-Siveres¹⁶, R.W. Gardner³³, N. Garelli¹⁴⁵,
 V. Garonne¹²¹, A. Gascon Bravo⁴⁵, K. Gasnikova⁴⁵, C. Gatti⁵⁰, A. Gaudiello^{53a,53b}, G. Gaudio^{123a},
 I.L. Gavrilenko⁹⁸, C. Gay¹⁷¹, G. Gaycken²³, E.N. Gazis¹⁰, C.N.P. Gee¹³³, J. Geisen⁵⁷, M. Geisen⁸⁶,
 M.P. Geisler^{60a}, K. Gellerstedt^{148a,148b}, C. Gemme^{53a}, M.H. Genest⁵⁸, C. Geng⁹², S. Gentile^{134a,134b},
 C. Gentsos¹⁵⁶, S. George⁸⁰, D. Gerbaudo¹³, A. Gershon¹⁵⁵, S. Ghasemi¹⁴³, M. Ghneimat²³,
 B. Giacobbe^{22a}, S. Giagu^{134a,134b}, P. Giannetti^{126a,126b}, S.M. Gibson⁸⁰, M. Gignac¹⁷¹, M. Gilchriese¹⁶,
 D. Gillberg³¹, G. Gilles¹⁷⁸, D.M. Gingrich^{3,d}, N. Giokaris^{9,*}, M.P. Giordani^{167a,167c}, F.M. Giorgi^{22a},
 P.F. Giraud¹³⁸, P. Giromini⁵⁹, D. Giugni^{94a}, F. Giuli¹²², C. Giuliani¹⁰³, M. Giulini^{60b}, B.K. Gjelsten¹²¹,
 S. Gkaitatzis¹⁵⁶, I. Gkialas^{9,s}, E.L. Gkougkousis¹³⁹, L.K. Gladilin¹⁰¹, C. Glasman⁸⁵, J. Glatzer¹³,
 P.C.F. Glaysher⁴⁵, A. Glazov⁴⁵, M. Goblirsch-Kolb²⁵, J. Godlewski⁴², S. Goldfarb⁹¹, T. Golling⁵²,
 D. Golubkov¹³², A. Gomes^{128a,128b,128d}, R. Gonçalo^{128a}, R. Goncalves Gama^{26a},
 J. Goncalves Pinto Firmino Da Costa¹³⁸, G. Gonella⁵¹, L. Gonella¹⁹, A. Gongadze⁶⁸,
 S. González de la Hoz¹⁷⁰, S. Gonzalez-Sevilla⁵², L. Goossens³², P.A. Gorbounov⁹⁹, H.A. Gordon²⁷,
 I. Gorelov¹⁰⁷, B. Gorini³², E. Gorini^{76a,76b}, A. Gorišek⁷⁸, A.T. Goshaw⁴⁸, C. Gössling⁴⁶, M.I. Gostkin⁶⁸,
 C.R. Goudet¹¹⁹, D. Goujdami^{137c}, A.G. Goussiou¹⁴⁰, N. Govender^{147b,t}, E. Gozani¹⁵⁴, L. Graber⁵⁷,
 I. Grabowska-Bold^{41a}, P.O.J. Gradin¹⁶⁸, J. Gramling¹⁶⁶, E. Gramstad¹²¹, S. Grancagnolo¹⁷,
 V. Gratchev¹²⁵, P.M. Gravila^{28f}, C. Gray⁵⁶, H.M. Gray³², Z.D. Greenwood^{82,u}, C. Grefe²³,
 K. Gregersen⁸¹, I.M. Gregor⁴⁵, P. Grenier¹⁴⁵, K. Grevtsov⁵, J. Griffiths⁸, A.A. Grillo¹³⁹, K. Grimm⁷⁵,
 S. Grinstein^{13,v}, Ph. Gris³⁷, J.-F. Grivaz¹¹⁹, S. Groh⁸⁶, E. Gross¹⁷⁵, J. Grosse-Knetter⁵⁷, G.C. Grossi⁸²,
 Z.J. Grout⁸¹, A. Grummer¹⁰⁷, L. Guan⁹², W. Guan¹⁷⁶, J. Guenther⁶⁵, F. Guescini^{163a}, D. Guest¹⁶⁶,
 O. Gueta¹⁵⁵, B. Gui¹¹³, E. Guido^{53a,53b}, T. Guillemin⁵, S. Guindon², U. Gul⁵⁶, C. Gumpert³², J. Guo^{36c},
 W. Guo⁹², Y. Guo^{36a,w}, R. Gupta⁴³, S. Gupta¹²², G. Gustavino^{134a,134b}, P. Gutierrez¹¹⁵,
 N.G. Gutierrez Ortiz⁸¹, C. Gutschow⁸¹, C. Guyot¹³⁸, M.P. Guzik^{41a}, C. Gwenlan¹²², C.B. Gwilliam⁷⁷,
 A. Haas¹¹², C. Haber¹⁶, H.K. Hadavand⁸, N. Haddad^{137e}, A. Hadef⁸⁸, S. Hageböck²³, M. Hagihara¹⁶⁴,
 H. Hakobyan^{180,*}, M. Haleem⁴⁵, J. Haley¹¹⁶, G. Halladjian⁹³, G.D. Hallewell⁸⁸, K. Hamacher¹⁷⁸,
 P. Hamal¹¹⁷, K. Hamano¹⁷², A. Hamilton^{147a}, G.N. Hamity¹⁴¹, P.G. Hamnett⁴⁵, L. Han^{36a}, S. Han^{35a,35d},
 K. Hanagaki^{69,x}, K. Hanawa¹⁵⁷, M. Hance¹³⁹, B. Haney¹²⁴, P. Hanke^{60a}, J.B. Hansen³⁹, J.D. Hansen³⁹,
 M.C. Hansen²³, P.H. Hansen³⁹, K. Hara¹⁶⁴, A.S. Hard¹⁷⁶, T. Harenberg¹⁷⁸, F. Hariri¹¹⁹, S. Harkusha⁹⁵,
 R.D. Harrington⁴⁹, P.F. Harrison¹⁷³, N.M. Hartmann¹⁰², M. Hasegawa⁷⁰, Y. Hasegawa¹⁴², A. Hasib⁴⁹,
 S. Hassani¹³⁸, S. Haug¹⁸, R. Hauser⁹³, L. Hauswald⁴⁷, L.B. Havener³⁸, M. Havranek¹³⁰,
 C.M. Hawkes¹⁹, R.J. Hawkings³², D. Hayakawa¹⁵⁹, D. Hayden⁹³, C.P. Hays¹²², J.M. Hays⁷⁹,
 H.S. Hayward⁷⁷, S.J. Haywood¹³³, S.J. Head¹⁹, T. Heck⁸⁶, V. Hedberg⁸⁴, L. Heelan⁸, K.K. Heidegger⁵¹,
 S. Heim⁴⁵, T. Heim¹⁶, B. Heinemann^{45,y}, J.J. Heinrich¹⁰², L. Heinrich¹¹², C. Heinz⁵⁵, J. Hejbal¹²⁹,
 L. Helary³², A. Held¹⁷¹, S. Hellman^{148a,148b}, C. Helsens³², R.C.W. Henderson⁷⁵, Y. Heng¹⁷⁶,
 S. Henkelmann¹⁷¹, A.M. Henriques Correia³², S. Henrot-Versille¹¹⁹, G.H. Herbert¹⁷, H. Herde²⁵,
 V. Herget¹⁷⁷, Y. Hernández Jiménez^{147c}, G. Herten⁵¹, R. Hertenberger¹⁰², L. Hervas³², T.C. Herwig¹²⁴,
 G.G. Hesketh⁸¹, N.P. Hessey^{163a}, J.W. Hetherly⁴³, S. Higashino⁶⁹, E. Higón-Rodriguez¹⁷⁰, E. Hill¹⁷²,
 J.C. Hill³⁰, K.H. Hiller⁴⁵, S.J. Hillier¹⁹, I. Hinchliffe¹⁶, M. Hirose⁵¹, D. Hirschbuehl¹⁷⁸, B. Hiti⁷⁸,
 O. Hladík¹²⁹, X. Hoad⁴⁹, J. Hobbs¹⁵⁰, N. Hod^{163a}, M.C. Hodgkinson¹⁴¹, P. Hodgson¹⁴¹, A. Hoecker³²,
 M.R. Hoeferkamp¹⁰⁷, F. Hoenig¹⁰², D. Hohn²³, T.R. Holmes³³, M. Homann⁴⁶, S. Honda¹⁶⁴, T. Honda⁶⁹,
 T.M. Hong¹²⁷, B.H. Hooberman¹⁶⁹, W.H. Hopkins¹¹⁸, Y. Horii¹⁰⁵, A.J. Horton¹⁴⁴, J.-Y. Hostachy⁵⁸,
 S. Hou¹⁵³, A. Hoummada^{137a}, J. Howarth⁴⁵, J. Hoya⁷⁴, M. Hrabovsky¹¹⁷, I. Hristova¹⁷, J. Hrvnac¹¹⁹,
 T. Hrynevich⁹⁶, P.J. Hsu⁶³, S.-C. Hsu¹⁴⁰, Q. Hu^{36a}, S. Hu^{36c}, Y. Huang^{35a}, Z. Hubacek¹³⁰,
 F. Hubaut⁸⁸, F. Huegging²³, T.B. Huffman¹²², E.W. Hughes³⁸, G. Hughes⁷⁵, M. Huhtinen³², P. Huo¹⁵⁰,
 N. Huseynov^{68,b}, J. Huston⁹³, J. Huth⁵⁹, G. Iacobucci⁵², G. Iakovidis²⁷, I. Ibragimov¹⁴³,

L. Iconomidou-Fayard¹¹⁹, Z. Idrissi^{137e}, P. Iengo³², O. Igonkina^{109,z}, T. Iizawa¹⁷⁴, Y. Ikegami⁶⁹,
 M. Ikeno⁶⁹, Y. Ilchenko^{11,aa}, D. Iliadis¹⁵⁶, N. Illic¹⁴⁵, G. Introzzi^{123a,123b}, P. Ioannou^{9,*}, M. Iodice^{136a},
 K. Iordanidou³⁸, V. Ippolito⁵⁹, M.F. Isacson¹⁶⁸, N. Ishijima¹²⁰, M. Ishino¹⁵⁷, M. Ishitsuka¹⁵⁹,
 C. Issever¹²², S. Istin^{20a}, F. Ito¹⁶⁴, J.M. Iturbe Ponce⁸⁷, R. Iuppa^{162a,162b}, H. Iwasaki⁶⁹, J.M. Izen⁴⁴,
 V. Izzo^{106a}, S. Jabbar³, P. Jackson¹, R.M. Jacobs²³, V. Jain², K.B. Jakobi⁸⁶, K. Jakobs⁵¹, S. Jakobsen⁶⁵,
 T. Jakoubek¹²⁹, D.O. Jamin¹¹⁶, D.K. Jana⁸², R. Jansky⁶⁵, J. Janssen²³, M. Janus⁵⁷, P.A. Janus^{41a},
 G. Jarlskog⁸⁴, N. Javadov^{68,b}, T. Javůrek⁵¹, M. Javurkova⁵¹, F. Jeanneau¹³⁸, L. Jeanty¹⁶, J. Jejelava^{54a,ab},
 A. Jelinskas¹⁷³, P. Jenni^{51,ac}, C. Jeske¹⁷³, S. Jézéquel⁵, H. Ji¹⁷⁶, J. Jia¹⁵⁰, H. Jiang⁶⁷, Y. Jiang^{36a},
 Z. Jiang¹⁴⁵, S. Jiggins⁸¹, J. Jimenez Pena¹⁷⁰, S. Jin^{35a}, A. Jinaru^{28b}, O. Jinnouchi¹⁵⁹, H. Jivan^{147c},
 P. Johansson¹⁴¹, K.A. Johns⁷, C.A. Johnson⁶⁴, W.J. Johnson¹⁴⁰, K. Jon-And^{148a,148b}, R.W.L. Jones⁷⁵,
 S.D. Jones¹⁵¹, S. Jones⁷, T.J. Jones⁷⁷, J. Jongmanns^{60a}, P.M. Jorge^{128a,128b}, J. Jovicevic^{163a}, X. Ju¹⁷⁶,
 A. Juste Rozas^{13,v}, M.K. Köhler¹⁷⁵, A. Kaczmarska⁴², M. Kado¹¹⁹, H. Kagan¹¹³, M. Kagan¹⁴⁵,
 S.J. Kahn⁸⁸, T. Kaji¹⁷⁴, E. Kajomovitz⁴⁸, C.W. Kalderon⁸⁴, A. Kaluza⁸⁶, S. Kama⁴³,
 A. Kamenshchikov¹³², N. Kanaya¹⁵⁷, L. Kanjir⁷⁸, V.A. Kantserov¹⁰⁰, J. Kanzaki⁶⁹, B. Kaplan¹¹²,
 L.S. Kaplan¹⁷⁶, D. Kar^{147c}, K. Karakostas¹⁰, N. Karastathis¹⁰, M.J. Kareem⁵⁷, E. Karentzos¹⁰,
 S.N. Karpov⁶⁸, Z.M. Karpova⁶⁸, K. Karthik¹¹², V. Kartvelishvili⁷⁵, A.N. Karyukhin¹³², K. Kasahara¹⁶⁴,
 L. Kashif¹⁷⁶, R.D. Kass¹¹³, A. Kastanas¹⁴⁹, Y. Kataoka¹⁵⁷, C. Kato¹⁵⁷, A. Katre⁵², J. Katzy⁴⁵,
 K. Kawade¹⁰⁵, K. Kawagoe⁷³, T. Kawamoto¹⁵⁷, G. Kawamura⁵⁷, E.F. Kay⁷⁷, V.F. Kazanin^{111,c},
 R. Keeler¹⁷², R. Kehoe⁴³, J.S. Keller⁴⁵, J.J. Kempster⁸⁰, H. Keoshkerian¹⁶¹, O. Kepka¹²⁹,
 B.P. Kerševan⁷⁸, S. Kersten¹⁷⁸, R.A. Keyes⁹⁰, M. Khader¹⁶⁹, F. Khalil-zada¹², A. Khanov¹¹⁶,
 A.G. Kharlamov^{111,c}, T. Kharlamova^{111,c}, A. Khodinov¹⁶⁰, T.J. Khoo⁵², V. Khovanskiy^{99,*},
 E. Khramov⁶⁸, J. Khubua^{54b,ad}, S. Kido⁷⁰, C.R. Kilby⁸⁰, H.Y. Kim⁸, S.H. Kim¹⁶⁴, Y.K. Kim³³,
 N. Kimura¹⁵⁶, O.M. Kind¹⁷, B.T. King⁷⁷, D. Kirchmeier⁴⁷, J. Kirk¹³³, A.E. Kiryunin¹⁰³,
 T. Kishimoto¹⁵⁷, D. Kisielewska^{41a}, K. Kiuchi¹⁶⁴, O. Kivernyk⁵, E. Kladiva^{146b},
 T. Klapdor-Kleingrothaus⁵¹, M.H. Klein³⁸, M. Klein⁷⁷, U. Klein⁷⁷, K. Kleinknecht⁸⁶, P. Klimek¹¹⁰,
 A. Klimentov²⁷, R. Klingenberg⁴⁶, T. Klingl²³, T. Klioutchnikova³², E.-E. Kluge^{60a}, P. Kluit¹⁰⁹,
 S. Kluth¹⁰³, J. Knapik⁴², E. Knerner⁶⁵, E.B.F.G. Knoops⁸⁸, A. Knue¹⁰³, A. Kobayashi¹⁵⁷,
 D. Kobayashi¹⁵⁹, T. Kobayashi¹⁵⁷, M. Kobel⁴⁷, M. Kocian¹⁴⁵, P. Kodys¹³¹, T. Koffas³¹, E. Koffeman¹⁰⁹,
 N.M. Köhler¹⁰³, T. Koi¹⁴⁵, M. Kolb^{60b}, I. Koletsou⁵, A.A. Komar^{98,*}, Y. Komori¹⁵⁷, T. Kondo⁶⁹,
 N. Kondrashova^{36c}, K. Köneke⁵¹, A.C. König¹⁰⁸, T. Kono^{69,ae}, R. Konoplich^{112,af}, N. Konstantinidis⁸¹,
 R. Kopeliansky⁶⁴, S. Koperny^{41a}, A.K. Kopp⁵¹, K. Korcyl⁴², K. Kordas¹⁵⁶, A. Korn⁸¹, A.A. Korol^{111,c},
 I. Korolkov¹³, E.V. Korolkova¹⁴¹, O. Kortner¹⁰³, S. Kortner¹⁰³, T. Kosek¹³¹, V.V. Kostyukhin²³,
 A. Kotwal⁴⁸, A. Koulouris¹⁰, A. Kourkoumeli-Charalampidi^{123a,123b}, C. Kourkoumelis⁹, E. Kourlitis¹⁴¹,
 V. Kouskoura²⁷, A.B. Kowalewska⁴², R. Kowalewski¹⁷², T.Z. Kowalski^{41a}, C. Kozakai¹⁵⁷,
 W. Kozanecki¹³⁸, A.S. Kozhin¹³², V.A. Kramarenko¹⁰¹, G. Kramberger⁷⁸, D. Krasnopalovtsev¹⁰⁰,
 M.W. Krasny⁸³, A. Krasznahorkay³², D. Krauss¹⁰³, J.A. Kremer^{41a}, J. Kretzschmar⁷⁷, K. Kreutzfeldt⁵⁵,
 P. Krieger¹⁶¹, K. Krizka³³, K. Kroeninger⁴⁶, H. Kroha¹⁰³, J. Kroll¹²⁹, J. Kroll¹²⁴, J. Kroseberg²³,
 J. Krstic¹⁴, U. Kruchonak⁶⁸, H. Krüger²³, N. Krumnack⁶⁷, M.C. Kruse⁴⁸, T. Kubota⁹¹, H. Kucuk⁸¹,
 S. Kuday^{4b}, J.T. Kuechler¹⁷⁸, S. Kuehn³², A. Kugel^{60c}, F. Kuger¹⁷⁷, T. Kuhl⁴⁵, V. Kukhtin⁶⁸, R. Kukla⁸⁸,
 Y. Kulchitsky⁹⁵, S. Kuleshov^{34b}, Y.P. Kulinich¹⁶⁹, M. Kuna^{134a,134b}, T. Kunigo⁷¹, A. Kupco¹²⁹,
 O. Kuprash¹⁵⁵, H. Kurashige⁷⁰, L.L. Kurchaninov^{163a}, Y.A. Kurochkin⁹⁵, M.G. Kurth^{35a,35d}, V. Kus¹²⁹,
 E.S. Kuwertz¹⁷², M. Kuze¹⁵⁹, J. Kvita¹¹⁷, T. Kwan¹⁷², D. Kyriazopoulos¹⁴¹, A. La Rosa¹⁰³,
 J.L. La Rosa Navarro^{26d}, L. La Rotonda^{40a,40b}, C. Lacasta¹⁷⁰, F. Lacava^{134a,134b}, J. Lacey⁴⁵, H. Lacker¹⁷,
 D. Lacour⁸³, E. Ladygin⁶⁸, R. Lafaye⁵, B. Laforge⁸³, T. Lagouri¹⁷⁹, S. Lai⁵⁷, S. Lammers⁶⁴, W. Lamp⁷,
 E. Lançon²⁷, U. Landgraf⁵¹, M.P.J. Landon⁷⁹, M.C. Lanfermann⁵², V.S. Lang^{60a}, J.C. Lange¹³,
 A.J. Lankford¹⁶⁶, F. Lanni²⁷, K. Lantzsch²³, A. Lanza^{123a}, A. Lapertosa^{53a,53b}, S. Laplace⁸³,
 J.F. Laporte¹³⁸, T. Lari^{94a}, F. Lasagni Manghi^{22a,22b}, M. Lassnig³², P. Laurelli⁵⁰, W. Lavrijssen¹⁶,

A.T. Law¹³⁹, P. Laycock⁷⁷, T. Lazovich⁵⁹, M. Lazzaroni^{94a,94b}, B. Le⁹¹, O. Le Dertz⁸³, E. Le Guirriec⁸⁸,
 E.P. Le Quilleuc¹³⁸, M. LeBlanc¹⁷², T. LeCompte⁶, F. Ledroit-Guillon⁵⁸, C.A. Lee²⁷, G.R. Lee^{133,ag},
 S.C. Lee¹⁵³, L. Lee⁵⁹, B. Lefebvre⁹⁰, G. Lefebvre⁸³, M. Lefebvre¹⁷², F. Legger¹⁰², C. Leggett¹⁶,
 A. Lehan⁷⁷, G. Lehmann Miotto³², X. Lei⁷, W.A. Leight⁴⁵, M.A.L. Leite^{26d}, R. Leitner¹³¹,
 D. Lellouch¹⁷⁵, B. Lemmer⁵⁷, K.J.C. Leney⁸¹, T. Lenz²³, B. Lenzi³², R. Leone⁷, S. Leone^{126a,126b},
 C. Leonidopoulos⁴⁹, G. Lerner¹⁵¹, C. Leroy⁹⁷, A.A.J. Lesage¹³⁸, C.G. Lester³⁰, M. Levchenko¹²⁵,
 J. Levêque⁵, D. Levin⁹², L.J. Levinson¹⁷⁵, M. Levy¹⁹, D. Lewis⁷⁹, B. Li^{36a,w}, Changqiao Li^{36a}, H. Li¹⁵⁰,
 L. Li^{36c}, Q. Li^{35a,35d}, S. Li⁴⁸, X. Li^{36c}, Y. Li¹⁴³, Z. Liang^{35a}, B. Liberti^{135a}, A. Liblong¹⁶¹, K. Lie^{62c},
 J. Liebal²³, W. Liebig¹⁵, A. Limosani¹⁵², S.C. Lin^{153,ah}, T.H. Lin⁸⁶, B.E. Lindquist¹⁵⁰, A.E. Lioni⁵²,
 E. Lipeles¹²⁴, A. Lipniacka¹⁵, M. Lisovyi^{60b}, T.M. Liss^{169,ai}, A. Lister¹⁷¹, A.M. Litke¹³⁹, B. Liu^{153,aj},
 H. Liu⁹², H. Liu²⁷, J.K.K. Liu¹²², J. Liu^{36b}, J.B. Liu^{36a}, K. Liu⁸⁸, L. Liu¹⁶⁹, M. Liu^{36a}, Y.L. Liu^{36a},
 Y. Liu^{36a}, M. Livan^{123a,123b}, A. Lleres⁵⁸, J. Llorente Merino^{35a}, S.L. Lloyd⁷⁹, C.Y. Lo^{62b},
 F. Lo Sterzo¹⁵³, E.M. Lobodzinska⁴⁵, P. Loch⁷, F.K. Loebinger⁸⁷, K.M. Loew²⁵, A. Loginov^{179,*},
 T. Lohse¹⁷, K. Lohwasser⁴⁵, M. Lokajicek¹²⁹, B.A. Long²⁴, J.D. Long¹⁶⁹, R.E. Long⁷⁵, L. Longo^{76a,76b},
 K.A.Looper¹¹³, J.A. Lopez^{34b}, D. Lopez Mateos⁵⁹, I. Lopez Paz¹³, A. Lopez Solis⁸³, J. Lorenz¹⁰²,
 N. Lorenzo Martinez⁵, M. Losada²¹, P.J. Lösel¹⁰², X. Lou^{35a}, A. Lounis¹¹⁹, J. Love⁶, P.A. Love⁷⁵,
 H. Lu^{62a}, N. Lu⁹², Y.J. Lu⁶³, H.J. Lubatti¹⁴⁰, C. Luci^{134a,134b}, A. Lucotte⁵⁸, C. Luedtke⁵¹, F. Luehring⁶⁴,
 W. Lukas⁶⁵, L. Luminari^{134a}, O. Lundberg^{148a,148b}, B. Lund-Jensen¹⁴⁹, P.M. Luzi⁸³, D. Lynn²⁷,
 R. Lysak¹²⁹, E. Lytken⁸⁴, V. Lyubushkin⁶⁸, H. Ma²⁷, L.L. Ma^{36b}, Y. Ma^{36b}, G. Maccarrone⁵⁰,
 A. Macchiolo¹⁰³, C.M. Macdonald¹⁴¹, B. Maček⁷⁸, J. Machado Miguens^{124,128b}, D. Madaffari⁸⁸,
 R. Madar³⁷, H.J. Maddocks¹⁶⁸, W.F. Mader⁴⁷, A. Madsen⁴⁵, J. Maeda⁷⁰, S. Maeland¹⁵, T. Maeno²⁷,
 A.S. Maevskiy¹⁰¹, E. Magradze⁵⁷, J. Mahlstedt¹⁰⁹, C. Maiani¹¹⁹, C. Maidantchik^{26a}, A.A. Maier¹⁰³,
 T. Maier¹⁰², A. Maio^{128a,128b,128d}, S. Majewski¹¹⁸, Y. Makida⁶⁹, N. Makovec¹¹⁹, B. Malaescu⁸³,
 Pa. Malecki⁴², V.P. Maleev¹²⁵, F. Malek⁵⁸, U. Mallik⁶⁶, D. Malon⁶, C. Malone³⁰, S. Maltezos¹⁰,
 S. Malyukov³², J. Mamuzic¹⁷⁰, G. Mancini⁵⁰, L. Mandelli^{94a}, I. Mandić⁷⁸, J. Maneira^{128a,128b},
 L. Manhaes de Andrade Filho^{26b}, J. Manjarres Ramos⁴⁷, A. Mann¹⁰², A. Manousos³², B. Mansoulié¹³⁸,
 J.D. Mansour^{35a}, R. Mantifel⁹⁰, M. Mantoani⁵⁷, S. Manzoni^{94a,94b}, L. Mapelli³², G. Marceca²⁹,
 L. March⁵², L. Marchese¹²², G. Marchiori⁸³, M. Marcisovsky¹²⁹, M. Marjanovic³⁷, D.E. Marley⁹²,
 F. Marroquim^{26a}, S.P. Marsden⁸⁷, Z. Marshall¹⁶, M.U.F Martensson¹⁶⁸, S. Marti-Garcia¹⁷⁰,
 C.B. Martin¹¹³, T.A. Martin¹⁷³, V.J. Martin⁴⁹, B. Martin dit Latour¹⁵, M. Martinez^{13,v},
 VI. Martinez Outschoorn¹⁶⁹, S. Martin-Haugh¹³³, V.S. Martoiu^{28b}, A.C. Martyniuk⁸¹, A. Marzin³²,
 L. Masetti⁸⁶, T. Mashimo¹⁵⁷, R. Mashinistov⁹⁸, J. Masik⁸⁷, A.L. Maslennikov^{111,c}, L. Massa^{135a,135b},
 P. Mastrandrea⁵, A. Mastroberardino^{40a,40b}, T. Masubuchi¹⁵⁷, P. Mättig¹⁷⁸, J. Maurer^{28b}, S.J. Maxfield⁷⁷,
 D.A. Maximov^{111,c}, R. Mazini¹⁵³, I. Maznias¹⁵⁶, S.M. Mazza^{94a,94b}, N.C. Mc Fadden¹⁰⁷,
 G. Mc Goldrick¹⁶¹, S.P. Mc Kee⁹², A. McCarn⁹², R.L. McCarthy¹⁵⁰, T.G. McCarthy¹⁰³,
 L.I. McClymont⁸¹, E.F. McDonald⁹¹, J.A. McFayden⁸¹, G. Mchedlidze⁵⁷, S.J. McMahon¹³³,
 P.C. McNamara⁹¹, R.A. McPherson^{172,o}, S. Meehan¹⁴⁰, T.J. Megy⁵¹, S. Mehlhase¹⁰², A. Mehta⁷⁷,
 T. Meideck⁵⁸, K. Meier^{60a}, B. Meirose⁴⁴, D. Melini^{170,ak}, B.R. Mellado Garcia^{147c}, J.D. Mellenthin⁵⁷,
 M. Melo^{146a}, F. Meloni¹⁸, S.B. Menary⁸⁷, L. Meng⁷⁷, X.T. Meng⁹², A. Mengarelli^{22a,22b}, S. Menke¹⁰³,
 E. Meoni^{40a,40b}, S. Mergelmeyer¹⁷, P. Mermod⁵², L. Merola^{106a,106b}, C. Meroni^{94a}, F.S. Merritt³³,
 A. Messina^{134a,134b}, J. Metcalfe⁶, A.S. Mete¹⁶⁶, C. Meyer¹²⁴, J.-P. Meyer¹³⁸, J. Meyer¹⁰⁹,
 H. Meyer Zu Theenhausen^{60a}, F. Miano¹⁵¹, R.P. Middleton¹³³, S. Miglioranzi^{53a,53b}, L. Mijović⁴⁹,
 G. Mikenberg¹⁷⁵, M. Mikestikova¹²⁹, M. Mikuž⁷⁸, M. Milesi⁹¹, A. Milic²⁷, D.W. Miller³³, C. Mills⁴⁹,
 A. Milov¹⁷⁵, D.A. Milstead^{148a,148b}, A.A. Minaenko¹³², Y. Minami¹⁵⁷, I.A. Minashvili^{54b},
 A.I. Mincer¹¹², B. Mindur^{41a}, M. Mineev⁶⁸, Y. Minegishi¹⁵⁷, Y. Ming¹⁷⁶, L.M. Mir¹³, K.P. Mistry¹²⁴,
 T. Mitani¹⁷⁴, J. Mitrevski¹⁰², V.A. Mitsou¹⁷⁰, A. Miucci¹⁸, P.S. Miyagawa¹⁴¹, A. Mizukami⁶⁹,
 J.U. Mjörnmark⁸⁴, T. Mkrtchyan¹⁸⁰, M. Mlynarikova¹³¹, T. Moa^{148a,148b}, K. Mochizuki⁹⁷, P. Mogg⁵¹,

S. Mohapatra³⁸, S. Molander^{148a,148b}, R. Moles-Valls²³, R. Monden⁷¹, M.C. Mondragon⁹³, K. Mönig⁴⁵, J. Monk³⁹, E. Monnier⁸⁸, A. Montalbano¹⁵⁰, J. Montejo Berlingen³², F. Monticelli⁷⁴, S. Monzani^{94a,94b}, R.W. Moore³, N. Morange¹¹⁹, D. Moreno²¹, M. Moreno Llácer⁵⁷, P. Morettini^{53a}, S. Morgenstern³², D. Mori¹⁴⁴, T. Mori¹⁵⁷, M. Morii⁵⁹, M. Morinaga¹⁵⁷, V. Morisbak¹²¹, A.K. Morley¹⁵², G. Mornacchi³², J.D. Morris⁷⁹, L. Morvaj¹⁵⁰, P. Moschovakos¹⁰, M. Mosidze^{54b}, H.J. Moss¹⁴¹, J. Moss^{145,al}, K. Motohashi¹⁵⁹, R. Mount¹⁴⁵, E. Mountricha²⁷, E.J.W. Moyse⁸⁹, S. Muanza⁸⁸, R.D. Mudd¹⁹, F. Mueller¹⁰³, J. Mueller¹²⁷, R.S.P. Mueller¹⁰², D. Muenstermann⁷⁵, P. Mullen⁵⁶, G.A. Mullier¹⁸, F.J. Munoz Sanchez⁸⁷, W.J. Murray^{173,133}, H. Musheghyan³², M. Muškinja⁷⁸, A.G. Myagkov^{132,am}, M. Myska¹³⁰, B.P. Nachman¹⁶, O. Nackenhorst⁵², K. Nagai¹²², R. Nagai^{69,ae}, K. Nagano⁶⁹, Y. Nagasaka⁶¹, K. Nagata¹⁶⁴, M. Nagel⁵¹, E. Nagy⁸⁸, A.M. Nairz³², Y. Nakahama¹⁰⁵, K. Nakamura⁶⁹, T. Nakamura¹⁵⁷, I. Nakano¹¹⁴, R.F. Naranjo Garcia⁴⁵, R. Narayan¹¹, D.I. Narrias Villar^{60a}, I. Naryshkin¹²⁵, T. Naumann⁴⁵, G. Navarro²¹, R. Nayyar⁷, H.A. Neal⁹², P.Yu. Nechaeva⁹⁸, T.J. Neep¹³⁸, A. Negri^{123a,123b}, M. Negrini^{22a}, S. Nektarijevic¹⁰⁸, C. Nellist¹¹⁹, A. Nelson¹⁶⁶, M.E. Nelson¹²², S. Nemecek¹²⁹, P. Nemethy¹¹², M. Nessi^{32,an}, M.S. Neubauer¹⁶⁹, M. Neumann¹⁷⁸, P.R. Newman¹⁹, T.Y. Ng^{62c}, T. Nguyen Manh⁹⁷, R.B. Nickerson¹²², R. Nicolaïdou¹³⁸, J. Nielsen¹³⁹, V. Nikolaenko^{132,am}, I. Nikolic-Audit⁸³, K. Nikolopoulos¹⁹, J.K. Nilsen¹²¹, P. Nilsson²⁷, Y. Ninomiya¹⁵⁷, A. Nisati^{134a}, N. Nishu^{35c}, R. Nisius¹⁰³, T. Nobe¹⁵⁷, Y. Noguchi⁷¹, M. Nomachi¹²⁰, I. Nomidis³¹, M.A. Nomura²⁷, T. Nooney⁷⁹, M. Nordberg³², N. Norjoharuddeen¹²², O. Novgorodova⁴⁷, M. Nozaki⁶⁹, L. Nozka¹¹⁷, K. Ntekas¹⁶⁶, E. Nurse⁸¹, F. Nuti⁹¹, K. O'connor²⁵, D.C. O'Neil¹⁴⁴, A.A. O'Rourke⁴⁵, V. O'Shea⁵⁶, F.G. Oakham^{31,d}, H. Oberlack¹⁰³, T. Obermann²³, J. Ocariz⁸³, A. Ochi⁷⁰, I. Ochoa³⁸, J.P. Ochoa-Ricoux^{34a}, S. Oda⁷³, S. Odaka⁶⁹, H. Ogren⁶⁴, A. Oh⁸⁷, S.H. Oh⁴⁸, C.C. Ohm¹⁶, H. Ohman¹⁶⁸, H. Oide^{53a,53b}, H. Okawa¹⁶⁴, Y. Okumura¹⁵⁷, T. Okuyama⁶⁹, A. Olariu^{28b}, L.F. Oleiro Seabra^{128a}, S.A. Olivares Pino⁴⁹, D. Oliveira Damazio²⁷, A. Olszewski⁴², J. Olszowska⁴², A. Onofre^{128a,128e}, K. Onogi¹⁰⁵, P.U.E. Onyisi^{11,aa}, M.J. Oreglia³³, Y. Oren¹⁵⁵, D. Orestano^{136a,136b}, N. Orlando^{62b}, R.S. Orr¹⁶¹, B. Osculati^{53a,53b,*}, R. Osipanov^{36a}, G. Otero y Garzon²⁹, H. Otono⁷³, M. Ouchrif^{137d}, F. Ould-Saada¹²¹, A. Ouraou¹³⁸, K.P. Oussoren¹⁰⁹, Q. Ouyang^{35a}, M. Owen⁵⁶, R.E. Owen¹⁹, V.E. Ozcan^{20a}, N. Ozturk⁸, K. Pachal¹⁴⁴, A. Pacheco Pages¹³, L. Pacheco Rodriguez¹³⁸, C. Padilla Aranda¹³, S. Pagan Griso¹⁶, M. Paganini¹⁷⁹, F. Paige²⁷, G. Palacino⁶⁴, S. Palazzo^{40a,40b}, S. Palestini³², M. Palka^{41b}, D. Pallin³⁷, E.St. Panagiotopoulou¹⁰, I. Panagoulias¹⁰, C.E. Pandini⁸³, J.G. Panduro Vazquez⁸⁰, P. Pani³², S. Panitkin²⁷, D. Pantea^{28b}, L. Paolozzi⁵², Th.D. Papadopoulou¹⁰, K. Papageorgiou^{9,s}, A. Paramonov⁶, D. Paredes Hernandez¹⁷⁹, A.J. Parker⁷⁵, M.A. Parker³⁰, K.A. Parker⁴⁵, F. Parodi^{53a,53b}, J.A. Parsons³⁸, U. Parzefall⁵¹, V.R. Pascuzzi¹⁶¹, J.M. Pasner¹³⁹, E. Pasqualucci^{134a}, S. Passaggio^{53a}, Fr. Pastore⁸⁰, S. Pataraia¹⁷⁸, J.R. Pater⁸⁷, T. Pauly³², B. Pearson¹⁰³, S. Pedraza Lopez¹⁷⁰, R. Pedro^{128a,128b}, S.V. Peleganchuk^{111,c}, O. Penc¹²⁹, C. Peng^{35a,35d}, H. Peng^{36a}, J. Penwell⁶⁴, B.S. Peralva^{26b}, M.M. Perego¹³⁸, D.V. Perepelitsa²⁷, L. Perini^{94a,94b}, H. Pernegger³², S. Perrella^{106a,106b}, R. Peschke⁴⁵, V.D. Peshekhanov^{68,*}, K. Peters⁴⁵, R.F.Y. Peters⁸⁷, B.A. Petersen³², T.C. Petersen³⁹, E. Petit⁵⁸, A. Petridis¹, C. Petridou¹⁵⁶, P. Petroff¹¹⁹, E. Petrolo^{134a}, M. Petrov¹²², F. Petrucci^{136a,136b}, N.E. Pettersson⁸⁹, A. Peyaud¹³⁸, R. Pezoa^{34b}, F.H. Phillips⁹³, P.W. Phillips¹³³, G. Piacquadio¹⁵⁰, E. Pianori¹⁷³, A. Picazio⁸⁹, E. Piccaro⁷⁹, M.A. Pickering¹²², R. Piegai²⁹, J.E. Pilcher³³, A.D. Pilkington⁸⁷, A.W.J. Pin⁸⁷, M. Pinamonti^{135a,135b}, J.L. Pinfold³, H. Pirumov⁴⁵, M. Pitt¹⁷⁵, L. Plazak^{146a}, M.-A. Pleier²⁷, V. Pleskot⁸⁶, E. Plotnikova⁶⁸, D. Pluth⁶⁷, P. Podberezko¹¹¹, R. Poettgen^{148a,148b}, R. Poggi^{123a,123b}, L. Poggioli¹¹⁹, D. Pohl²³, G. Polesello^{123a}, A. Poley⁴⁵, A. Policicchio^{40a,40b}, R. Polifka³², A. Polini^{22a}, C.S. Pollard⁵⁶, V. Polychronakos²⁷, K. Pommès³², D. Ponomarenko¹⁰⁰, L. Pontecorvo^{134a}, B.G. Pope⁹³, G.A. Popeneciu^{28d}, A. Poppleton³², S. Pospisil¹³⁰, K. Potamianos¹⁶, I.N. Potrap⁶⁸, C.J. Potter³⁰, G. Poulard³², T. Poulsen⁸⁴, J. Poveda³², M.E. Pozo Astigarraga³², P. Pralavorio⁸⁸, A. Pranko¹⁶, S. Prell⁶⁷, D. Price⁸⁷, L.E. Price⁶, M. Primavera^{76a}, S. Prince⁹⁰, N. Proklova¹⁰⁰, K. Prokofiev^{62c}, F. Prokoshin^{34b}, S. Protopopescu²⁷,

J. Proudfoot⁶, M. Przybycien^{41a}, A. Puri¹⁶⁹, P. Puzo¹¹⁹, J. Qian⁹², G. Qin⁵⁶, Y. Qin⁸⁷, A. Quadt⁵⁷,
 M. Queitsch-Maitland⁴⁵, D. Quilty⁵⁶, S. Raddum¹²¹, V. Radeka²⁷, V. Radescu¹²²,
 S.K. Radhakrishnan¹⁵⁰, P. Radloff¹¹⁸, P. Rados⁹¹, F. Ragusa^{94a,94b}, G. Rahal¹⁸¹, J.A. Raine⁸⁷,
 S. Rajagopalan²⁷, C. Rangel-Smith¹⁶⁸, T. Rashid¹¹⁹, M.G. Ratti^{94a,94b}, D.M. Rauch⁴⁵, F. Rauscher¹⁰²,
 S. Rave⁸⁶, I. Ravinovich¹⁷⁵, J.H. Rawling⁸⁷, M. Raymond³², A.L. Read¹²¹, N.P. Readioff⁵⁸,
 M. Reale^{76a,76b}, D.M. Rebuzzi^{123a,123b}, A. Redelbach¹⁷⁷, G. Redlinger²⁷, R. Reece¹³⁹, R.G. Reed^{147c},
 K. Reeves⁴⁴, L. Rehnisch¹⁷, J. Reichert¹²⁴, A. Reiss⁸⁶, C. Rembser³², H. Ren^{35a,35d}, M. Rescigno^{134a},
 S. Resconi^{94a}, E.D. Ressegue¹²⁴, S. Rettie¹⁷¹, E. Reynolds¹⁹, O.L. Rezanova^{111,c}, P. Reznicek¹³¹,
 R. Rezvani⁹⁷, R. Richter¹⁰³, S. Richter⁸¹, E. Richter-Was^{41b}, O. Ricken²³, M. Ridel⁸³, P. Rieck¹⁰³,
 C.J. Riegel¹⁷⁸, J. Rieger⁵⁷, O. Rifki¹¹⁵, M. Rijssenbeek¹⁵⁰, A. Rimoldi^{123a,123b}, M. Rimoldi¹⁸,
 L. Rinaldi^{22a}, B. Ristic⁵², E. Ritsch³², I. Riu¹³, F. Rizatdinova¹¹⁶, E. Rizvi⁷⁹, C. Rizzi¹³, R.T. Roberts⁸⁷,
 S.H. Robertson^{90,o}, A. Robichaud-Veronneau⁹⁰, D. Robinson³⁰, J.E.M. Robinson⁴⁵, A. Robson⁵⁶,
 E. Rocco⁸⁶, C. Roda^{126a,126b}, Y. Rodina^{88,ao}, S. Rodriguez Bosca¹⁷⁰, A. Rodriguez Perez¹³,
 D. Rodriguez Rodriguez¹⁷⁰, S. Roe³², C.S. Rogan⁵⁹, O. Røhne¹²¹, J. Roloff⁵⁹, A. Romaniouk¹⁰⁰,
 M. Romano^{22a,22b}, S.M. Romano Saez³⁷, E. Romero Adam¹⁷⁰, N. Rompotis⁷⁷, M. Ronzani⁵¹, L. Roos⁸³,
 S. Rosati^{134a}, K. Rosbach⁵¹, P. Rose¹³⁹, N.-A. Rosien⁵⁷, E. Rossi^{106a,106b}, L.P. Rossi^{53a}, J.H.N. Rosten³⁰,
 R. Rosten¹⁴⁰, M. Rotaru^{28b}, I. Roth¹⁷⁵, J. Rothberg¹⁴⁰, D. Rousseau¹¹⁹, A. Rozanova⁸⁸, Y. Rozen¹⁵⁴,
 X. Ruan^{147c}, F. Rubbo¹⁴⁵, F. Rühr⁵¹, A. Ruiz-Martinez³¹, Z. Rurikova⁵¹, N.A. Rusakovich⁶⁸,
 H.L. Russell⁹⁰, J.P. Rutherford⁷, N. Ruthmann³², Y.F. Ryabov¹²⁵, M. Rybar¹⁶⁹, G. Rybkin¹¹⁹, S. Ryu⁶,
 A. Ryzhov¹³², G.F. Rzehorz⁵⁷, A.F. Saavedra¹⁵², G. Sabato¹⁰⁹, S. Sacerdoti²⁹, H.F-W. Sadrozinski¹³⁹,
 R. Sadykov⁶⁸, F. Safai Tehrani^{134a}, P. Saha¹¹⁰, M. Sahinsoy^{60a}, M. Saimpert⁴⁵, M. Saito¹⁵⁷, T. Saito¹⁵⁷,
 H. Sakamoto¹⁵⁷, Y. Sakurai¹⁷⁴, G. Salamanna^{136a,136b}, J.E. Salazar Loyola^{34b}, D. Salek¹⁰⁹,
 P.H. Sales De Bruin¹⁶⁸, D. Salihagic¹⁰³, A. Salnikov¹⁴⁵, J. Salt¹⁷⁰, D. Salvatore^{40a,40b}, F. Salvatore¹⁵¹,
 A. Salvucci^{62a,62b,62c}, A. Salzburger³², D. Sammel⁵¹, D. Sampsonidis¹⁵⁶, D. Sampsonidou¹⁵⁶,
 J. Sánchez¹⁷⁰, V. Sanchez Martinez¹⁷⁰, A. Sanchez Pineda^{167a,167c}, H. Sandaker¹²¹, R.L. Sandbach⁷⁹,
 C.O. Sander⁴⁵, M. Sandhoff¹⁷⁸, C. Sandoval²¹, D.P.C. Sankey¹³³, M. Sannino^{53a,53b}, A. Sansoni⁵⁰,
 C. Santoni³⁷, R. Santonico^{135a,135b}, H. Santos^{128a}, I. Santoyo Castillo¹⁵¹, A. Sapronov⁶⁸,
 J.G. Saraiva^{128a,128d}, B. Sarrazin²³, O. Sasaki⁶⁹, K. Sato¹⁶⁴, E. Sauvan⁵, G. Savage⁸⁰, P. Savard^{161,d},
 N. Savic¹⁰³, C. Sawyer¹³³, L. Sawyer^{82,u}, J. Saxon³³, C. Sbarra^{22a}, A. Sbrizzi^{22a,22b}, T. Scanlon⁸¹,
 D.A. Scannicchio¹⁶⁶, M. Scarcella¹⁵², V. Scarfone^{40a,40b}, J. Schaarschmidt¹⁴⁰, P. Schacht¹⁰³,
 B.M. Schachtner¹⁰², D. Schaefer³², L. Schaefer¹²⁴, R. Schaefer⁴⁵, J. Schaeffer⁸⁶, S. Schaepe²³,
 S. Schaetzl^{60b}, U. Schäfer⁸⁶, A.C. Schaffer¹¹⁹, D. Schaile¹⁰², R.D. Schamberger¹⁵⁰, V. Scharf^{60a},
 V.A. Schegelsky¹²⁵, D. Scheirich¹³¹, M. Schernau¹⁶⁶, C. Schiavi^{53a,53b}, S. Schier¹³⁹, L.K. Schildgen²³,
 C. Schillo⁵¹, M. Schioppa^{40a,40b}, S. Schlenker³², K.R. Schmidt-Sommerfeld¹⁰³, K. Schmieden³²,
 C. Schmitt⁸⁶, S. Schmitt⁴⁵, S. Schmitz⁸⁶, U. Schnoor⁵¹, L. Schoeffel¹³⁸, A. Schoening^{60b},
 B.D. Schoenrock⁹³, E. Schopf²³, M. Schott⁸⁶, J.F.P. Schouwenberg¹⁰⁸, J. Schovancova³², S. Schramm⁵²,
 N. Schuh⁸⁶, A. Schulte⁸⁶, M.J. Schultens²³, H.-C. Schultz-Coulon^{60a}, H. Schulz¹⁷, M. Schumacher⁵¹,
 B.A. Schumm¹³⁹, Ph. Schune¹³⁸, A. Schwartzman¹⁴⁵, T.A. Schwarz⁹², H. Schweiger⁸⁷,
 Ph. Schwemling¹³⁸, R. Schwienhorst⁹³, J. Schwindling¹³⁸, A. Sciandra²³, G. Sciolla²⁵, F. Scuri^{126a,126b},
 F. Scutti⁹¹, J. Searcy⁹², P. Seema²³, S.C. Seidel¹⁰⁷, A. Seiden¹³⁹, J.M. Seixas^{26a}, G. Sekhniaidze^{106a},
 K. Sekhon⁹², S.J. Sekula⁴³, N. Semprini-Cesari^{22a,22b}, S. Senkin³⁷, C. Serfon¹²¹, L. Serin¹¹⁹,
 L. Serkin^{167a,167b}, M. Sessa^{136a,136b}, R. Seuster¹⁷², H. Severini¹¹⁵, T. Sfiligoj⁷⁸, F. Sforza³², A. Sfyrla⁵²,
 E. Shabalina⁵⁷, N.W. Shaikh^{148a,148b}, L.Y. Shan^{35a}, R. Shang¹⁶⁹, J.T. Shank²⁴, M. Shapiro¹⁶,
 P.B. Shatalov⁹⁹, K. Shaw^{167a,167b}, S.M. Shaw⁸⁷, A. Shcherbakova^{148a,148b}, C.Y. Shehu¹⁵¹, Y. Shen¹¹⁵,
 P. Sherwood⁸¹, L. Shi^{153,ap}, S. Shimizu⁷⁰, C.O. Shimmin¹⁷⁹, M. Shimojima¹⁰⁴, I.P.J. Shipsey¹²²,
 S. Shirabe⁷³, M. Shiyakova^{68,aq}, J. Shlomi¹⁷⁵, A. Shmeleva⁹⁸, D. Shoaleh Saadi⁹⁷, M.J. Shochet³³,
 S. Shojaii^{94a}, D.R. Shope¹¹⁵, S. Shrestha¹¹³, E. Shulga¹⁰⁰, M.A. Shupe⁷, P. Sicho¹²⁹, A.M. Sickles¹⁶⁹,

P.E. Sidebo¹⁴⁹, E. Sideras Haddad^{147c}, O. Sidiropoulou¹⁷⁷, D. Sidorov¹¹⁶, A. Sidoti^{22a,22b}, F. Siegert⁴⁷, Dj. Sijacki¹⁴, J. Silva^{128a,128d}, S.B. Silverstein^{148a}, V. Simak¹³⁰, L. Simic¹⁴, S. Simion¹¹⁹, E. Simioni⁸⁶, B. Simmons⁸¹, M. Simon⁸⁶, P. Sinervo¹⁶¹, N.B. Sinev¹¹⁸, M. Sioli^{22a,22b}, G. Siragusa¹⁷⁷, I. Siral⁹², S.Yu. Sivoklokov¹⁰¹, J. Sjölin^{148a,148b}, M.B. Skinner⁷⁵, P. Skubic¹¹⁵, M. Slater¹⁹, T. Slavicek¹³⁰, M. Slawinska⁴², K. Sliwa¹⁶⁵, R. Slovak¹³¹, V. Smakhtin¹⁷⁵, B.H. Smart⁵, J. Smiesko^{146a}, N. Smirnov¹⁰⁰, S.Yu. Smirnov¹⁰⁰, Y. Smirnov¹⁰⁰, L.N. Smirnova^{101,ar}, O. Smirnova⁸⁴, J.W. Smith⁵⁷, M.N.K. Smith³⁸, R.W. Smith³⁸, M. Smizanska⁷⁵, K. Smolek¹³⁰, A.A. Snesarev⁹⁸, I.M. Snyder¹¹⁸, S. Snyder²⁷, R. Sobie^{172,o}, F. Socher⁴⁷, A. Soffer¹⁵⁵, D.A. Soh¹⁵³, G. Sokhrannyi⁷⁸, C.A. Solans Sanchez³², M. Solar¹³⁰, E.Yu. Soldatov¹⁰⁰, U. Soldevila¹⁷⁰, A.A. Solodkov¹³², A. Soloshenko⁶⁸, O.V. Solovyanov¹³², V. Solovyev¹²⁵, P. Sommer⁵¹, H. Son¹⁶⁵, H.Y. Song^{36a,as}, A. Sopczak¹³⁰, D. Sosa^{60b}, C.L. Sotiropoulou^{126a,126b}, R. Soualah^{167a,167c}, A.M. Soukharev^{111,c}, D. South⁴⁵, B.C. Sowden⁸⁰, S. Spagnolo^{76a,76b}, M. Spalla^{126a,126b}, M. Spangenberg¹⁷³, F. Spanò⁸⁰, D. Sperlich¹⁷, F. Spettel¹⁰³, T.M. Spieker^{60a}, R. Spighi^{22a}, G. Spigo³², L.A. Spiller⁹¹, M. Spousta¹³¹, R.D. St. Denis^{56,*}, A. Stabile^{94a}, R. Stamen^{60a}, S. Stamm¹⁷, E. Stanecka⁴², R.W. Stanek⁶, C. Stanescu^{136a}, M.M. Stanitzki⁴⁵, S. Stapnes¹²¹, E.A. Starchenko¹³², G.H. Stark³³, J. Stark⁵⁸, S.H Stark³⁹, P. Staroba¹²⁹, P. Starovoitov^{60a}, S. Stärz³², R. Staszewski⁴², P. Steinberg²⁷, B. Stelzer¹⁴⁴, H.J. Stelzer³², O. Stelzer-Chilton^{163a}, H. Stenzel⁵⁵, G.A. Stewart⁵⁶, M.C. Stockton¹¹⁸, M. Stoebe⁹⁰, G. Stoica^{28b}, P. Stolte⁵⁷, S. Stonjek¹⁰³, A.R. Stradling⁸, A. Straessner⁴⁷, M.E. Stramaglia¹⁸, J. Strandberg¹⁴⁹, S. Strandberg^{148a,148b}, A. Strandlie¹²¹, M. Strauss¹¹⁵, P. Strizenec^{146b}, R. Ströhmer¹⁷⁷, D.M. Strom¹¹⁸, R. Stroynowski⁴³, A. Strubig¹⁰⁸, S.A. Stucci²⁷, B. Stugu¹⁵, N.A. Styles⁴⁵, D. Su¹⁴⁵, J. Su¹²⁷, S. Suchek^{60a}, Y. Sugaya¹²⁰, M. Suk¹³⁰, V.V. Sulin⁹⁸, S. Sultansoy^{4c}, T. Sumida⁷¹, S. Sun⁵⁹, X. Sun³, K. Suruliz¹⁵¹, C.J.E. Suster¹⁵², M.R. Sutton¹⁵¹, S. Suzuki⁶⁹, M. Svatos¹²⁹, M. Swiatlowski³³, S.P. Swift², I. Sykora^{146a}, T. Sykora¹³¹, D. Ta⁵¹, K. Tackmann⁴⁵, J. Taenzer¹⁵⁵, A. Taffard¹⁶⁶, R. Tafirout^{163a}, N. Taiblum¹⁵⁵, H. Takai²⁷, R. Takashima⁷², T. Takeshita¹⁴², Y. Takubo⁶⁹, M. Talby⁸⁸, A.A. Talyshев^{111,c}, J. Tanaka¹⁵⁷, M. Tanaka¹⁵⁹, R. Tanaka¹¹⁹, S. Tanaka⁶⁹, R. Tanioka⁷⁰, B.B. Tannenwald¹¹³, S. Tapia Araya^{34b}, S. Tapprogge⁸⁶, S. Tarem¹⁵⁴, G.F. Tartarelli^{94a}, P. Tas¹³¹, M. Tasevsky¹²⁹, T. Tashiro⁷¹, E. Tassi^{40a,40b}, A. Tavares Delgado^{128a,128b}, Y. Tayalati^{137e}, A.C. Taylor¹⁰⁷, G.N. Taylor⁹¹, P.T.E. Taylor⁹¹, W. Taylor^{163b}, P. Teixeira-Dias⁸⁰, D. Temple¹⁴⁴, H. Ten Kate³², P.K. Teng¹⁵³, J.J. Teoh¹²⁰, F. Tepel¹⁷⁸, S. Terada⁶⁹, K. Terashi¹⁵⁷, J. Terron⁸⁵, S. Terzo¹³, M. Testa⁵⁰, R.J. Teuscher^{161,o}, T. Theveneaux-Pelzer⁸⁸, J.P. Thomas¹⁹, J. Thomas-Wilsker⁸⁰, P.D. Thompson¹⁹, A.S. Thompson⁵⁶, L.A. Thomsen¹⁷⁹, E. Thomson¹²⁴, M.J. Tibbetts¹⁶, R.E. Ticse Torres⁸⁸, V.O. Tikhomirov^{98,at}, Yu.A. Tikhonov^{111,c}, S. Timoshenko¹⁰⁰, P. Tipton¹⁷⁹, S. Tisserant⁸⁸, K. Todome¹⁵⁹, S. Todorova-Nova⁵, J. Tojo⁷³, S. Tokár^{146a}, K. Tokushuku⁶⁹, E. Tolley⁵⁹, L. Tomlinson⁸⁷, M. Tomoto¹⁰⁵, L. Tompkins^{145,au}, K. Toms¹⁰⁷, B. Tong⁵⁹, P. Tornambe⁵¹, E. Torrence¹¹⁸, H. Torres¹⁴⁴, E. Torró Pastor¹⁴⁰, J. Toth^{88,av}, F. Touchard⁸⁸, D.R. Tovey¹⁴¹, C.J. Treado¹¹², T. Trefzger¹⁷⁷, F. Tresoldi¹⁵¹, A. Tricoli²⁷, I.M. Trigger^{163a}, S. Trincaz-Duvold⁸³, M.F. Tripiana¹³, W. Trischuk¹⁶¹, B. Trocmé⁵⁸, A. Trofymov⁴⁵, C. Troncon^{94a}, M. Trottier-McDonald¹⁶, M. Trovatelli¹⁷², L. Truong^{167a,167c}, M. Trzebinski⁴², A. Trzupek⁴², K.W. Tsang^{62a}, J.C-L. Tseng¹²², P.V. Tsiareshka⁹⁵, G. Tsipolitis¹⁰, N. Tsirintanis⁹, S. Tsiskaridze¹³, V. Tsiskaridze⁵¹, E.G. Tskhadadze^{54a}, K.M. Tsui^{62a}, I.I. Tsukerman⁹⁹, V. Tsulaia¹⁶, S. Tsuno⁶⁹, D. Tsybychev¹⁵⁰, Y. Tu^{62b}, A. Tudorache^{28b}, V. Tudorache^{28b}, T.T. Tulbure^{28a}, A.N. Tuna⁵⁹, S.A. Tupputi^{22a,22b}, S. Turchikhin⁶⁸, D. Turgeman¹⁷⁵, I. Turk Cakir^{4b,aw}, R. Turra^{94a}, P.M. Tuts³⁸, G. Ucchielli^{22a,22b}, I. Ueda⁶⁹, M. Ughetto^{148a,148b}, F. Ukegawa¹⁶⁴, G. Unal³², A. Undrus²⁷, G. Unel¹⁶⁶, F.C. Ungaro⁹¹, Y. Unno⁶⁹, C. Unverdorben¹⁰², J. Urban^{146b}, P. Urquijo⁹¹, P. Urrejola⁸⁶, G. Usai⁸, J. Usui⁶⁹, L. Vacavant⁸⁸, V. Vacek¹³⁰, B. Vachon⁹⁰, C. Valderanis¹⁰², E. Valdes Santurio^{148a,148b}, S. Valentini^{22a,22b}, A. Valero¹⁷⁰, L. Valéry¹³, S. Valkar¹³¹, A. Vallier⁵, J.A. Valls Ferrer¹⁷⁰, W. Van Den Wollenberg¹⁰⁹, H. van der Graaf¹⁰⁹, P. van Gemmeren⁶, J. Van Nieuwkoop¹⁴⁴, I. van Vulpen¹⁰⁹, M.C. van Woerden¹⁰⁹, M. Vanadia^{135a,135b},

W. Vandelli³², A. Vaniachine¹⁶⁰, P. Vankov¹⁰⁹, G. Vardanyan¹⁸⁰, R. Vari^{134a}, E.W. Varnes⁷,
 C. Varni^{53a,53b}, T. Varol⁴³, D. Varouchas¹¹⁹, A. Vartapetian⁸, K.E. Varvell¹⁵², J.G. Vasquez¹⁷⁹,
 G.A. Vasquez^{34b}, F. Vazeille³⁷, T. Vazquez Schroeder⁹⁰, J. Veatch⁵⁷, V. Veeraraghavan⁷, L.M. Veloce¹⁶¹,
 F. Veloso^{128a,128c}, S. Veneziano^{134a}, A. Ventura^{76a,76b}, M. Venturi¹⁷², N. Venturi¹⁶¹, A. Venturini²⁵,
 V. Vercesi^{123a}, M. Verducci^{136a,136b}, W. Verkerke¹⁰⁹, J.C. Vermeulen¹⁰⁹, M.C. Vetterli^{144,d},
 N. Viaux Maira^{34b}, O. Viazlo⁸⁴, I. Vichou^{169,*}, T. Vickey¹⁴¹, O.E. Vickey Boeriu¹⁴¹,
 G.H.A. Viehhauser¹²², S. Viel¹⁶, L. Vigani¹²², M. Villa^{22a,22b}, M. Villaplana Perez^{94a,94b}, E. Vilucchi⁵⁰,
 M.G. Vincter³¹, V.B. Vinogradov⁶⁸, A. Vishwakarma⁴⁵, C. Vittori^{22a,22b}, I. Vivarelli¹⁵¹, S. Vlachos¹⁰,
 M. Vlasak¹³⁰, M. Vogel¹⁷⁸, P. Vokac¹³⁰, G. Volpi^{126a,126b}, H. von der Schmitt¹⁰³, E. von Toerne²³,
 V. Vorobel¹³¹, K. Vorobev¹⁰⁰, M. Vos¹⁷⁰, R. Voss³², J.H. Vossebeld⁷⁷, N. Vranjes¹⁴,
 M. Vranjes Milosavljevic¹⁴, V. Vrba¹³⁰, M. Vreeswijk¹⁰⁹, R. Vuillermet³², I. Vukotic³³, P. Wagner²³,
 W. Wagner¹⁷⁸, J. Wagner-Kuhr¹⁰², H. Wahlberg⁷⁴, S. Wahrmund⁴⁷, J. Wakabayashi¹⁰⁵, J. Walder⁷⁵,
 R. Walker¹⁰², W. Walkowiak¹⁴³, V. Wallangen^{148a,148b}, C. Wang^{35b}, C. Wang^{36b,ax}, F. Wang¹⁷⁶,
 H. Wang¹⁶, H. Wang³, J. Wang⁴⁵, J. Wang¹⁵², Q. Wang¹¹⁵, R. Wang⁶, S.M. Wang¹⁵³, T. Wang³⁸,
 W. Wang^{153,ay}, W. Wang^{36a,as}, Z. Wang^{36c}, C. Wanotayaroj¹¹⁸, A. Warburton⁹⁰, C.P. Ward³⁰,
 D.R. Wardrope⁸¹, A. Washbrook⁴⁹, P.M. Watkins¹⁹, A.T. Watson¹⁹, M.F. Watson¹⁹, G. Watts¹⁴⁰,
 S. Watts⁸⁷, B.M. Waugh⁸¹, A.F. Webb¹¹, S. Webb⁸⁶, M.S. Weber¹⁸, S.W. Weber¹⁷⁷, S.A. Weber³¹,
 J.S. Webster⁶, A.R. Weidberg¹²², B. Weinert⁶⁴, J. Weingarten⁵⁷, C. Weiser⁵¹, H. Weits¹⁰⁹, P.S. Wells³²,
 T. Wenaus²⁷, T. Wengler³², S. Wenig³², N. Wermes²³, M.D. Werner⁶⁷, P. Werner³², M. Wessels^{60a},
 K. Whalen¹¹⁸, N.L. Whallon¹⁴⁰, A.M. Wharton⁷⁵, A.S. White⁹², A. White⁸, M.J. White¹, R. White^{34b},
 D. Whiteson¹⁶⁶, F.J. Wickens¹³³, W. Wiedenmann¹⁷⁶, M. Wielers¹³³, C. Wiglesworth³⁹,
 L.A.M. Wiik-Fuchs²³, A. Wildauer¹⁰³, F. Wilk⁸⁷, H.G. Wilkens³², H.H. Williams¹²⁴, S. Williams¹⁰⁹,
 C. Willis⁹³, S. Willocq⁸⁹, J.A. Wilson¹⁹, I. Wingerter-Seez⁵, E. Winkels¹⁵¹, F. Winklmeier¹¹⁸,
 O.J. Winston¹⁵¹, B.T. Winter²³, M. Wittgen¹⁴⁵, M. Wobisch^{82,u}, T.M.H. Wolf¹⁰⁹, R. Wolff⁸⁸,
 M.W. Wolter⁴², H. Wolters^{128a,128c}, V.W.S. Wong¹⁷¹, S.D. Worm¹⁹, B.K. Wosiek⁴², J. Wotschack³²,
 K.W. Wozniak⁴², M. Wu³³, S.L. Wu¹⁷⁶, X. Wu⁵², Y. Wu⁹², T.R. Wyatt⁸⁷, B.M. Wynne⁴⁹, S. Xella³⁹,
 Z. Xi⁹², L. Xia^{35c}, D. Xu^{35a}, L. Xu²⁷, B. Yabsley¹⁵², S. Yacoob^{147a}, D. Yamaguchi¹⁵⁹, Y. Yamaguchi¹²⁰,
 A. Yamamoto⁶⁹, S. Yamamoto¹⁵⁷, T. Yamanaka¹⁵⁷, K. Yamauchi¹⁰⁵, Y. Yamazaki⁷⁰, Z. Yan²⁴,
 H. Yang^{36c}, H. Yang¹⁶, Y. Yang¹⁵³, Z. Yang¹⁵, W.-M. Yao¹⁶, Y.C. Yap⁸³, Y. Yasu⁶⁹, E. Yatsenko⁵,
 K.H. Yau Wong²³, J. Ye⁴³, S. Ye²⁷, I. Yeletskikh⁶⁸, E. Yigitbasi²⁴, E. Yildirim⁸⁶, K. Yorita¹⁷⁴,
 K. Yoshihara¹²⁴, C. Young¹⁴⁵, C.J.S. Young³², D.R. Yu¹⁶, J. Yu⁸, J. Yu⁶⁷, S.P.Y. Yuen²³, I. Yusuff^{30,az},
 B. Zabinski⁴², G. Zacharis¹⁰, R. Zaidan¹³, A.M. Zaitsev^{132,am}, N. Zakharchuk⁴⁵, J. Zalieckas¹⁵,
 A. Zaman¹⁵⁰, S. Zambito⁵⁹, D. Zanzi⁹¹, C. Zeitnitz¹⁷⁸, A. Zemla^{41a}, J.C. Zeng¹⁶⁹, Q. Zeng¹⁴⁵,
 O. Zenin¹³², T. Ženiš^{146a}, D. Zerwas¹¹⁹, D. Zhang⁹², F. Zhang¹⁷⁶, G. Zhang^{36a,as}, H. Zhang^{35b},
 J. Zhang⁶, L. Zhang⁵¹, L. Zhang^{36a}, M. Zhang¹⁶⁹, P. Zhang^{35b}, R. Zhang²³, R. Zhang^{36a,ax}, X. Zhang^{36b},
 Y. Zhang^{35a,35d}, Z. Zhang¹¹⁹, X. Zhao⁴³, Y. Zhao^{36b,ba}, Z. Zhao^{36a}, A. Zhemchugov⁶⁸, B. Zhou⁹²,
 C. Zhou¹⁷⁶, L. Zhou⁴³, M. Zhou^{35a,35d}, M. Zhou¹⁵⁰, N. Zhou^{35c}, C.G. Zhu^{36b}, H. Zhu^{35a}, J. Zhu⁹²,
 Y. Zhu^{36a}, X. Zhuang^{35a}, K. Zhukov⁹⁸, A. Zibell¹⁷⁷, D. Ziemska⁶⁴, N.I. Zimine⁶⁸, C. Zimmermann⁸⁶,
 S. Zimmermann⁵¹, Z. Zinonos¹⁰³, M. Zinser⁸⁶, M. Ziolkowski¹⁴³, L. Živković¹⁴, G. Zobernig¹⁷⁶,
 A. Zoccoli^{22a,22b}, R. Zou³³, M. zur Nedden¹⁷, L. Zwalski³².

¹ Department of Physics, University of Adelaide, Adelaide, Australia

² Physics Department, SUNY Albany, Albany NY, United States of America

³ Department of Physics, University of Alberta, Edmonton AB, Canada

⁴ ^(a) Department of Physics, Ankara University, Ankara; ^(b) Istanbul Aydin University, Istanbul; ^(c) Division of Physics, TOBB University of Economics and Technology, Ankara, Turkey

⁵ LAPP, CNRS/IN2P3 and Université Savoie Mont Blanc, Annecy-le-Vieux, France

- ⁶ High Energy Physics Division, Argonne National Laboratory, Argonne IL, United States of America
⁷ Department of Physics, University of Arizona, Tucson AZ, United States of America
⁸ Department of Physics, The University of Texas at Arlington, Arlington TX, United States of America
⁹ Physics Department, National and Kapodistrian University of Athens, Athens, Greece
¹⁰ Physics Department, National Technical University of Athens, Zografou, Greece
¹¹ Department of Physics, The University of Texas at Austin, Austin TX, United States of America
¹² Institute of Physics, Azerbaijan Academy of Sciences, Baku, Azerbaijan
¹³ Institut de Física d'Altes Energies (IFAE), The Barcelona Institute of Science and Technology, Barcelona, Spain
¹⁴ Institute of Physics, University of Belgrade, Belgrade, Serbia
¹⁵ Department for Physics and Technology, University of Bergen, Bergen, Norway
¹⁶ Physics Division, Lawrence Berkeley National Laboratory and University of California, Berkeley CA, United States of America
¹⁷ Department of Physics, Humboldt University, Berlin, Germany
¹⁸ Albert Einstein Center for Fundamental Physics and Laboratory for High Energy Physics, University of Bern, Bern, Switzerland
¹⁹ School of Physics and Astronomy, University of Birmingham, Birmingham, United Kingdom
²⁰ ^(a) Department of Physics, Bogazici University, Istanbul; ^(b) Department of Physics Engineering, Gaziantep University, Gaziantep; ^(d) Istanbul Bilgi University, Faculty of Engineering and Natural Sciences, Istanbul; ^(e) Bahcesehir University, Faculty of Engineering and Natural Sciences, Istanbul, Turkey
²¹ Centro de Investigaciones, Universidad Antonio Narino, Bogota, Colombia
²² ^(a) INFN Sezione di Bologna; ^(b) Dipartimento di Fisica e Astronomia, Università di Bologna, Bologna, Italy
²³ Physikalisches Institut, University of Bonn, Bonn, Germany
²⁴ Department of Physics, Boston University, Boston MA, United States of America
²⁵ Department of Physics, Brandeis University, Waltham MA, United States of America
²⁶ ^(a) Universidade Federal do Rio De Janeiro COPPE/EE/IF, Rio de Janeiro; ^(b) Electrical Circuits Department, Federal University of Juiz de Fora (UFJF), Juiz de Fora; ^(c) Federal University of Sao Joao del Rei (UFSJ), Sao Joao del Rei; ^(d) Instituto de Fisica, Universidade de Sao Paulo, Sao Paulo, Brazil
²⁷ Physics Department, Brookhaven National Laboratory, Upton NY, United States of America
²⁸ ^(a) Transilvania University of Brasov, Brasov; ^(b) Horia Hulubei National Institute of Physics and Nuclear Engineering, Bucharest; ^(c) Department of Physics, Alexandru Ioan Cuza University of Iasi, Iasi; ^(d) National Institute for Research and Development of Isotopic and Molecular Technologies, Physics Department, Cluj Napoca; ^(e) University Politehnica Bucharest, Bucharest; ^(f) West University in Timisoara, Timisoara, Romania
²⁹ Departamento de Física, Universidad de Buenos Aires, Buenos Aires, Argentina
³⁰ Cavendish Laboratory, University of Cambridge, Cambridge, United Kingdom
³¹ Department of Physics, Carleton University, Ottawa ON, Canada
³² CERN, Geneva, Switzerland
³³ Enrico Fermi Institute, University of Chicago, Chicago IL, United States of America
³⁴ ^(a) Departamento de Física, Pontificia Universidad Católica de Chile, Santiago; ^(b) Departamento de Física, Universidad Técnica Federico Santa María, Valparaíso, Chile
³⁵ ^(a) Institute of High Energy Physics, Chinese Academy of Sciences, Beijing; ^(b) Department of Physics, Nanjing University, Jiangsu; ^(c) Physics Department, Tsinghua University, Beijing 100084; ^(d) University of Chinese Academy of Science (UCAS), Beijing, China
³⁶ ^(a) Department of Modern Physics and State Key Laboratory of Particle Detection and Electronics,

University of Science and Technology of China, Anhui; ^(b) School of Physics, Shandong University, Shandong; ^(c) Department of Physics and Astronomy, Key Laboratory for Particle Physics, Astrophysics and Cosmology, Ministry of Education; Shanghai Key Laboratory for Particle Physics and Cosmology, Shanghai Jiao Tong University, Shanghai(also at PKU-CHEP), China

³⁷ Université Clermont Auvergne, CNRS/IN2P3, LPC, Clermont-Ferrand, France

³⁸ Nevis Laboratory, Columbia University, Irvington NY, United States of America

³⁹ Niels Bohr Institute, University of Copenhagen, Kobenhavn, Denmark

⁴⁰ ^(a) INFN Gruppo Collegato di Cosenza, Laboratori Nazionali di Frascati; ^(b) Dipartimento di Fisica, Università della Calabria, Rende, Italy

⁴¹ ^(a) AGH University of Science and Technology, Faculty of Physics and Applied Computer Science, Krakow; ^(b) Marian Smoluchowski Institute of Physics, Jagiellonian University, Krakow, Poland

⁴² Institute of Nuclear Physics Polish Academy of Sciences, Krakow, Poland

⁴³ Physics Department, Southern Methodist University, Dallas TX, United States of America

⁴⁴ Physics Department, University of Texas at Dallas, Richardson TX, United States of America

⁴⁵ DESY, Hamburg and Zeuthen, Germany

⁴⁶ Lehrstuhl für Experimentelle Physik IV, Technische Universität Dortmund, Dortmund, Germany

⁴⁷ Institut für Kern- und Teilchenphysik, Technische Universität Dresden, Dresden, Germany

⁴⁸ Department of Physics, Duke University, Durham NC, United States of America

⁴⁹ SUPA - School of Physics and Astronomy, University of Edinburgh, Edinburgh, United Kingdom

⁵⁰ INFN e Laboratori Nazionali di Frascati, Frascati, Italy

⁵¹ Fakultät für Mathematik und Physik, Albert-Ludwigs-Universität, Freiburg, Germany

⁵² Departement de Physique Nucleaire et Corpusculaire, Université de Genève, Geneva, Switzerland

⁵³ ^(a) INFN Sezione di Genova; ^(b) Dipartimento di Fisica, Università di Genova, Genova, Italy

⁵⁴ ^(a) E. Andronikashvili Institute of Physics, Iv. Javakhishvili Tbilisi State University, Tbilisi; ^(b) High Energy Physics Institute, Tbilisi State University, Tbilisi, Georgia

⁵⁵ II Physikalisches Institut, Justus-Liebig-Universität Giessen, Giessen, Germany

⁵⁶ SUPA - School of Physics and Astronomy, University of Glasgow, Glasgow, United Kingdom

⁵⁷ II Physikalisches Institut, Georg-August-Universität, Göttingen, Germany

⁵⁸ Laboratoire de Physique Subatomique et de Cosmologie, Université Grenoble-Alpes, CNRS/IN2P3, Grenoble, France

⁵⁹ Laboratory for Particle Physics and Cosmology, Harvard University, Cambridge MA, United States of America

⁶⁰ ^(a) Kirchhoff-Institut für Physik, Ruprecht-Karls-Universität Heidelberg, Heidelberg; ^(b) Physikalisches Institut, Ruprecht-Karls-Universität Heidelberg, Heidelberg; ^(c) ZITI Institut für technische Informatik, Ruprecht-Karls-Universität Heidelberg, Mannheim, Germany

⁶¹ Faculty of Applied Information Science, Hiroshima Institute of Technology, Hiroshima, Japan

⁶² ^(a) Department of Physics, The Chinese University of Hong Kong, Shatin, N.T., Hong Kong; ^(b) Department of Physics, The University of Hong Kong, Hong Kong; ^(c) Department of Physics and Institute for Advanced Study, The Hong Kong University of Science and Technology, Clear Water Bay, Kowloon, Hong Kong, China

⁶³ Department of Physics, National Tsing Hua University, Taiwan, Taiwan

⁶⁴ Department of Physics, Indiana University, Bloomington IN, United States of America

⁶⁵ Institut für Astro- und Teilchenphysik, Leopold-Franzens-Universität, Innsbruck, Austria

⁶⁶ University of Iowa, Iowa City IA, United States of America

⁶⁷ Department of Physics and Astronomy, Iowa State University, Ames IA, United States of America

⁶⁸ Joint Institute for Nuclear Research, JINR Dubna, Dubna, Russia

⁶⁹ KEK, High Energy Accelerator Research Organization, Tsukuba, Japan

- ⁷⁰ Graduate School of Science, Kobe University, Kobe, Japan
⁷¹ Faculty of Science, Kyoto University, Kyoto, Japan
⁷² Kyoto University of Education, Kyoto, Japan
⁷³ Research Center for Advanced Particle Physics and Department of Physics, Kyushu University, Fukuoka, Japan
⁷⁴ Instituto de Física La Plata, Universidad Nacional de La Plata and CONICET, La Plata, Argentina
⁷⁵ Physics Department, Lancaster University, Lancaster, United Kingdom
⁷⁶ ^(a) INFN Sezione di Lecce; ^(b) Dipartimento di Matematica e Fisica, Università del Salento, Lecce, Italy
⁷⁷ Oliver Lodge Laboratory, University of Liverpool, Liverpool, United Kingdom
⁷⁸ Department of Experimental Particle Physics, Jožef Stefan Institute and Department of Physics, University of Ljubljana, Ljubljana, Slovenia
⁷⁹ School of Physics and Astronomy, Queen Mary University of London, London, United Kingdom
⁸⁰ Department of Physics, Royal Holloway University of London, Surrey, United Kingdom
⁸¹ Department of Physics and Astronomy, University College London, London, United Kingdom
⁸² Louisiana Tech University, Ruston LA, United States of America
⁸³ Laboratoire de Physique Nucléaire et de Hautes Energies, UPMC and Université Paris-Diderot and CNRS/IN2P3, Paris, France
⁸⁴ Fysiska institutionen, Lunds universitet, Lund, Sweden
⁸⁵ Departamento de Fisica Teorica C-15, Universidad Autonoma de Madrid, Madrid, Spain
⁸⁶ Institut für Physik, Universität Mainz, Mainz, Germany
⁸⁷ School of Physics and Astronomy, University of Manchester, Manchester, United Kingdom
⁸⁸ CPPM, Aix-Marseille Université and CNRS/IN2P3, Marseille, France
⁸⁹ Department of Physics, University of Massachusetts, Amherst MA, United States of America
⁹⁰ Department of Physics, McGill University, Montreal QC, Canada
⁹¹ School of Physics, University of Melbourne, Victoria, Australia
⁹² Department of Physics, The University of Michigan, Ann Arbor MI, United States of America
⁹³ Department of Physics and Astronomy, Michigan State University, East Lansing MI, United States of America
⁹⁴ ^(a) INFN Sezione di Milano; ^(b) Dipartimento di Fisica, Università di Milano, Milano, Italy
⁹⁵ B.I. Stepanov Institute of Physics, National Academy of Sciences of Belarus, Minsk, Republic of Belarus
⁹⁶ Research Institute for Nuclear Problems of Byelorussian State University, Minsk, Republic of Belarus
⁹⁷ Group of Particle Physics, University of Montreal, Montreal QC, Canada
⁹⁸ P.N. Lebedev Physical Institute of the Russian Academy of Sciences, Moscow, Russia
⁹⁹ Institute for Theoretical and Experimental Physics (ITEP), Moscow, Russia
¹⁰⁰ National Research Nuclear University MEPhI, Moscow, Russia
¹⁰¹ D.V. Skobeltsyn Institute of Nuclear Physics, M.V. Lomonosov Moscow State University, Moscow, Russia
¹⁰² Fakultät für Physik, Ludwig-Maximilians-Universität München, München, Germany
¹⁰³ Max-Planck-Institut für Physik (Werner-Heisenberg-Institut), München, Germany
¹⁰⁴ Nagasaki Institute of Applied Science, Nagasaki, Japan
¹⁰⁵ Graduate School of Science and Kobayashi-Maskawa Institute, Nagoya University, Nagoya, Japan
¹⁰⁶ ^(a) INFN Sezione di Napoli; ^(b) Dipartimento di Fisica, Università di Napoli, Napoli, Italy
¹⁰⁷ Department of Physics and Astronomy, University of New Mexico, Albuquerque NM, United States of America
¹⁰⁸ Institute for Mathematics, Astrophysics and Particle Physics, Radboud University Nijmegen/Nikhef,

- Nijmegen, Netherlands
- ¹⁰⁹ Nikhef National Institute for Subatomic Physics and University of Amsterdam, Amsterdam, Netherlands
- ¹¹⁰ Department of Physics, Northern Illinois University, DeKalb IL, United States of America
- ¹¹¹ Budker Institute of Nuclear Physics, SB RAS, Novosibirsk, Russia
- ¹¹² Department of Physics, New York University, New York NY, United States of America
- ¹¹³ Ohio State University, Columbus OH, United States of America
- ¹¹⁴ Faculty of Science, Okayama University, Okayama, Japan
- ¹¹⁵ Homer L. Dodge Department of Physics and Astronomy, University of Oklahoma, Norman OK, United States of America
- ¹¹⁶ Department of Physics, Oklahoma State University, Stillwater OK, United States of America
- ¹¹⁷ Palacký University, RCPTM, Olomouc, Czech Republic
- ¹¹⁸ Center for High Energy Physics, University of Oregon, Eugene OR, United States of America
- ¹¹⁹ LAL, Univ. Paris-Sud, CNRS/IN2P3, Université Paris-Saclay, Orsay, France
- ¹²⁰ Graduate School of Science, Osaka University, Osaka, Japan
- ¹²¹ Department of Physics, University of Oslo, Oslo, Norway
- ¹²² Department of Physics, Oxford University, Oxford, United Kingdom
- ¹²³ ^(a) INFN Sezione di Pavia; ^(b) Dipartimento di Fisica, Università di Pavia, Pavia, Italy
- ¹²⁴ Department of Physics, University of Pennsylvania, Philadelphia PA, United States of America
- ¹²⁵ National Research Centre "Kurchatov Institute" B.P.Konstantinov Petersburg Nuclear Physics Institute, St. Petersburg, Russia
- ¹²⁶ ^(a) INFN Sezione di Pisa; ^(b) Dipartimento di Fisica E. Fermi, Università di Pisa, Pisa, Italy
- ¹²⁷ Department of Physics and Astronomy, University of Pittsburgh, Pittsburgh PA, United States of America
- ¹²⁸ ^(a) Laboratório de Instrumentação e Física Experimental de Partículas - LIP, Lisboa; ^(b) Faculdade de Ciências, Universidade de Lisboa, Lisboa; ^(c) Department of Physics, University of Coimbra, Coimbra; ^(d) Centro de Física Nuclear da Universidade de Lisboa, Lisboa; ^(e) Departamento de Física, Universidade do Minho, Braga; ^(f) Departamento de Física Teórica y del Cosmos, Universidad de Granada, Granada; ^(g) Dep Física and CEFITEC of Faculdade de Ciencias e Tecnologia, Universidade Nova de Lisboa, Caparica, Portugal
- ¹²⁹ Institute of Physics, Academy of Sciences of the Czech Republic, Praha, Czech Republic
- ¹³⁰ Czech Technical University in Prague, Praha, Czech Republic
- ¹³¹ Charles University, Faculty of Mathematics and Physics, Prague, Czech Republic
- ¹³² State Research Center Institute for High Energy Physics (Protvino), NRC KI, Russia
- ¹³³ Particle Physics Department, Rutherford Appleton Laboratory, Didcot, United Kingdom
- ¹³⁴ ^(a) INFN Sezione di Roma; ^(b) Dipartimento di Fisica, Sapienza Università di Roma, Roma, Italy
- ¹³⁵ ^(a) INFN Sezione di Roma Tor Vergata; ^(b) Dipartimento di Fisica, Università di Roma Tor Vergata, Roma, Italy
- ¹³⁶ ^(a) INFN Sezione di Roma Tre; ^(b) Dipartimento di Matematica e Fisica, Università Roma Tre, Roma, Italy
- ¹³⁷ ^(a) Faculté des Sciences Ain Chock, Réseau Universitaire de Physique des Hautes Energies - Université Hassan II, Casablanca; ^(b) Centre National de l'Energie des Sciences Techniques Nucléaires, Rabat; ^(c) Faculté des Sciences Semlalia, Université Cadi Ayyad, LPHEA-Marrakech; ^(d) Faculté des Sciences, Université Mohammed Premier and LPTPM, Oujda; ^(e) Faculté des sciences, Université Mohammed V, Rabat, Morocco
- ¹³⁸ DSM/IRFU (Institut de Recherches sur les Lois Fondamentales de l'Univers), CEA Saclay (Commissariat à l'Energie Atomique et aux Energies Alternatives), Gif-sur-Yvette, France

- ¹³⁹ Santa Cruz Institute for Particle Physics, University of California Santa Cruz, Santa Cruz CA, United States of America
- ¹⁴⁰ Department of Physics, University of Washington, Seattle WA, United States of America
- ¹⁴¹ Department of Physics and Astronomy, University of Sheffield, Sheffield, United Kingdom
- ¹⁴² Department of Physics, Shinshu University, Nagano, Japan
- ¹⁴³ Department Physik, Universität Siegen, Siegen, Germany
- ¹⁴⁴ Department of Physics, Simon Fraser University, Burnaby BC, Canada
- ¹⁴⁵ SLAC National Accelerator Laboratory, Stanford CA, United States of America
- ¹⁴⁶ ^(a) Faculty of Mathematics, Physics & Informatics, Comenius University, Bratislava; ^(b) Department of Subnuclear Physics, Institute of Experimental Physics of the Slovak Academy of Sciences, Kosice, Slovak Republic
- ¹⁴⁷ ^(a) Department of Physics, University of Cape Town, Cape Town; ^(b) Department of Physics, University of Johannesburg, Johannesburg; ^(c) School of Physics, University of the Witwatersrand, Johannesburg, South Africa
- ¹⁴⁸ ^(a) Department of Physics, Stockholm University; ^(b) The Oskar Klein Centre, Stockholm, Sweden
- ¹⁴⁹ Physics Department, Royal Institute of Technology, Stockholm, Sweden
- ¹⁵⁰ Departments of Physics & Astronomy and Chemistry, Stony Brook University, Stony Brook NY, United States of America
- ¹⁵¹ Department of Physics and Astronomy, University of Sussex, Brighton, United Kingdom
- ¹⁵² School of Physics, University of Sydney, Sydney, Australia
- ¹⁵³ Institute of Physics, Academia Sinica, Taipei, Taiwan
- ¹⁵⁴ Department of Physics, Technion: Israel Institute of Technology, Haifa, Israel
- ¹⁵⁵ Raymond and Beverly Sackler School of Physics and Astronomy, Tel Aviv University, Tel Aviv, Israel
- ¹⁵⁶ Department of Physics, Aristotle University of Thessaloniki, Thessaloniki, Greece
- ¹⁵⁷ International Center for Elementary Particle Physics and Department of Physics, The University of Tokyo, Tokyo, Japan
- ¹⁵⁸ Graduate School of Science and Technology, Tokyo Metropolitan University, Tokyo, Japan
- ¹⁵⁹ Department of Physics, Tokyo Institute of Technology, Tokyo, Japan
- ¹⁶⁰ Tomsk State University, Tomsk, Russia
- ¹⁶¹ Department of Physics, University of Toronto, Toronto ON, Canada
- ¹⁶² ^(a) INFN-TIFPA; ^(b) University of Trento, Trento, Italy
- ¹⁶³ ^(a) TRIUMF, Vancouver BC; ^(b) Department of Physics and Astronomy, York University, Toronto ON, Canada
- ¹⁶⁴ Faculty of Pure and Applied Sciences, and Center for Integrated Research in Fundamental Science and Engineering, University of Tsukuba, Tsukuba, Japan
- ¹⁶⁵ Department of Physics and Astronomy, Tufts University, Medford MA, United States of America
- ¹⁶⁶ Department of Physics and Astronomy, University of California Irvine, Irvine CA, United States of America
- ¹⁶⁷ ^(a) INFN Gruppo Collegato di Udine, Sezione di Trieste, Udine; ^(b) ICTP, Trieste; ^(c) Dipartimento di Chimica, Fisica e Ambiente, Università di Udine, Udine, Italy
- ¹⁶⁸ Department of Physics and Astronomy, University of Uppsala, Uppsala, Sweden
- ¹⁶⁹ Department of Physics, University of Illinois, Urbana IL, United States of America
- ¹⁷⁰ Instituto de Física Corpuscular (IFIC), Centro Mixto Universidad de Valencia - CSIC, Spain
- ¹⁷¹ Department of Physics, University of British Columbia, Vancouver BC, Canada
- ¹⁷² Department of Physics and Astronomy, University of Victoria, Victoria BC, Canada
- ¹⁷³ Department of Physics, University of Warwick, Coventry, United Kingdom

- ¹⁷⁴ Waseda University, Tokyo, Japan
¹⁷⁵ Department of Particle Physics, The Weizmann Institute of Science, Rehovot, Israel
¹⁷⁶ Department of Physics, University of Wisconsin, Madison WI, United States of America
¹⁷⁷ Fakultät für Physik und Astronomie, Julius-Maximilians-Universität, Würzburg, Germany
¹⁷⁸ Fakultät für Mathematik und Naturwissenschaften, Fachgruppe Physik, Bergische Universität Wuppertal, Wuppertal, Germany
¹⁷⁹ Department of Physics, Yale University, New Haven CT, United States of America
¹⁸⁰ Yerevan Physics Institute, Yerevan, Armenia
¹⁸¹ Centre de Calcul de l’Institut National de Physique Nucléaire et de Physique des Particules (IN2P3), Villeurbanne, France
^a Also at Department of Physics, King’s College London, London, United Kingdom
^b Also at Institute of Physics, Azerbaijan Academy of Sciences, Baku, Azerbaijan
^c Also at Novosibirsk State University, Novosibirsk, Russia
^d Also at TRIUMF, Vancouver BC, Canada
^e Also at Department of Physics & Astronomy, University of Louisville, Louisville, KY, United States of America
^f Also at Physics Department, An-Najah National University, Nablus, Palestine
^g Also at Department of Physics, California State University, Fresno CA, United States of America
^h Also at Department of Physics, University of Fribourg, Fribourg, Switzerland
ⁱ Also at II Physikalisches Institut, Georg-August-Universität, Göttingen, Germany
^j Also at Departament de Fisica de la Universitat Autònoma de Barcelona, Barcelona, Spain
^k Also at Departamento de Fisica e Astronomia, Faculdade de Ciencias, Universidade do Porto, Portugal
^l Also at Tomsk State University, Tomsk, and Moscow Institute of Physics and Technology State University, Dolgoprudny, Russia
^m Also at The Collaborative Innovation Center of Quantum Matter (CICQM), Beijing, China
ⁿ Also at Universita di Napoli Parthenope, Napoli, Italy
^o Also at Institute of Particle Physics (IPP), Canada
^p Also at Horia Hulubei National Institute of Physics and Nuclear Engineering, Bucharest, Romania
^q Also at Department of Physics, St. Petersburg State Polytechnical University, St. Petersburg, Russia
^r Also at Borough of Manhattan Community College, City University of New York, New York City, United States of America
^s Also at Department of Financial and Management Engineering, University of the Aegean, Chios, Greece
^t Also at Centre for High Performance Computing, CSIR Campus, Rosebank, Cape Town, South Africa
^u Also at Louisiana Tech University, Ruston LA, United States of America
^v Also at Institucio Catalana de Recerca i Estudis Avancats, ICREA, Barcelona, Spain
^w Also at Department of Physics, The University of Michigan, Ann Arbor MI, United States of America
^x Also at Graduate School of Science, Osaka University, Osaka, Japan
^y Also at Fakultät für Mathematik und Physik, Albert-Ludwigs-Universität, Freiburg, Germany
^z Also at Institute for Mathematics, Astrophysics and Particle Physics, Radboud University Nijmegen/Nikhef, Nijmegen, Netherlands
^{aa} Also at Department of Physics, The University of Texas at Austin, Austin TX, United States of America
^{ab} Also at Institute of Theoretical Physics, Ilia State University, Tbilisi, Georgia
^{ac} Also at CERN, Geneva, Switzerland
^{ad} Also at Georgian Technical University (GTU), Tbilisi, Georgia
^{ae} Also at Ochadai Academic Production, Ochanomizu University, Tokyo, Japan

- af* Also at Manhattan College, New York NY, United States of America
ag Also at Departamento de Física, Pontificia Universidad Católica de Chile, Santiago, Chile
ah Also at Academia Sinica Grid Computing, Institute of Physics, Academia Sinica, Taipei, Taiwan
ai Also at The City College of New York, New York NY, United States of America
aj Also at School of Physics, Shandong University, Shandong, China
ak Also at Departamento de Física Teórica y del Cosmos, Universidad de Granada, Granada, Portugal
al Also at Department of Physics, California State University, Sacramento CA, United States of America
am Also at Moscow Institute of Physics and Technology State University, Dolgoprudny, Russia
an Also at Departement de Physique Nucléaire et Corpusculaire, Université de Genève, Geneva, Switzerland
ao Also at Institut de Física d'Altes Energies (IFAE), The Barcelona Institute of Science and Technology, Barcelona, Spain
ap Also at School of Physics, Sun Yat-sen University, Guangzhou, China
aq Also at Institute for Nuclear Research and Nuclear Energy (INRNE) of the Bulgarian Academy of Sciences, Sofia, Bulgaria
ar Also at Faculty of Physics, M.V.Lomonosov Moscow State University, Moscow, Russia
as Also at Institute of Physics, Academia Sinica, Taipei, Taiwan
at Also at National Research Nuclear University MEPhI, Moscow, Russia
au Also at Department of Physics, Stanford University, Stanford CA, United States of America
av Also at Institute for Particle and Nuclear Physics, Wigner Research Centre for Physics, Budapest, Hungary
aw Also at Giresun University, Faculty of Engineering, Turkey
ax Also at CPPM, Aix-Marseille Université and CNRS/IN2P3, Marseille, France
ay Also at Department of Physics, Nanjing University, Jiangsu, China
az Also at University of Malaya, Department of Physics, Kuala Lumpur, Malaysia
ba Also at LAL, Univ. Paris-Sud, CNRS/IN2P3, Université Paris-Saclay, Orsay, France
* Deceased